TRIBHUVAN UNIVERSITY

INSTITUTE OF ENGINEERING

PULCHOWK CAMPUS

THESIS NO. PUL080MSGtE006

Numerical Investigation on Influence of Excavation Sequence and Parametric Analysis on Cavern Interaction (A Case Study of Tamakoshi V Hydroelectric Project)

by

Gyanu Pathak

A THESIS

SUBMITTED TO THE DEPARTMENT OF CIVIL ENGINEERING IN PARTIAL FULFILLMENT OF THE REQUIREMENTS FOR THE DEGREE OF MASTER IN SCIENCE IN GEOTECHICAL ENGINEERING

DEPARTMENT OF CIVIL ENGINEERING.

LALITPUR, NEPAL

APRIL, 2026

COPYRIGHT

TRIBHUVAN UNIVERSITY

INSTITUTE OF ENGINEERING

PULCHOWK CAMPUS

DEPARTMENT OF CIVIL ENGINEERING

The thesis titled “Numerical Investigation on Influence of Excavation Sequence and Parametric Analysis on Cavern Interaction (A Case Study of Tamakoshi V Hydroelectric Project)” prepared and submitted by Gyanu Pathak in partial fulfilment of the requirements for the degree of Master of Science (M. Sc.) in Geotechnical Engineering has been examined by us and is accepted for the award of M. Sc. In Geotechnical Engineering by Tribhuvan University.

The undersigned certify that they have read, and recommended to the Institute of Engineering for acceptance, a thesis report entitled “Numerical Investigation on Influence of Excavation Sequence and Parametric Analysis on Cavern Interaction (A Case Study of Tamakoshi V Hydroelectric Project)" submitted by Gyanu Pathak in partial fulfillment of the requirements for the degree of Master in Geotechnical Engineering

Supervisor:
Assist. Prof. Santosh Kumar Yadav
Department of Civil Engineering
IOE, Pulchowk Campus

External Examiner:
Dr. Gyanendra Lal Shrestha
Immediate Past President
Nepal Tunneling Association

Program Coordinator:
Assist. Prof. Bhim Kumar Dahal
M.Sc. in Geotechnical Engineering
Department of Civil Engineering
IOE, Pulchowk Campus

Date: April 27, 2026

DECLARATION

I hereby declare that this study, titled "**Numerical Investigation on Influence of Excavation Sequence and Parametric Analysis on Cavern Interaction (A Case Study of Tamakoshi V Hydroelectric Project)** "is based on my original research work. Related works on the topic by other researchers have been duly acknowledged. I owe all the liabilities relating to the accuracy and authenticity of the data and any other information included hereunder.

Gyanu Pathak

080/MSGtE/006

MSc in Geotechnical Engineering

Date: 27th April, 2026

ACKNOWLEDGEMENTS

I want to express my sincere gratitude to my supervisor, Dr. Santosh Kumar Yadav, for his invaluable guidance, continuous support, and encouragement throughout this research. His insightful suggestions significantly enhanced the quality of this work, and his expertise was instrumental in shaping the direction of this study.

I am equally grateful to my external examiner, Dr. Gyanendra Lal Shrestha, for his constructive feedback and thoughtful guidance on my thesis.

I extend my heartfelt thanks to Professor Indra Prasad Acharya, Assistant Professor Bhim Kumar Dahal, and Assistant Professor Ram Chandra Tiwari, along with all members of the Geotechnical Engineering Department at Pulchowk Campus. Their constant support and the opportunities they provided have greatly enriched my academic journey and broadened my knowledge.

I would like to thank Mr. Surya Krishna Prajapati for his dedicated efforts in support of the Geotechnical Engineering Department at Pulchowk Campus, and Hydro Consult Engineering for their cooperation during this study. I am particularly grateful to Er. Sulabh Majgainya for his technical assistance, which was essential to the successful completion of this thesis.

I am thankful to the Department of Civil Engineering, Pulchowk Campus, Institute of Engineering, for providing the necessary resources and a conducive research environment.

Finally, I would like to express my deepest gratitude to my parents, family and friends for their unwavering support, encouragement, and inspiration throughout my studies. Special gratitude goes to my wife, Kabita Bhusal, and my sister, Sushmita Pathak, for their unwavering support during the course of my study and research. I also extend my thanks to all those who contributed to this work, directly or indirectly.

Gyanu Pathak

080/MSGtE/006

ABSTRACT

Caverns are essential components of hydropower projects in Nepal where the stability of the excavations needs to be carefully assessed in order to design safe and economically viable structures. This research examines the effects of excavation on the behaviour of the rock mass in a parallel cavern system by studying three parameters: rock mass quality in terms of the Geological Strength Index (GSI), cavern spacing and excavation sequence, through a numerical model. The findings reveal that the most important governing parameter is rock mass quality, with an increase in GSI from 35 to 60 resulting in a considerable decrease in the deformation amplification factor from greater than 2.0 to 1.0, and a significant reduction in the plastic zone around the caverns. Spacing is observed to be dependent on the rock mass quality, where in poor quality rock mass, spacing equal to or greater than the full height of the largest cavern is necessary to avoid interaction between plastic zones around the caverns, while in good quality rock mass, the spacing can be reduced to two-thirds the height of the largest cavern without significant cavern interaction. In terms of excavation sequence, it is observed that the deformation in the smaller cavern is reduced by excavating the larger cavern first, which confirms that this is an important governing factor in cavern stability.

Keywords: Cavern; Amplification Factor; Plastic Zone; Geological Strength Index (GSI); Deformation Behavior; Excavation Sequence

TABLE OF CONTENTS

LIST OF FIGURES

LIST OF TABLES

ABBREVIATIONS AND ACRONYMS

2D	:	Two Dimensional
3D	:	Three Dimensional
AF	:	Amplification Factor
D	:	Disturbance Factor
E	:	Modulus of Elasticity
GPa	:	Giga Pascal
GSI	:	Geological Strength Index
HEP	:	Hydroelectric Project
MPa	:	Mega Pascal
PHC	:	Powerhouse Cavern
Q	:	Rock Mass Quality Index
RMR	:	Rock Mass Rating
RS2	:	Finite Element Software (Rocscience)
TKV	:	Tamakoshi V Hydroelectric Project
TRC	:	Transformer Cavern
UCS	:	Unconfined Compressive Strength
γ	:	Unit Weight
ν	:	Poisson's Ratio
σ	:	Stress

1 INTRODUCTION

1.1 Background

The construction of underground structures for hydropower development in Nepal has grown considerably over recent decades. The country's rugged Himalayan topography, characterized by steep terrain and limited flat land along river valleys, makes underground placement of key components such as tunnels, settling basins, surge shafts, and powerhouses both practical and often necessary. Underground construction in Nepal has a long history; the Churia Tunnel, regarded as one of the country's earliest highway tunnels, was completed in 1917. The Tinau Hydropower Plant (commissioned 1978) incorporates a 2.462 km headrace tunnel and underground desilting chambers, while the Andhikhola Hydropower Station (commissioned 1995) features a powerhouse excavated within slate with quartize vein.

Underground facilities are favoured in mountainous terrain because steep slopes hinder large surface structures and increase slope instability risk. However, underground facilities reduce environmental disturbance, limit surface land use, and offer protection from surface hazards such as landslides and rockfall. Nevertheless, the Himalayan region's geological complexity, marked by highly fractured rock masses, active tectonics, and variable in-situ stress conditions, presents substantial challenges for underground cavern design and construction. Long-term structural stability, therefore, demands thorough geotechnical investigation and rigorous engineering design (Krishna K. Panthi (2006)).

Large underground hydropower schemes typically comprise multiple adjacent caverns: a main powerhouse cavern, transformer cavern, surge chamber, and settling basins. The interaction among these openings significantly influences stress redistribution and deformation in the adjacent rock mass. When caverns remain positioned in proximity, stress concentration can develop in the intervening rock pillar, potentially causing excessive deformation or instability. Consequently, pillar width, cavern spacing, and excavation sequence are critical design parameters. Numerical and empirical studies confirm that adequate pillar

dimensions are necessary to prevent the coalescence of plastic zones and to maintain stable stress distributions (Shukla et al., 2024).

In most underground hydropower layouts, the transformer cavern is positioned immediately adjacent to the powerhouse cavern to accommodate electrical equipment efficiently while optimising overall cavern dimensions. The stability of the cavern is controlled by the virgin stress, discontinuities present, and the mechanical properties of the rockmass present at the location of interest.

A further governing parameter is the rock mass deformation modulus, which quantifies rock stiffness and its capacity to resist excavation-induced displacement. Higher modulus values correlate with reduced deformation around openings, whereas weak or fractured rock masses exhibiting low modulus values tend to experience larger displacements and more extensive plastic zones. Numerical simulations and field data from hydropower cavern projects consistently demonstrate that rock mass stiffness and excavation-induced stress redistribution are the primary controls on surrounding rock behaviour (Sun et al., 2023).

In view of these considerations, this thesis investigates the deformation behaviour of adjacent powerhouse and transformer caverns, with particular focus on the influence of excavation sequence, rock mass deformation modulus, and distance between caverns. Numerical simulations using the finite element method are conducted using geological and geotechnical data obtained from the Tamakoshi V Hydroelectric Project.

1.2 Research Gaps and Problem Statement

In a typical underground hydropower layout, a transformer cavern (TRC) is built parallel to the powerhouse cavern (PHC) to step up electrical voltage while optimizing underground space utilization. However, constructing two caverns in proximity introduces complex rock mass behaviour governed primarily by geomechanical properties of the rock mass present at area of interest.

Underground excavation disturbs the natural virgin stress field, resulting in stress re-distribution and deformation in the rock mass. When caverns are positioned in proximity, the intervening rock pillar becomes subject to elevated stress concentrations, potentially leading to progressive deformation or pillar failure if

dimensions are insufficient (Brady & Brown, 2004). A key parameter in the response of the structure is the deformation modulus of the rock mass, which defines the deformation and stiffness characteristics of the rock mass present at area of interest. Rock masses exhibiting low deformation modulus are significantly more susceptible to large displacements, plastic zone development, and wall convergence following excavation (Bellapu et al., 2023).

Inadequate pillar width within the adjacent caverns can develop overlapping in plastic zones, amplifying instability in both openings simultaneously (Zhang & Goh, 2015). Furthermore inappropriate excavation sequencing further increase in stress concentrations and deformation and thus increasing the risk of structural failure (Wang et al., 2023). However, with growing research and study related to different cavern, the combined influence of deformation modulus, rock pillar thickness and excavation sequence due to cavern interaction in Himalayan geological conditions are not adequate studied which is the motivation for this study.

1.3 Objectives

1.3.1 General objective

- To assess the deformation behaviour due to cavern interaction (powerhouse and transformer cavern) with different excavation sequences, rock mass properties, and cavern spacing.

1.3.2 Specific objective

- Analyze the effects of various excavation sequences of the PHC and TRC on induced deformation.
- To study the effects of the deformation modulus of the rock mass on the deformation behavior of the surrounding rock mass, and also to investigate the influence of different rock mass stiffness conditions on the wall convergence of the cavern.
- To investigate the influence of different cavern spacing between powerhouse and transformer cavern on deformation, and to study the suitable excavation method, cavern distance and rock mass properties.

1.4 Limitations

- The study is based on the available literature on tunnelling principles of rock mechanics and geotechnical engineering, and the findings are interpreted within the framework of established empirical and analytical methods.
- Factors such as seismic forces, groundwater pressure, seepage flow, and discontinuities (joints, faults, and fractures) are not considered in the study; only the geotechnical parameters influencing the static stability of the rock mass are taken into account, which may underestimate actual field conditions.
- The analysis is conducted under two-dimensional (2D) plane strain assumptions using a 2D numerical modelling tool, and a full three-dimensional (3D) numerical simulation of cavern interaction, which would more accurately capture spatial stress redistribution, arching effects, and pillar behaviour between adjacent caverns, is beyond the scope of this study.
- The rock mass is assumed to be isotropic and homogeneous, and the in-situ stress used in the analysis is based on empirical relationships, which may not fully represent the actual stress conditions in the area of interest.

2 LITERATURE REVIEW

The stability of underground caverns has been a subject of extensive research in the field of rock mechanics and geotechnical engineering. The behavior of rock mass around underground excavations is controlled by a complex interplay of geological, geomechanical, and structural parameters. Numerous studies have investigated the influence of rock mass properties, in-situ stress conditions and excavation geometry on the stability of underground openings (Brady & Brown, 2004).

The interaction between adjacent caverns is a critical feature of underground space utilization especially, when multiple caverns are excavated in each other proximity. The distance between caverns which is commonly referred as the pillar width, plays a significant role in determining the stress redistribution and deformation behavior of the surrounding rock mass (Hoek et al., 2006). As the inter-cavern spacing decreases, the zones of influence overlap, leading to amplified stress concentrations and potential instability (Zhao & Ma, 2009).

Rock mass classification systems such as the Rock Mass Rating (RMR) by (Bieniawski & Bieniawski, 1989), the Q-system by (Barton et al., 1974), and the Geological Strength Index (GSI) (Carranza-Torres & Fairhurst, 2000; Vlachopoulos & Diederichs, 2009) have been widely employed to characterize the geotechnical properties of rock masses and assess the stability of underground excavations. These classification systems form the basis for determining input parameters in numerical modelling studies and support the determination.

Numerical methods such as finite element method (FEM) and finite difference method (FDM) have been widely applied to model the response of underground caverns under different rock mass and geometrical conditions. These approaches enable the evaluation of stress, displacement and plastic zone around underground openings.

This literature review addresses the current research on the interaction of caverns, the impact of rock mass parameters on the stability of underground caverns, and the effect of cavern spacing on stress redistribution and deformation, and forms the basis of the numerical modeling strategy used in this study.

2.1 Underground Excavation and Tunnel Support System

The stability of modern rock tunnels is governed by the combined action of rock mass reinforcement and structural support systems (Hoek et al., 2008). The incorporation of structural design and geotechnical in tunneling recognizes that reinforcement generally in the form of cables or rockbolts, upgrade the mechanical properties of rock mass in a same way as reinforcement does to the concrete. Structural supports like lattice girders or steel sets surrounded by shotcrete, provide confinement and resistance to tunnel convergence. Optimizing tunnel design relies on the combined use of support and reinforcement, with particular importance placed on coupling geotechnical behavior with structural response (Hoek et al., 2008). Rockbolts act as tunnel reinforcement by modifying the mechanical properties of the rock mass surrounding the excavation, and this understanding has enabled numerical analyses of tunnels reinforced with rockbolts and supported by composite linings, demonstrating that the integration of geotechnical behavior with structural design has practical implications for ensuring that support systems are mobilized effectively at each stage of excavation. (Singh & Goel, 1999) emphasized the philosophy of rock reinforcement as stitching rock wedges together and restraining them from sliding from the roof and walls. The principles of rockbolting design, noting that the earlier method of choosing strong rockbolts is effective mainly under conditions of low virgin stresses (Li, 2017). In high in-situ stress environments, energy-absorbing rockbolts are preferred because they can accommodate the large deformations associated with deep excavations (Li, 2017). A pressure arch is formed in the rock at a certain distance behind the tunnel face. When the failure zone is small, the rockbolts should be sufficiently long to penetrate this pressure arch (Li, 2017). If the failure zone is large, short rockbolts are placed close to each other to form an artificial pressure arch in the failure zone (Li, 2017). The length of the roof bolts should preferably be less than half of the opening height. The length of wall bolts should not exceed half of the span for ease of installation. In regular bolting patterns, the spacing between bolts in a row and between rows are typically equal. The bolts should be spaced between 1.0 m and 2.5 m apart, the recommended spacing should be 3-4 times the average joint spacing when the joints are spaced 0.3-1.0 m apart (Li, 2017).

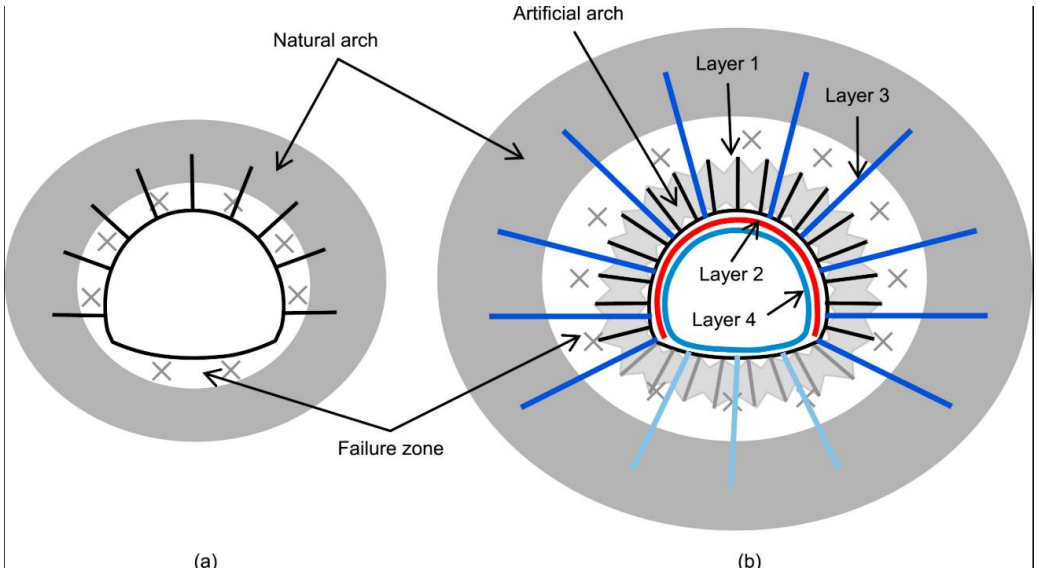

Figure 2.1: Rockbolting in different failure of rock conditions ((Li, 2017)

2.2 Large Underground Powerhouse Cavern

The design of large underground powerhouses in weak rocks presents unique stability challenges due to the heterogeneity of the rock mass and the large deformations that may occur during and after excavation(Wang et al., 2023). Evert Hoek reviewed several large powerhouse caverns in weak rock and highlighted the importance of understanding in-situ stress conditions, rock mass properties, and the limitations of traditional support systems such as concrete arches. He recommended the use of flexible support systems, including grouted cables and shotcrete linings capable of accommodating significant displacements to maintain stability throughout excavation. The role of excavation sequencing is particularly important in large cavern construction, as a staged excavation approach allows monitoring data to be gathered at each stage, enabling back-analysis and design adjustments as excavation progresses. Numerical modeling, combined with empirical data and continuous geotechnical inspection, is recommended for tailoring designs to the specific geological and geotechnical conditions encountered at each site. The observation that flexible support systems perform better than rigid concrete supports in weak rock conditions has been validated through numerous case histories, particularly in high-deformation environments such as the Himalayan region. The study conducted on the influence of the distance between caverns in large cavern complexes in hydraulic power stations shows that creating multiple caverns in close proximity to each other has a

significant impact on the stability of the rock pillar between them, with the extent of influence mainly dependent on the cavern's width-to-height ratio and the geotechnical conditions of the rock mass between the caverns (Zhao & Ma, 2009). Their study also demonstrated that an optimal cavern spacing exists beyond which further separation yields only marginal improvement in stability.

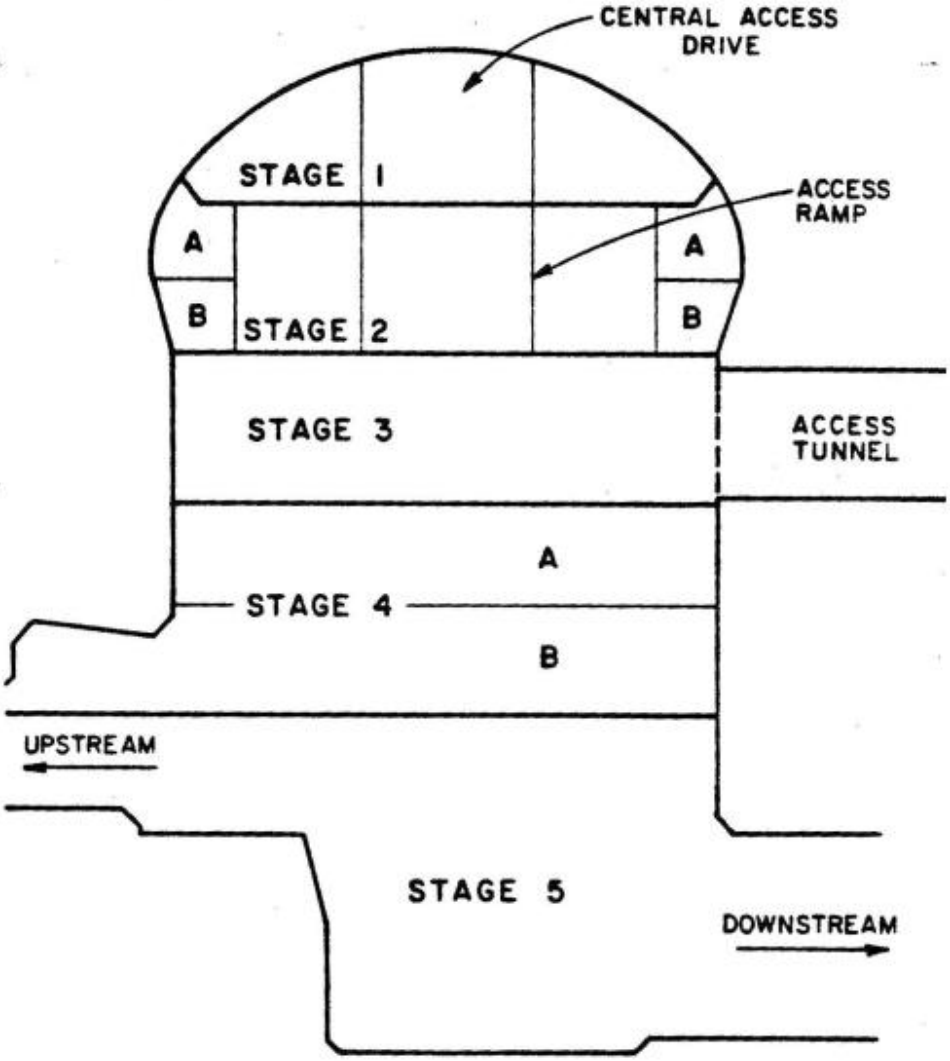

Figure 2.2: Excavation stages for cavern (Hammett & Hoek, 1981)

The stability of pillars between a machine hall and a transformer gallery in the Mingtan Pumped Storage Project, Taiwan, is optimized when the separation distance between the two caverns is about the same as the height of the larger cavern, which is a factor to be considered for designing underground caverns in weak rock masses (Hoek, 2007).

2.3 Rock Mass Classification System

Rock mass classification systems serves as the foundation of empirical approaches used to characterize the geotechnical properties of rock masses and evaluate the suitability of underground excavation designs (Bieniawski & Bieniawski, 1989; Palmstrom & Broch, 2006). The three most widely used systems in tunnel and cavern engineering are the Rock Mass Rating (RMR) developed (Bieniawski & Bieniawski, 1989) the Q-system developed by (Barton et al., 1974), and the Geological Strength Index (GSI) proposed by (Marions & Hoek, 2000)

The RMR system rates rock mass quality based on six parameters: uniaxial compressive strength of intact rock, rock quality designation (RQD), spacing of discontinuities, condition of discontinuities, groundwater conditions, and orientation of discontinuities (Bieniawski & Bieniawski, 1989; Singh & Goel, 1999). The total RMR score ranges from 0 to 100, and is used to assign a rock mass class that directly informs support recommendations and stand-up time estimates (Pantelidis, 2009; Singh & Goel, 1999).

Table 2.1: Engineering rock mass classification (Sivakugan et al., 2013)

Table 4.17 Rock mass classes based on RMR

RMR	81–100	61–80	41–60	21–40	0–20
Class number	I	II	III	IV	V
Description	Very good rock	Good rock	Fair rock	Poor rock	Very poor rock

Table 4.18 Meaning of rock mass class

Class number	*I*	*II*	*III*	*IV*	*V*
Average stand-up time of tunnel	20 years for 15-m span	1 year for 10-m span	1 week for 5-m span	10 hours for 2.5-m span	30 minutes for 1-m span
Cohesion of rock mass (kPa)	>400	300–400	200–300	100–200	<100
Friction angle of rock mass (°)	>45	35–45	25–35	15–25	<15

The Q-system, developed at the Norwegian Geotechnical Institute(Barton et al., 1974; Palmstrom & Broch, 2006), provides a quantitative measure of rock mass quality through six parameters: RQD, the number of joint sets, joint roughness, joint alteration, water reduction factor, and stress reduction(Barton, 2002; Barton et al., 1974). Q system is extensively used in a tunnelling project in Nepal

(especially in a hydropower project), and (Nilsen & Palmström, 2000) reviewed the Q-system application in various geological conditions, establishing guidelines for parameter determination in complex geological environments, adjustment factors for large-span excavations, and integration with other classification systems.

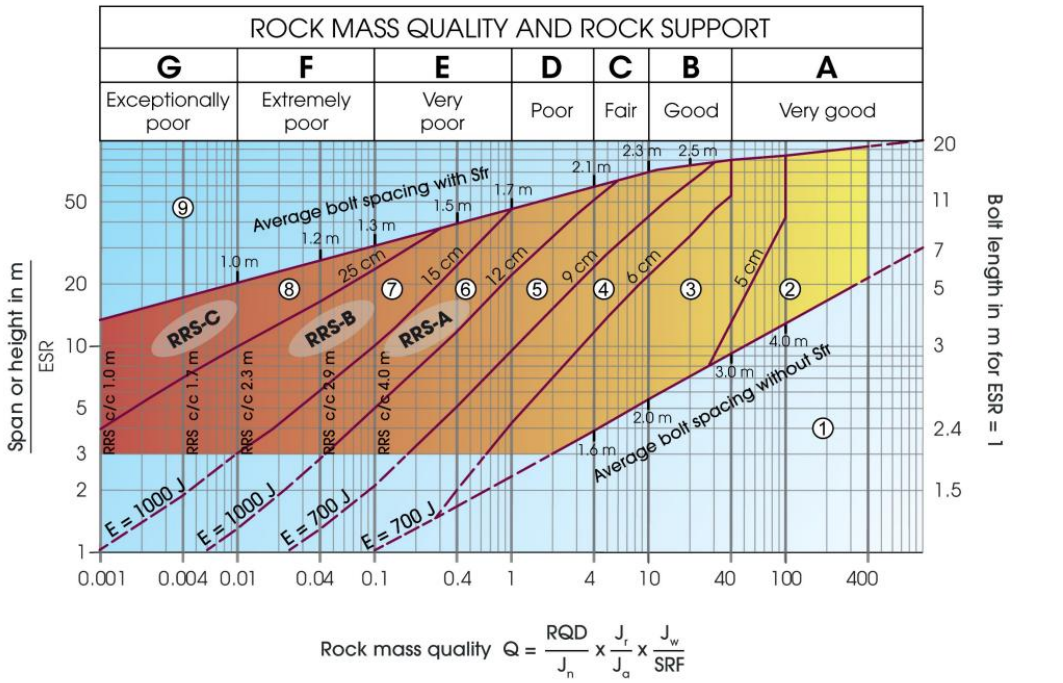

Figure 2.3: Support system based on Q (NGI, 2025)

The GSI system was originally proposed by (Hoek, 1994) and subsequently refined by (Hoek & Brown, 1997) (Marions & Hoek, 2000) later extended the GSI classification specifically for heterogeneous weak rock masses. It provides a way to predict the reduction in rock mass strength under different geological conditions, based on visual inspection of the structural conditions of the rock mass and surface conditions of discontinuities(Hoek, 2007) . Contrasting to Q and RMR ,GSI is specifically designed for use with the Hoek-Brown failure criterion. (Shrestha, 2021) provided comprehensive guidance on rock engineering design for tunnels and underground structures in the Himalayan context, emphasizing the limitations of empirical classification systems under highly stressed conditions and the need for site-specific calibration.

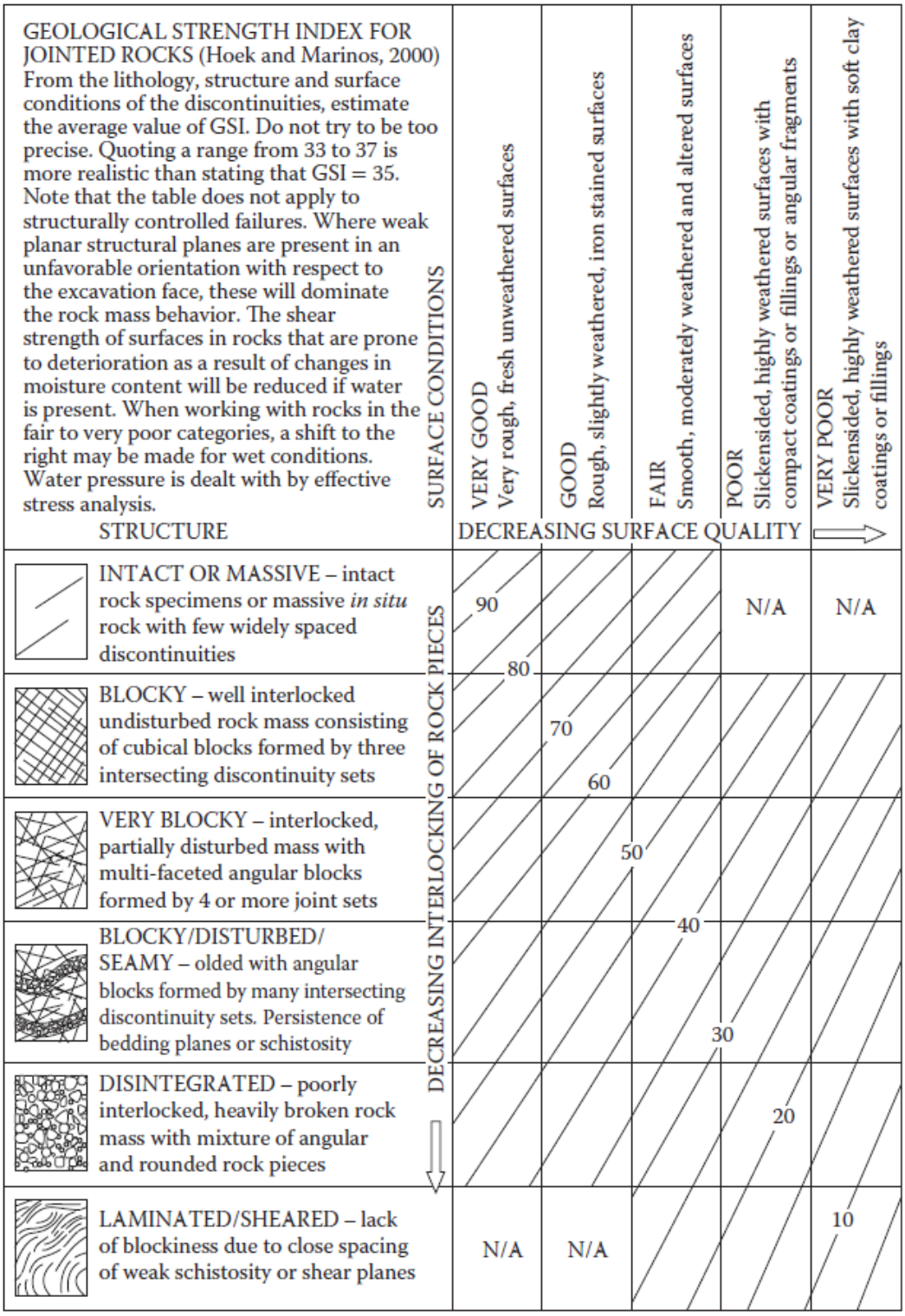

Figure 2.4: Geological Strength Index (GSI) for jointed rocks (Hoek, 2007)

2.4 Failure Criterion

Failure criteria are essential in rock mechanics that provides the mathematical framework to describe the strength of rock masses and intact rock for use in engineering design. (Ulusay, 2015) provides the basic guidelines for the selection

of failure criterion, which includes Mohr-Coulomb criterion, Hoek–Brown criterion, and Drucker-Prager Criterion. The two major criteria that have been more extensively used have been highlighted in this literature review.

2.4.1 Mohr-Coulomb failure criterion

Among the traditional methods that are used to describe the shear failure in materials likes soils and rocks, the Mohr-Coulomb (MC) criterion is one of the commonly preferred linear models(Jaeger et al., 2011; Labuz & Zang, 2012) . This approach defines that failure of a material commences when the shear stress component acting on a potential failure plane reaches a threshold value that depends on the normal stress component on that plane (Jaeger et al., 2011; Labuz & Zang, 2012).The model represents the failure envelope using two material parameters: cohesion (c) and the angle of internal friction (φ).

The shear strength of the material according to the Mohr–Coulomb criterion is expressed as:

$$\tau = c + \sigma_n \tan\emptyset \quad (1)$$

Where, c is the cohesion, σ_n the normal stress acting on the plane of failure, and ∅ is the angle of friction.

The other way to represent the Mohr-Coulomb criterion involves using principles stress components in which failure is assessed by the relationship among the minor principle stress (σ_3) and major principle stress (σ_1), with intermediate principle stress (σ_2) is neglected (Al-Ajmi & Zimmerman, 2005; Jaeger et al., 2011). This alternative representation is reasonably accurate for assessing rock mass behaviour under conditions where variations in mean stress remain limited and all principle stresses are compressive (Ulusay, 2015).

In the scenario of tunnelling, Mohr Coulomb criterion is generally employed for preliminary analysis, shallow tunnels, and cases where stress conditions vary within a limited range. However, it may not accurately represent rock mass behavior under high confining stresses or highly fractured conditions, where the strength envelope becomes nonlinear. In such cases, criteria such as Hoek Brown failure criterion generally provide a more accurate representation of mechanical properties of rock masses (Hoek et al., 2002).

2.4.2 Hoek Brown failure criterion

The Hoek-Brown failure criterion is a popular empirical method used for determining the strength of rock masses with fractures and intact rock and, particularly for the design and analysis of underground excavations like tunnels and caverns (Carranza-Torres & Fairhurst, 2000; Hoek, 2007). It was developed by Evert Hoek and Edward T. Brown based on a large number of laboratory triaxial tests on a wide range of igneous, sedimentary and metamorphic rocks(Cai, 2010; Hoek & Brown, 1980a) . Unlike the linear Mohr-Coulomb criterion, the Hoek-Brown criterion is non-linear and parabolic, making it a better fit for the growth in strength of rocks with the increase in confining stress (Labuz & Zang, 2012; Ulusay, 2015).

The original Hoek–Brown failure criterion for intact rock is expressed as:

$$\sigma_1 = \sigma_3 + \sigma_{ci}\sqrt{m_i\left(\frac{\sigma_3}{\sigma_{ci}}\right) + s} \tag{2}$$

Where σ1 and σ3 are the major and minor principal stresses. σci is the uniaxial compressive strength of intact rock, m and s being constants that depend on the rock mass properties (Hoek, 2007).

The criterion has been further modified to represent the behaviour of jointed rock masses. The generalized Hoek-Brown criterion is expressed as:

$$\sigma_1{}' = \sigma_3{}' + \sigma_{ci}\left(m_b\left(\frac{\sigma_3{}'}{\sigma_{ci}}\right) + s\right)^a \tag{3}$$

where σ1′ and σ3′ are the maximum and minimum effective principal stresses at failure, mb is the Hoek–Brown constant for the rock mass, and s and a are parameters that depend on the rock mass quality (Hoek et al., 2002). These parameters are determined using the Geological Strength Index (GSI) and a disturbance factor (D) that accounts for blast damage.

The Hoek–Brown criterion provides an empirical approach to estimate rock mass strength from intact rock properties, making it particularly useful when direct large-scale testing of rock masses is not feasible (Eberhardt, 2012). It is generally applicable to rock masses with closely spaced discontinuities and approximately

isotropic mechanical behavior, where the rock mass can be treated as an equivalent continuum (Hoek, 2007).

For many numerical modelling programs that use the Mohr–Coulomb model, the Hoek–Brown failure envelope can be converted into equivalent cohesion and friction angle parameters by fitting a linear relationship over a selected range of confining stresses (Hoek, 2007). This method is commonly used in numerical analysis of tunnels and underground excavations.

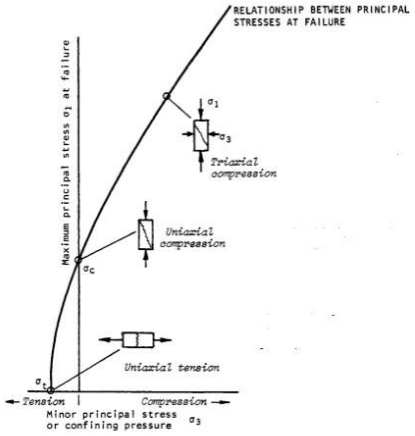

(a) Schematic Diagram of failure envelope (Brown and Hoek, 1980)

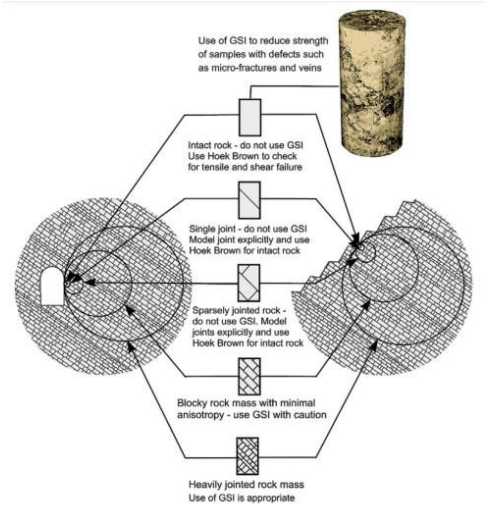

(b) Condition for selecting Generalized Hoek and Brown Criterion (Hoek and Brown, 2019). Modified after (Brown and Hoek, 1980)

Figure 2.5: Selection for Generalized Hoek-Brown criterion (Hoek, 2007)

The Mohr–Coulomb failure criterion is a simple linear model that uses cohesion and friction angle to describe rock strength and is commonly used for preliminary analysis and conditions with limited stress range. However, it may not accurately represent rock behaviour under high confining stresses.

The Hoek–Brown failure criterion is a non-linear empirical model developed from extensive rock testing and is more suitable for jointed rock masses and underground excavation analysis. In practice, Hoek–Brown parameters are often converted into equivalent Mohr–Coulomb parameters for numerical modelling in many geotechnical software programs.

2.5 Rock Stresses

The design of structures on rock foundation or in underground excavations shall carried out considering the in situ stress conditions any conceivable subsequent stress change brought about by:

a) Constructions of New Structures such as dams, tunnels, and powerhouses.
b) Self-Weight of New Structures;
c) Surface and/ or underground excavations
d) Changes Pore Pressure Regime

Virgin rock stresses may be attributed to the following origins or their combinations. Virgin stresses are the due to following components (Nilsen & Thidemann, 1993):

- Gravitational Stresses
- Topographic Stresses
- Tectonic Stresses
- Residual Stresses

Most commonly, gravity and tectonic stresses are the major components in applied rock mechanics and engineering. In assessing the stress field at a certain depth in a rock mass, it's typically assumed that the in situ stress field is comprised of three major components: a vertical stress brought about by the weight of the overlying mass and two horizontal stresses that could be either greater or smaller than the vertical stress (Ulusay, 2015).

2.5.1 Gravitational stresses

Rock masses subjected to overburden develop stress components in both vertical and horizontal orientations (Brady & Brown, 2004). For a point located at depth z beneath a horizontal ground surface, the vertical stress component attributable to gravitational loading can be expressed by the equation.

$$\sigma_v = \sigma_z = \gamma H \quad (4)$$

Where, σ_v is the vertical stress

γ = unit weight of the overlying rock

H = depth below surface

Field observation at various location around the world shows the relationship to be valid. Although as shown in Figure 2.6, the measurement shows considerate number of deviations in measurements (Hoek, 2007).

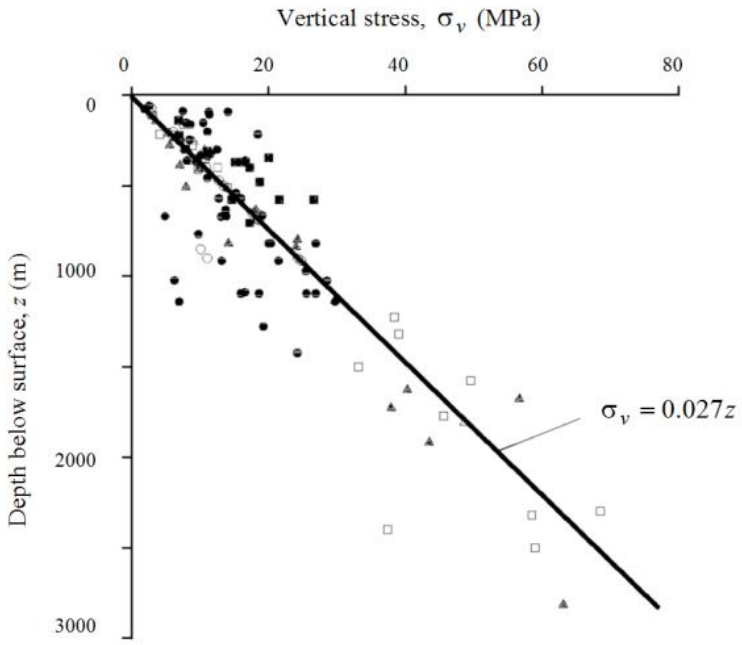

Figure 2.6: Result of vertical stress measurements (Hoek, 2007)

Unlike the vertical stresses, estimates of horizontal stresses on a rock element at a depth H below the surface are more difficult. In general, the ratio of the mean horizontal stress to the vertical stress is symbolised by k such that:

$$\sigma_h = k\sigma_v = k\gamma \mathrm{H} \tag{5}$$

where,

$$k = \frac{\upsilon}{1-\upsilon} \tag{6}$$

υ = Poisson's ratio

(Karl & Richart, 1952) recommends, "For a gravitationally loaded rock mass in which no lateral strain was permitted during formation of the overlying strata, the value of k is independent of depth." For Poisson's ratio of approx. 0.25, which is typical for many rock masses, the horizontal stress generated purely by gravitational loading is about one-third of the vertical stress (Hoek & Brown, 1997; Karl & Richart, 1952). However, this gravity-induced component represents only a minor portion of the total horizontal stress (Amadei & Stephansson, 1997; Zang & Stephansson, 2010). Field measurements from civil and mining sites worldwide indicate that the stress ratio k is generally higher at shallow depths and tends to decrease as depth increases (Brown & Hoek, 1978; Sheorey, 1994).

(Sheorey, 1994) Shorey developed an elasto-static thermal stress model of the Earth. This model takes into account the curvature of the Earth's crust and variation of elastic constants, density, and thermal expansion coefficient in the Earth's crust and mantle (Hoek, 2007; Ray, 2009).

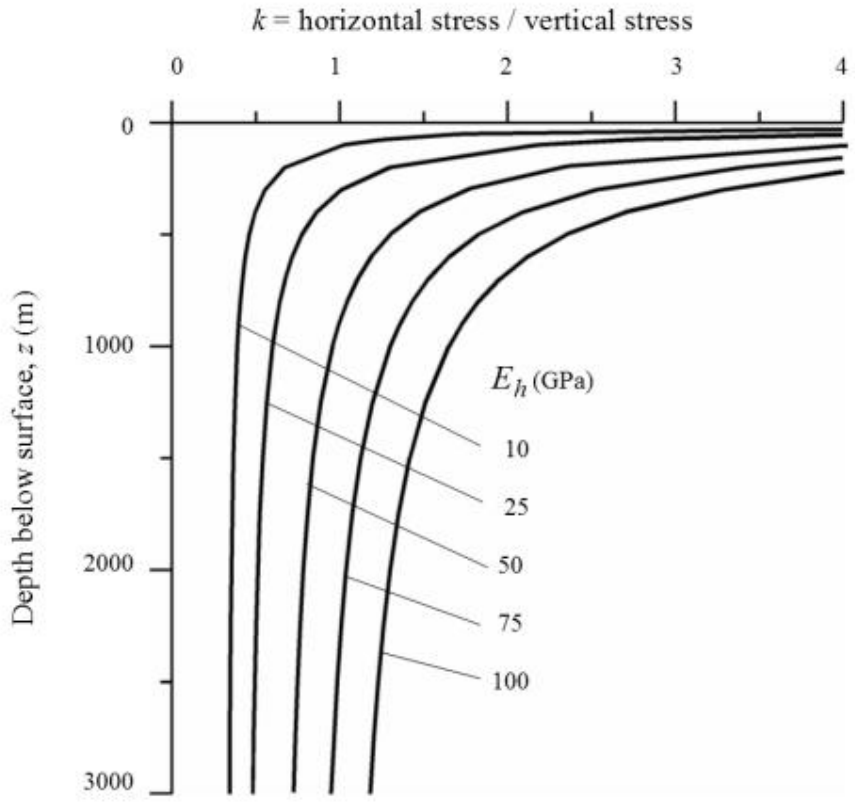

Figure 2.7: Value of K based upon Sheorey's equation (Hoek, 2007)

2.5.2 Topographic stresses

When the ground surface is not horizontal, virgin stress state is influenced by the topography. The stress that is induced due to topography is referred to as topographical stress. The characteristic feature of the topographic stresses is that topography affects the direction of the principal stress.

In steep valley territories, where numerous hydropower projects are positioned, the virgin stress condition is mostly controlled by the shape of the terrain. Instead of acting vertically, the stresses tend to adjust according to the valley slope. The major principal stress (σ_1) usually acts nearly parallel to the slope surface, while the minor principal stress (σ_3) acts roughly perpendicular to it (Nilsen & Thidemann, 1993). This means that even if the rock itself is uniform, the stress distribution becomes direction-dependent due to the valley geometry. As a result,

the rock mass experiences different stress magnitudes in different directions, which is important for the design and stability of underground facilities and tunnels in such areas.

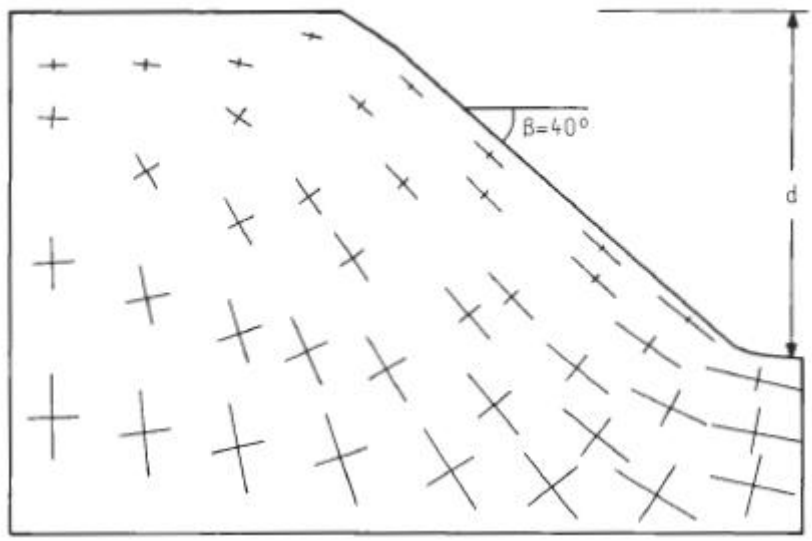

Figure 2.8: Effects of topography on stresses (Nilsen & Thidemann, 1993)

2.5.3 Tectonic stresses

The formation of the Himalayan Mountain range resulted from the collision between the Indian Plate and the Eurasian Plate that began about 50-60 million years ago (Molnar & Tapponnier, 1975; Yin, 2006). The Indian Plate is moving northward at a speed of 5 cm per year, compared with 2 cm per year for the Eurasian Plate, causing a continued convergence and compressional tectonic stresses in the area (Bilham et al., 1997; Copley et al., 2010).

This ongoing continental collision generates a stress regime in which the maximum horizontal stress is generally oriented perpendicular to the Himalayan arc, predominantly in a north-south direction. As a consequence of these intense tectonic forces, the horizontal stresses in the Himalayan region are significantly greater than those produced by gravitational loading alone. In non-tectonic activity, horizontal stress is generally in ranges from 0.5 to 0.3 times the vertical stress. However, in tectonically active regions like the Himalayas, the horizontal stress can be equal to or even exceed the vertical stress, with ratios commonly ranging from 0.5 to 2.0 or higher (Amadei & Stephansson, 1997).

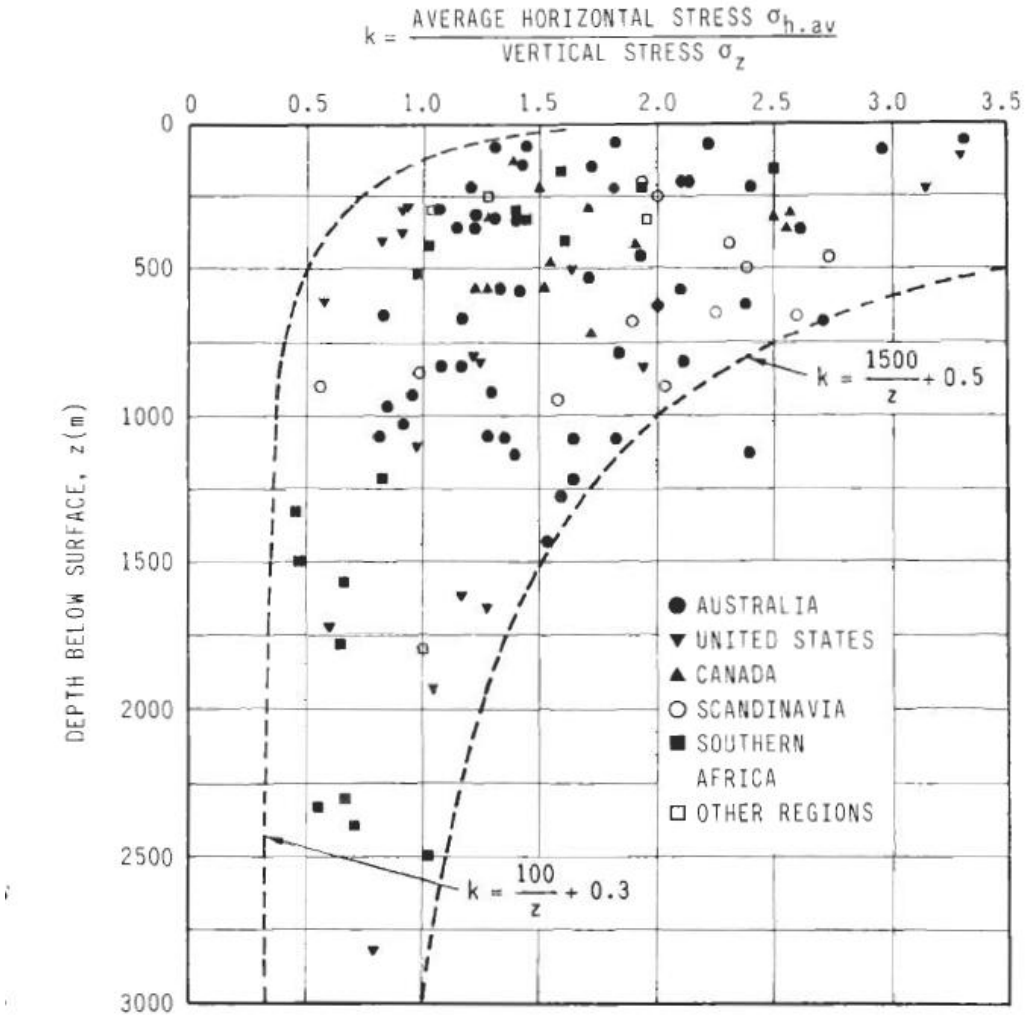

Figure 2.9: Variation of K with depth (Brown & Hoek, 1978)

(Stephansson, 1993) has provided the correlation for in situ horizontal stresses at shallow depth (z < 1000m) based on hydro-fracturing tests (Singh & Goel, 1999).

$$\sigma_H = 2.8 + 1.4\sigma_v \quad (7)$$

$$\sigma_h = 2.2 + 0.89\sigma_v \quad (8)$$

$$\sigma_v = \gamma H \quad (9)$$

(Sengupta, 1998) carried a series of hydro-fracturing tests on weak rocks in the Himalayan region. The correlation between σv and σh is not good, which may be due to the mountainous terrain. Thus, it is suggested that H < 400 meters (Singh & Goel, 1999).

$$\sigma_H = 1.5 + 1.2\sigma_v \quad (10)$$

$$\sigma_h = 1.0 + 0.5\sigma_v \quad (11)$$

$$\sigma_v = \gamma H \quad (12)$$

Stephansson's correlation provides a higher side, whereas Sengupta's correlation provides a lower side of the actual in situ stresses. In steeply inclined mountainous terrain, Sengupta's correlations can be applicable in the stress ($\sigma_H > \sigma_v > \sigma_h$) (Singh & Goel, 1999).

2.5.4 Stresses around the excavation boundary

Before excavation, the rock mass exists in a state of natural equilibrium, carrying the overburden stresses and maintaining stability under the existing stress field (Brady & Brown, 2004). The excavation process fundamentally disturbs this equilibrium state because the physical support previously provided by the rock material is removed from its original location. (Hoek & Brown, 1980b).

When rock is excavated, the virgin or primary stresses that were originally supported by excavated material are transferred and redistributed into the adjacent rock mass (Hudson & Harrison, 2009). This stress redistribution process inevitably leads to the growth of induced secondary stresses and corresponding rock mass displacements both in a immediate area of the excavation and in the adjacent rock mass ((Brady & Brown, 2004).

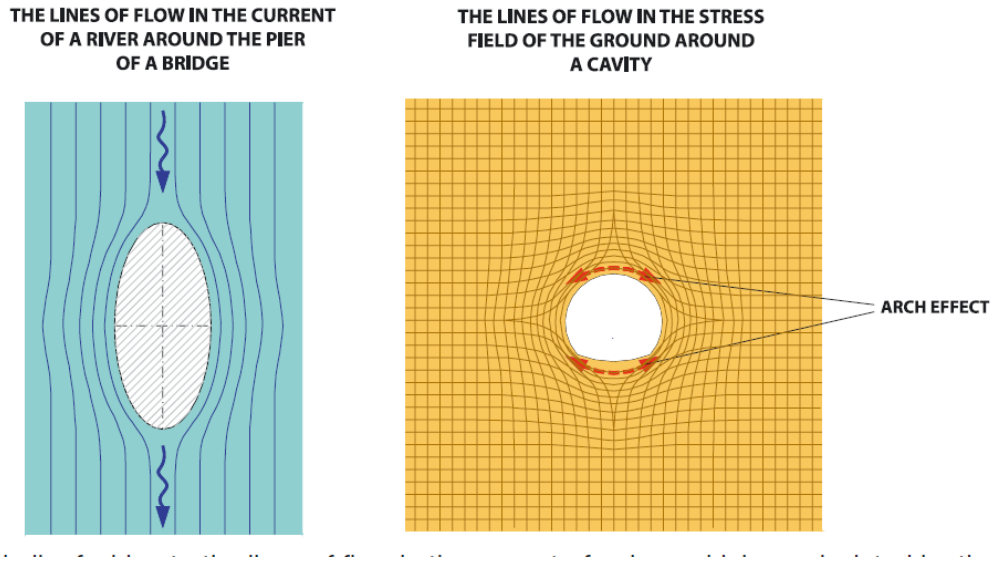

Figure 2.10: River flow and stress analogy (Lunardi, 2008)

Just as river flow lines are deflected and accelerated around a bridge pier, the stress flow lines in a rock mass are diverted around a cavity, forming a zone of increased stress along the excavation walls, and this phenomenon, known as the arch effect, contributes to the long-term stability of the cavity (Lunardi, 2008).

The stress condition nearby the boundary of the tunnel or rock cavern is an area of interest when assessing potential problems due to rock stresses.

An analytical relationship for stress and displacement distribution around a circular tunnel was developed in an ideal rock mass by Kirsch (1898). For the elastic material, homogeneous, isotropic, and isostatic virgin stresses $\sigma_1 = \sigma_2 = \sigma_3 = \sigma$ (Brady & Brown, 2004).

If the radius of the opening is a, the radial and tangential stresses of a cross-section (σ_r and σ_t , respectively) will be the following as functions of the distance r from the circle centre:

$$\sigma_r = \sigma\left(1 - \frac{a^2}{r^2}\right) \tag{13}$$

$$\sigma_t = \sigma\left(1 + \frac{a^2}{r^2}\right) \tag{14}$$

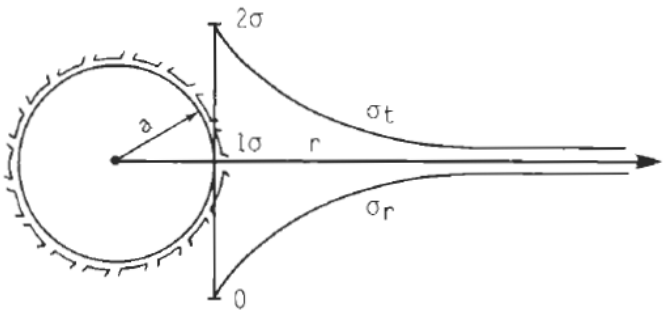

Figure 2.11: Tangential and radial stresses (Nilsen & Thidemann, 1993)

For non-isotropic stress conditions, the Kirsch solution indicates that the maximum tangential stress $\sigma tmax$ occurs at location where the major principal stress (σ_1) is tangent to excavation boundary. Similarly, minimum tangential stress (σ_{tmin}) occurs where the minor principal stress (σ_3) is tangent to the

excavation boundary (Nilsen & Thidemann, 1993). As per the Kirsch solution, tangential stress distribution is expressed as:

$$\sigma_{tmax} = 3\sigma_1 - \sigma_3 \quad (15)$$

$$\sigma_{tmin} = 3\sigma_3 - \sigma_1 \quad (16)$$

As described by (Jaeger et al., 2011)," Non- symmetrical geometry and sharp corner is particular, will strongly affect the magnitude of the tangential stress as described."

As the radius of curvature decreases, the tangential stress magnitude increases. In other words, sharper corners between the wall and roof of a cavern lead to higher stress concentrations at those locations. In extreme situations, these stress concentrations can exceed ten times the value of the major principal stress (Nilsen & Thidemann, 1993).

2.6 Numerical Modelling of Underground Excavation

Numerical modelling has become an necessary tool in the design and stability analysis of underground excavations. Methods such as the finite element method (FEM), finite difference method (FDM), boundary element method (BEM), and discrete element method (DEM) have been developed and updated over several years, each with specific strengths suited to different problem types. The finite difference program FLAC, developed by Itasca, and the finite element program Phase2 (now RS2), developed by Rocscience, are among the most widely used software in tunnel and cavern engineering.

(Carranza-Torres & Fairhurst, 2000) Applied the convergence-confinement method, a semi-analytical approach derived from elasto-plastic continuum mechanics, to analyze the behavior of circular tunnels in rock masses governed by the Hoek-Brown failure criterion. The method provides ground reaction curves, support characteristic curves, and longitudinal deformation profiles, which together define the equilibrium condition between the deforming rock mass and the installed support. While the method is limited to circular tunnels and homogeneous rock conditions, it remains a valuable tool for preliminary design and calibration of numerical models.

(Vlachopoulos & Diederichs, 2009) discussed the appropriate uses and practical limitations of two-dimensional numerical analyses of tunnels and tunnel support response, noting that 2D models operating in plane strain conditions cannot fully capture the three-dimensional stress redistribution that occurs at the tunnel face. They proposed correction factors for the longitudinal deformation profile to enable more realistic back-calculation of support loads from 2D analyses. Their work has direct relevance to cavern interaction studies conducted in 2D, where the omission of 3D effects may lead to either conservative or unconservative design conclusions depending on the geometry.

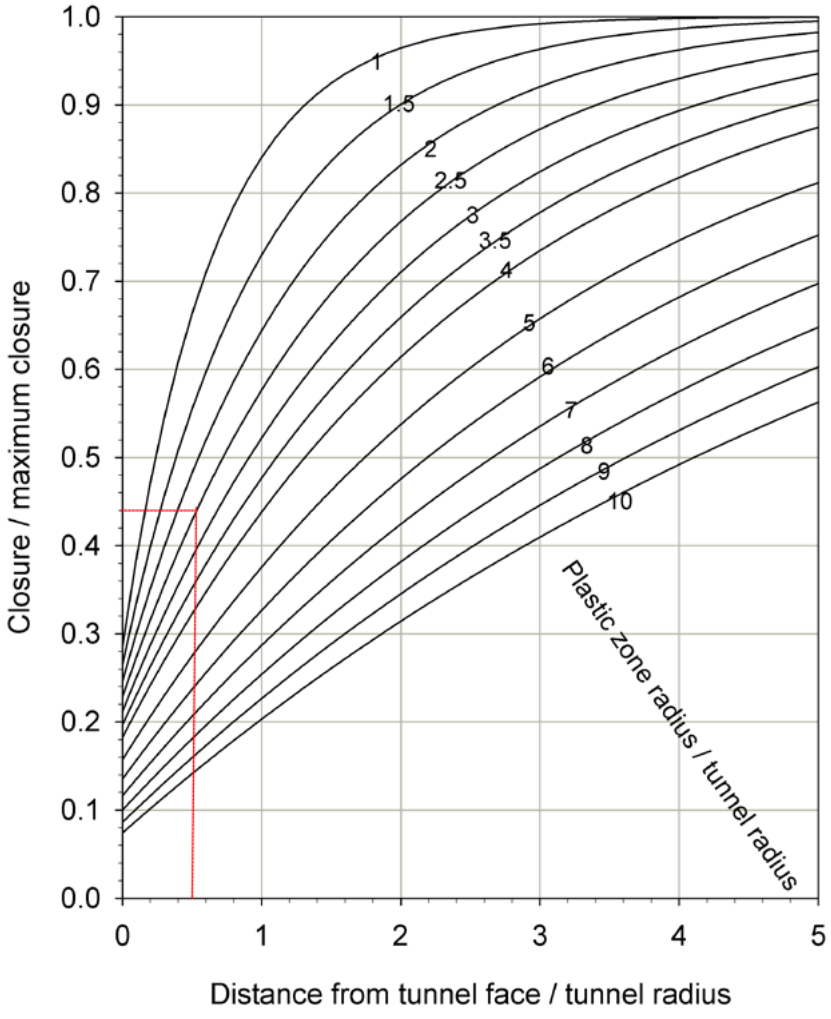

Figure 2.12: Support installation using (Vlachopoulos & Diederichs, 2009)

(Sakurai, 1983) states, "Tunnel strain levels in excess of approximately 1% are associated with the onset of tunnel instability and with difficulties in providing adequate support".

"Some tunnels experienced strains as high as 5% without showing stability issues. Although all tunnels identified as having stability problems were ultimately completed but with increase in strain level the construction difficulties also. Therefore, the 1% strain limit proposed by Sakurai should be taken only as an indicator of increasing construction difficulty, rather than consideration as a threshold value. In fact, in certain situations, it may be beneficial to allow tunnel strains to reach up to 5% before engaging the support system" (Hoek, 2007).

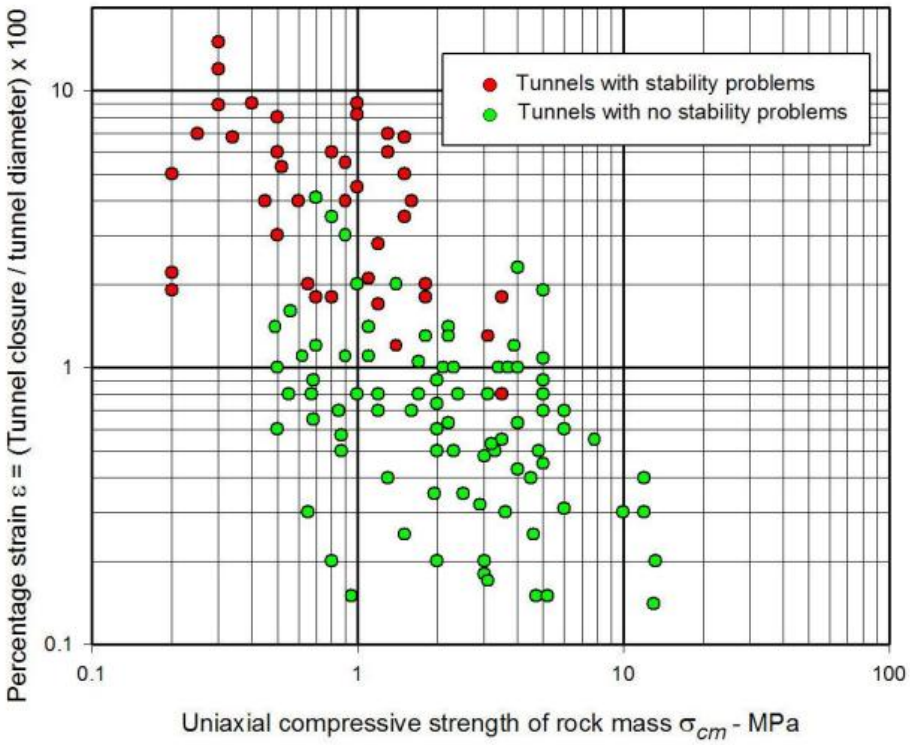

Figure 2.13: Field observations of HRT in Taiwan (Chern et al., 1998).

Systematic numerical simulation studies, such as those presented by (Zhu et al., 2003) based on construction process mechanics in Taiwan, demonstrated that different excavation and support schemes have significant impacts on tunneling stability and deformation. The studies showed that the timely installation of support is critical for weak rock masses and that numerical simulation should be performed before construction to select the optimal construction scheme. From a parametric study perspective, the deformation modulus and in situ stress ratio were identified as the most sensitive parameters governing tunnel convergence.

2.6.1 In-situ measurement

In-situ measurement of rock mass properties remains essential for the design and stability of underground openings. Techniques like pressuremeter test measure rock deformability and stress–strain behavior in boreholes, while the hydraulic - fracturing method determines the in-situ stress magnitude and orientation by inducing tensile fractures. Although both methods provide direct field data, limited point measurements may not capture overall stress variations caused by tectonic effects and overburden pressure, and deep underground applications can be technically challenging and costly. These approaches are critical for accurate rock mass characterization and numerical model calibration.

a. Hydraulic fracture method

Hydraulic-fracturing (HF) is a borehole-based field procedure used to measure absolute in-situ stresses by injecting fluid into a confined interval until new fractures are created or existing fractures are reopened. In an ideal HF test, the injected pressure causes tensile failure at the borehole wall when the fluid pressure exceeds the minimum principal stress, allowing the magnitude and orientation of in-situ stresses to be inferred from breakdown and shut-in pressures (Amadei & Stephansson, 1997).

For hydraulic fracturing to occur and yield meaningful stress data, the rock mass must be sufficiently intact and able to support stress without pre-existing, pervasive microcracking or extensive discontinuities. The technique generally assumes that failure initiation is controlled by the pre-existing stress state and that the rock behaves in a manner where tensile fractures can be induced and propagated perpendicular to the minimum principal stress (Hubbert & Willis, 1957).

Hydraulic Fracture Method tests to be successful in determining in-situ stress, the rock mass must support the development of a controlled tensile fracture, packers must isolate the test interval effectively, and fluid injection conditions should be such that pressure can rise to cause fracturing rather than leak away. In highly fractured, porous, or poorly isolated conditions, hydraulic fracturing may not produce reliable measurements.

b. Pressuremeter

The pressuremeter test is an established in-situ geomechanical testing method used to directly determine the deformation and strength properties of soils and rocks without disturbing their natural state. In this test, a cylindrical probe with an inflatable membrane is placed in a pre-drilled borehole and pressurized in controlled increments. As the membrane expands, it applies radial pressure to the borehole walls, and the corresponding radial deformation of the rock mass is recorded along with the applied pressure (Mair & Muir Wood, 1987).

From the measured pressure deformation relationship, a pressuremeter curve is obtained, which represents the in situ stress-strain response of the rock mass. Interpretation of this curve enables the estimation of key parameters such as deformation modulus (E_c) and limit pressure, which reflect the rock mass stiffness and strength characteristics (Mair & Muir Wood, 1987). Because the test occurs in the field under existing stress conditions, it inherently captures the combined effects of intact rock properties and discontinuities without reliance on laboratory sample extraction, making it especially valuable for rock masses that are difficult to sample (Phangkawira et al., 2025).

The pressuremeter test provides one of the few direct field measures of rock mass deformability, yielding parameters that are difficult to obtain through conventional laboratory testing or indirect empirical correlations. Its outputs are essential for calibrating numerical models, evaluating rock mass stiffness, and supporting the design of underground excavations such as tunnels, caverns, and shafts (Clarke, 2023).

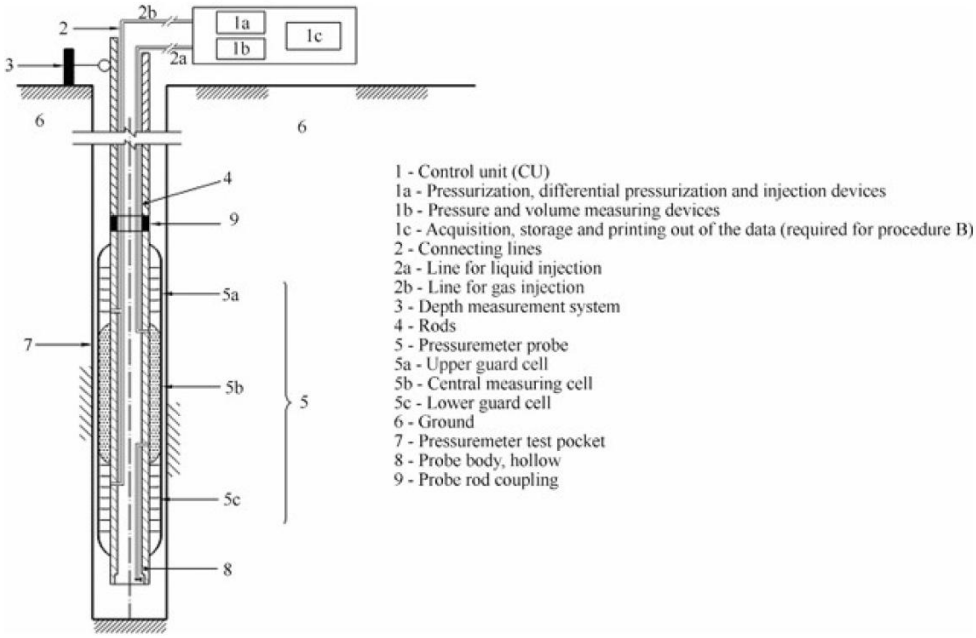

Figure 2.14: Representation diagram showing components of pressuremeter

2.7 Plastic Zone and Stress Redistribution

When an underground excavation is created; pre-existing in situ stresses are disturbed, and the rock mass around the opening must redistribute these stresses to be in a new equilibrium. In the region immediately surrounding the opening, stresses may exceed the strength of the rock mass, leading to the development of a plastic zone or failure zone. The extent of this zone depends on the ratio of in situ stress to rock mass strength, the shape and size of the opening, and the deformation modulus of the rock mass.

The ground reaction curve is a key concept in tunnel engineering that represents the relationship between the support pressure acting on the tunnel boundary and the corresponding inward displacement (convergence) of the tunnel wall. Its shape and position depend primarily on the strength and deformability of the rock mass, as well as the in-situ stress conditions. A softer rock mass (lower deformation modulus) will produce greater convergence at a given support pressure, while a stronger rock mass will exhibit less convergence. Understanding the ground reaction curve is essential for designing support systems that are mobilized at the appropriate stage of excavation.

3 STUDY AREA AND DATA

3.1 Description of Project

The Tamakoshi V Hydroelectric Project is a cascade development of the Upper Tamakoshi HEP with tandem operation. The project area is located on the right bank of the Tamakoshi River. The Project takes the discharge from the tailrace of the Upper Tamakoshi HEP through an underground interconnection arrangement (headworks) and conveys it to the headrace tunnel of this Project.

3.1.1 Powerhouse configuration

The powerhouse is provided at the right bank of the Tamakoshi River. The powerhouse station comprises a powerhouse cavern, a transformer cavern, an escape tunnel, Bus Duct Galleries, and Cable and Ventilation Tunnel (CVT). The provided powerhouse cavern is 82.00m (L) x 14.50m (W) x 33.14m (H).

The transformer cavern accommodating GIS is located 33.30m apart from the powerhouse cavern with dimensions of 13.8m (W) x 66.7m (L) x 12.8m (H).

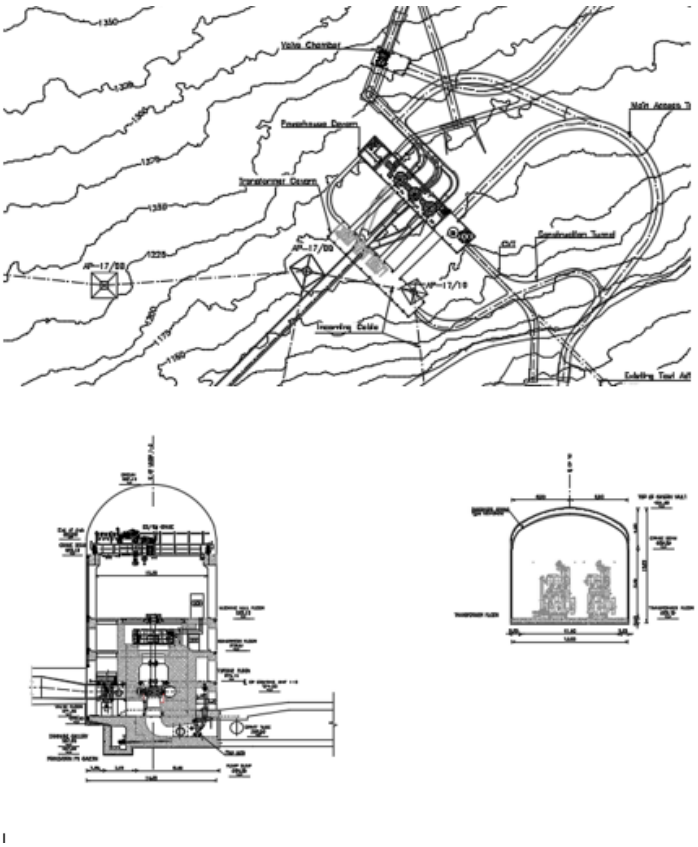

Figure 3.1: Powerhouse complex

3.1.2 Geological overview of the project

Geologically, the Tamakoshi V Hydroelectric Project belongs to the part of the Higher Himalayan crystalline succession and Lesser Himalayan succession, which consists mostly of Precambrian gneiss, quartzite, and marble. The Higher Himalayan crystalline succession is separated from the Lesser Himalaya by the Main Central Thrust (MCT). Schelling (1987) divided the Lesser and Higher Himalayan rocks of this area into the following units.

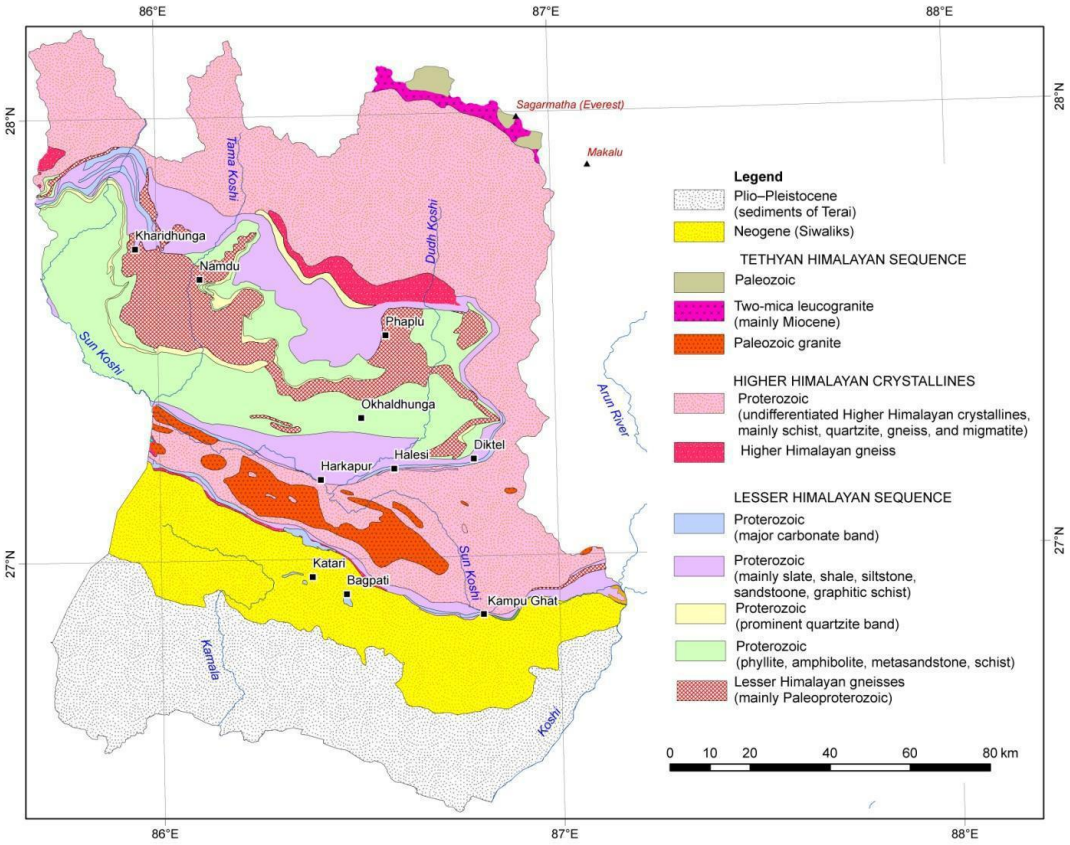

Figure 3.2: Regional geological map of project area
Source: Dhital (2015)

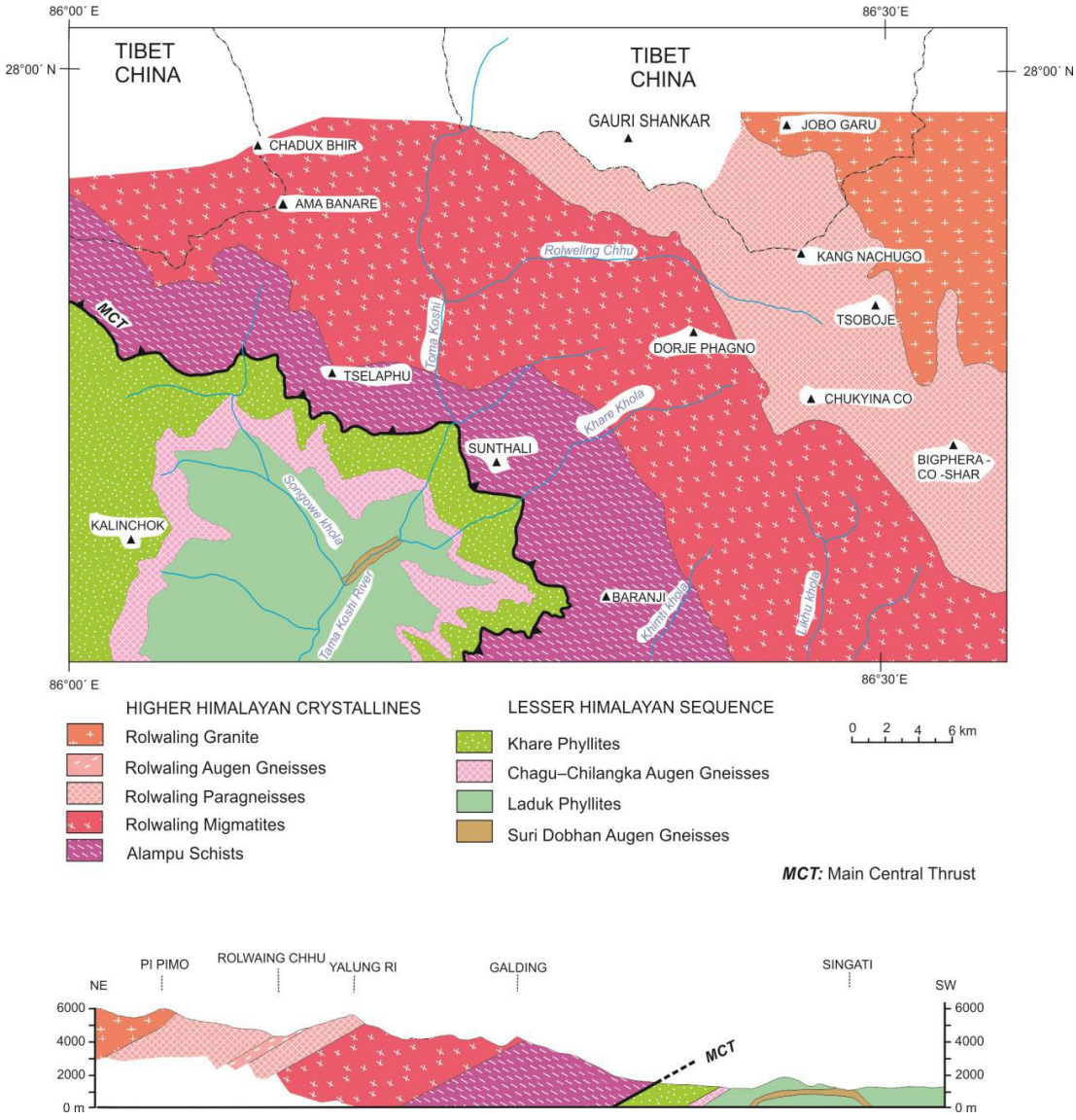

Figure 3.3: Geological subdivisions of the upper Tamakoshi area. Source: Modified from Schelling (1987)

The powerhouse is located at the downstream of MCT (Main Central Thrust) at the Lower Himalayan Succession. The powerhouse area has rock primary of augen gneiss with partings of chlorite schist. The texture of rock mass at powerhouse area is gneissic. It contains an assemblage of quartz, muscovite, feldspar and biotite, including phenocrysts of feldspar and quartz.

4 METHODOLOGY

This chapter outlines the approach considered for the numerical modeling of cavern interaction and how the mechanical properties of rock and excavation sequence affect the cavern. This chapter covers parameters adapted for the numerical analysis in the Finite Element Model, with the parameters available and determined.

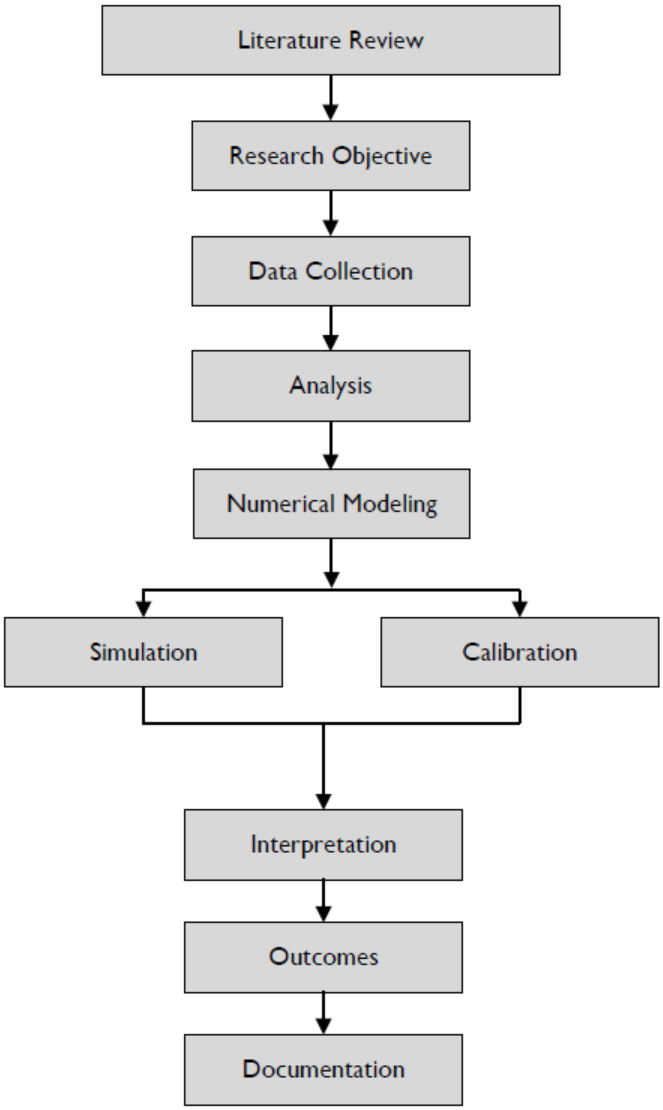

Figure 4.1: Flowchart of methodology

4.1 Preliminary Study

The preliminary stage of study includes the literature review, which includes, but is not limited to, articles, books, research papers, journal which align with the scope of work. The major literature reviewed was related to the Lecture Series by Dr. Hooke. The study also includes the outline of the research objective based on the gap of the study found from the literature review.

4.2 Data Collection

The data for the analysis has been considered from the Tamakoshi V Hydroelectric Project (TKV). The dimension, geometry, and spacing of both the cavern PHC and TRC were obtained from drawing and report of TKV. The available primary data of the project are the mechanical properties of intact rock, the deformation modulus of rockmass, and the convergence value.

4.3 Rock Mass Classification

The data for the analysis has been considered from the Tamakoshi V Hydroelectric Project (TKV).

Drilling at two different locations of the powerhouse cavern was performed. The lab testing of the recovered core was performed. The mechanical properties of intact rock after laboratory testing are presented in Table 4.1.

Figure 4.2: Drilling at powerhouse cavern

Table 4.1: Mechanical properties of intact rock

S.N	Sample ID	Depth (m)	Rock Type	UCS (Mpa)	Young's Modulus (Avg.) (Gpa)	Poisson's Ratio (Avg)
1	PH03	6.53-6.67	Gneiss	74.400	43.650	0.350
2		13.20-13.35	Gneiss	65.510	44.490	0.340
3		14-14.24	Gneiss	93.520	39.520	0.250
4		14.27-14.46	Gneiss	86.140	39.360	0.340
5		21-21.25	Gneiss	52.300	36.460	0.240
6	PH04	10-10.28	Gneiss	48.480	34.910	0.290
7		12-12.15	Gneiss	77.330	47.480	0.260
8		12.63-12.81	Gneiss	46.130	35.270	0.200
9		12.81-13	Gneiss	39.000	31.190	0.170
Average				64.757	39.148	0.271

4.3.1 In-situ deformation modulus of rock mass

The pressuremeter test at the powerhouse cavern has been performed at the sample location of drilling and core recovery. The result obtained from the test has been adopted for the numerical modelling.

Table 4.2: Summary of deformation modulus obtained from in-situ test

Hole No.	**Depth**	**E_m (MN/m²) 1st unload/reload cycle**	**E_m (MN/m²) 2nd unload/reload cycle**	**Remarks**
PH-03	13.55-14.20	5309.8	4188.8	
	18.65-19.30	975.3	2477	
	20.85-21.50	6944.1	8671.6	
PH-04	4.10-4.75	2610.8	4716.9	
	9.0-9.65	1693.5	3793.3	
	13.0-13.65	5229.3	7162.5	
Average		3793.8	5168.35	
		4481.075		

4.3.2 In-situ stress measurement

The hydraulic fracture method was performed at the test tunnel near the powerhouse cavern, and it was not successful. Hence, the in situ stress data for the project site are not available. In the absence of in situ stress data, the empirical relationship has been adopted for the determination of major, minor, and intermediate principal stress. The vertical stress has been determined using the height of overburden, and the major principal stress has been initially adopted as provided by Equation 10, which was further calibrated with the actual deformation observed at the site.

The pressuremeter test at the powerhouse cavern has been performed at the sample location of drilling and core recovery. The result obtained from the test has been adopted for the numerical modelling.

4.4 Numerical Modelling

The numerical analysis for two-dimensional (2D) modeling was conducted using Rocscience Phase2 Finite Element software. The type of analysis performed is Plain Strain Analysis. Plain strain is defined to be a state of strain in which the

strain normal to the x-y plane (< z) and shear strain (< xz and < yz) are assumed to be zero.

The distance between the excavation and the model boundary should generally be maintained at a minimum of four to five times the size of the underground opening. However, in weaker rock mass conditions, this boundary extent may need to be increased beyond this range. Providing such a distance helps minimize or eliminate the influence of boundary effects on the excavation response. The numerical model is restrained in both the X and Y directions, and the analysis is performed using six-noded triangular elements.

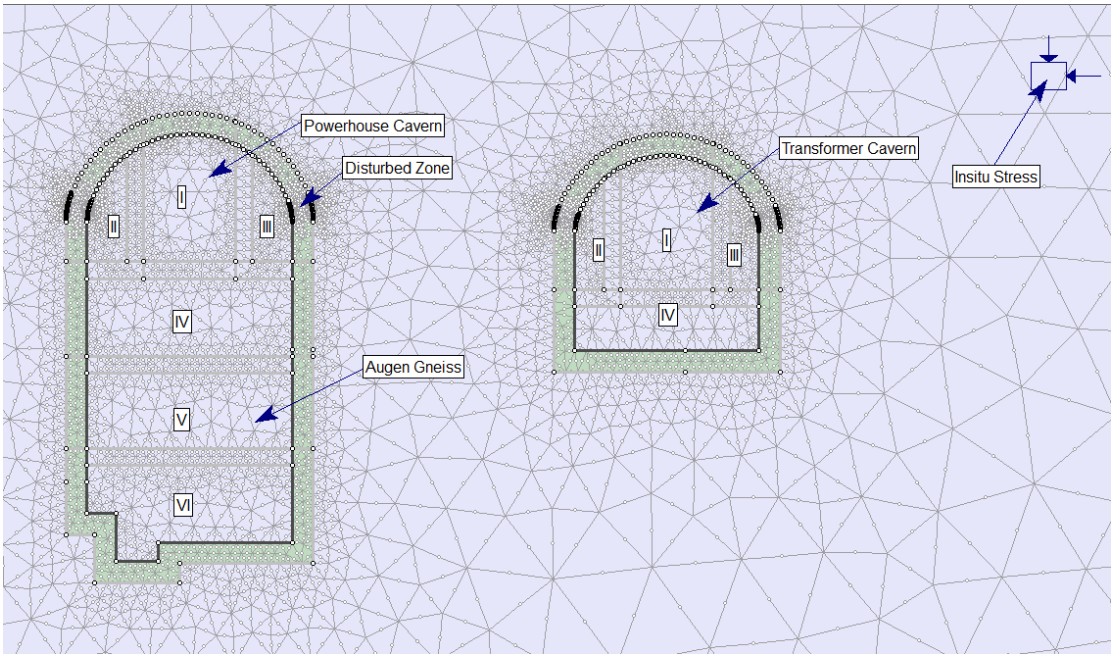

Figure 4.3: Phase 2 numerical model

3D Tunnel Simulation has been performed using the Core Replacement Technique. Phase 2 is employed to simulate the three-dimensional excavation process of a tunnel. In a 3D condition, the tunnel face initially provides a stabilizing effect. As the excavation face moves away from the region of interest, this support gradually diminishes until the stress conditions can be reasonably represented using a two-dimensional plane strain model. The approach incorporates soft inclusions to control tunnel deformation, and by progressively reducing the stiffness (modulus) of these inclusions, the tunnel characteristic curve can be determined. This method is considered more flexible and effective compared to the field stress vector approach (Hoek, 2011). The core softening values are based on the

relationship proposed by Vlachopoulos and Diederichs (2009), as suggested by Hoek (2011).

Disturbance factor (D) is a factor that depends upon the degree of disturbance due to blast damage and stress relaxation.(Hoek, 2007). The disturbance factor of 0.3 has been considered for the analysis. Where a disturbance factor is applied, there is a corresponding reduction in the rock mass strength. Hence, E-values for the disturbed zone are taken same as those for the undisturbed zone. (Shrestha, 2021).

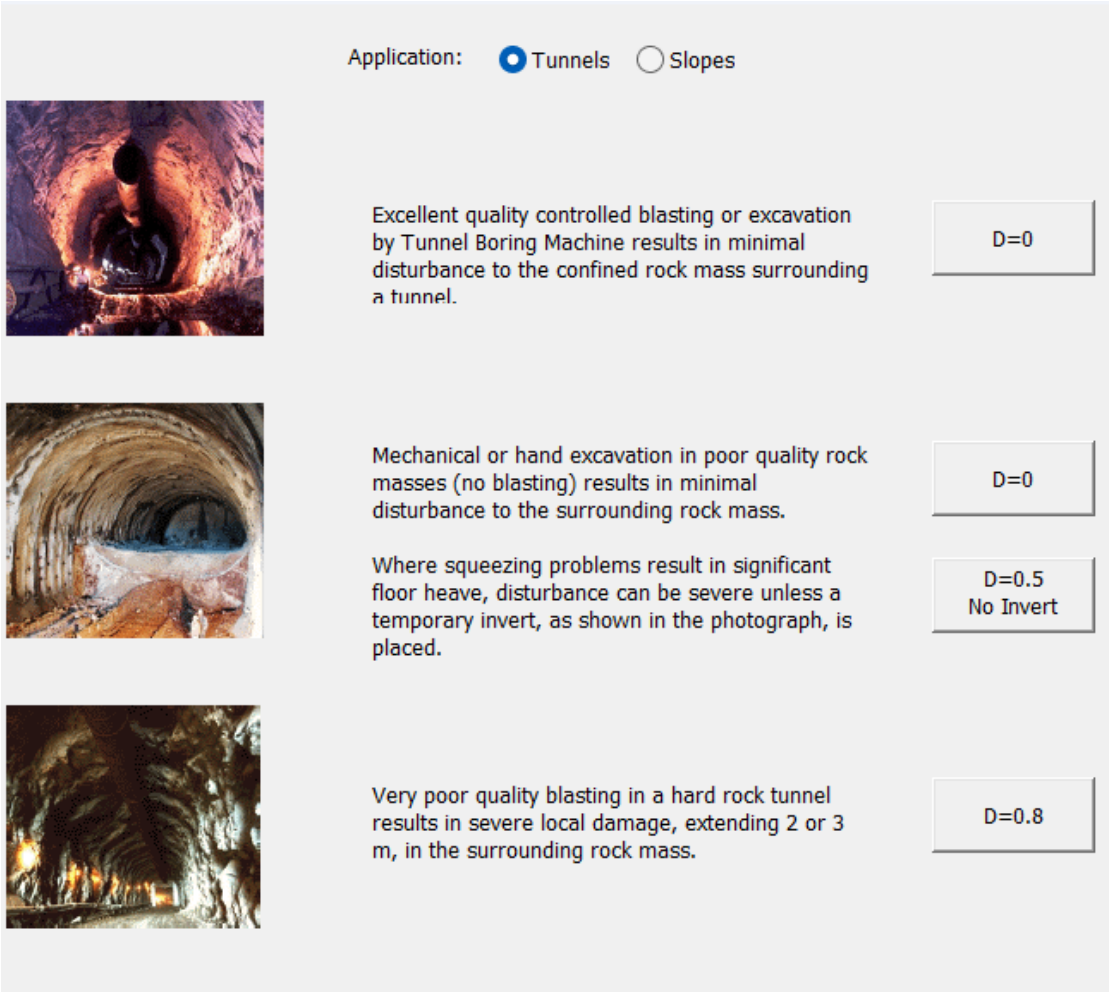

Figure 4.4: Disturbance factor (Phase 2)

4.4.1 Calibration of numerical model

The data of the bi-relex target at chainage 0+50m of powerhouse cavern was available on the basis of which the model has been calibrated. The crown and immediate bench of the powerhouse cavern have been excavated at the site. The model has been calibrated with the excavation sequence and height of each bench

adopted. The observed total convergence at the side wall was 55mm, on the basis of which the model has been calibrated, and the rock and stress properties have been determined. The 30% of the total deformation is induced at the face.(Hoek, 2007) During the calibration, in excess of the deformation observed at the site, 30% of the total deformation has been included. The support used for the analysis is 32mm dia., 12 m long and 9m long rockbolt at 1.5m spacing (alternative) in the crown and 32mm dia., 9m long and 28mm dia 6m long rockbolt at 1.5m spacing (alternative) in the side wall. The thickness of shotcrete at the crown is 200mm, and at the side wall, 150mm.

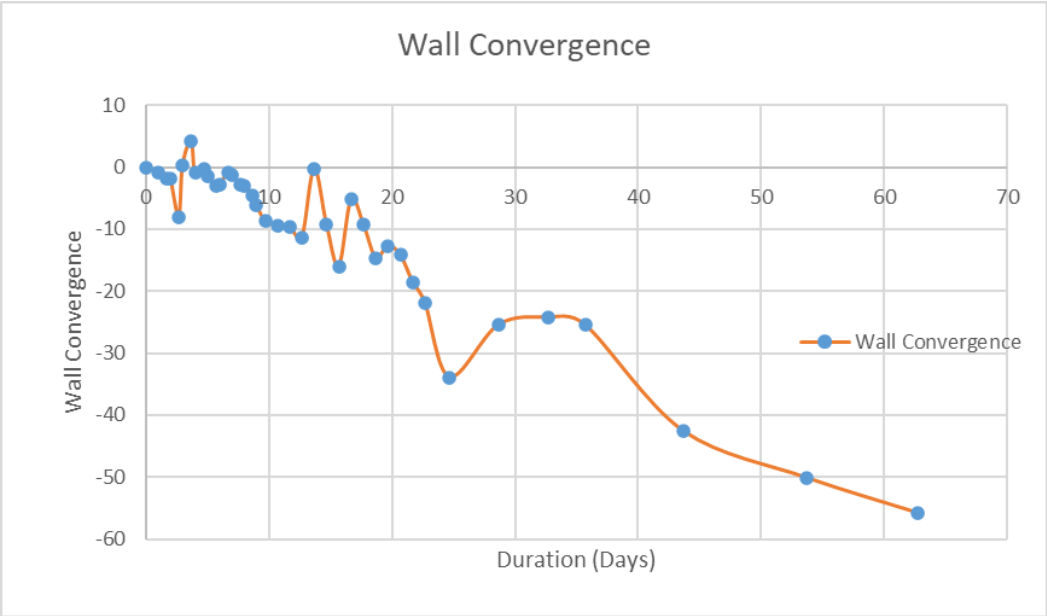

Figure 4.5: Plot of wall convergence

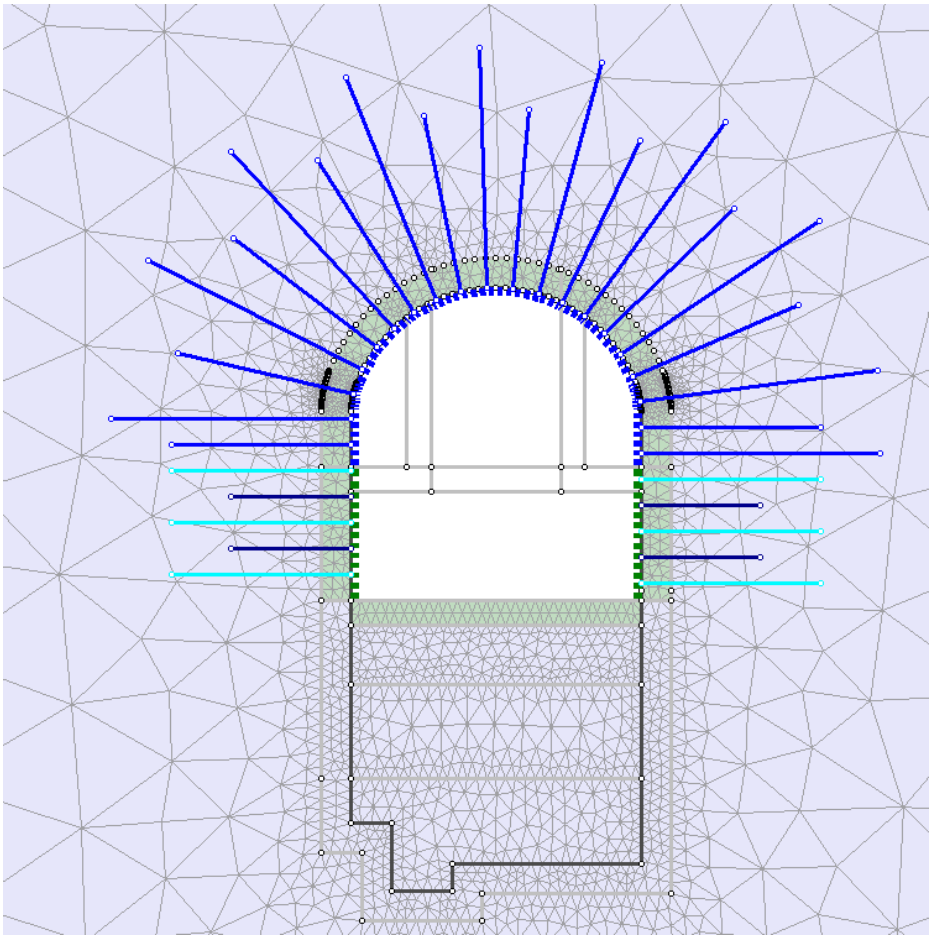

Figure 4.6: Model adopted for calibration

Table 4.3: Parameter after calibration of model

S. N.	**Parameter**	**Value**
1	Type of Material	Augen Gneiss
2	Failure Criteria	Generalized Hoek Brown (Material Type is Plastic)
3	Initial Element Loading	Field Stress Only
4	Unit Weight of Rock	27 kN/m^3
5	Intact Compressive Strength (UCS)	64.76 MPa
6	Intact Rock constant (m_i)	27
7	Disturbance Factor	0.0 for the Undisturbed zone and 0.3 for the Disturbed zone

S. N.	Parameter	Value
8	Modulus of Elasticity of Intact Rock	39,480 MPa
9	Stiffness Property	Isotropic
10	Poisson Ratio	0.27
Field Stress		
11	Major Principal Stress (sigma 1) (MPa)	8.073
12	Intermediate Principal Stress (sigma 2) (MPa)	7.14
13	Minor Principal Stress (Sigma 3) (MPa)	6.21
14	Rock mass parameters	IV
15	GSI	35
Undisturbed Rock Mass		
16	Modulus of Deformation of Rockmass (MPa)	4477.3
17	Parameter 'm_b' for rock mass	2.650
18	Parameters for rock mass	0.0007302
19	Parameter ' a ' for rock mass	0.5159
Distributed Rock Mass		
20	Parameter 'm_b' for rock mass	1.759
21	Parameters for rock mass	0.0003273
22	Parameter ' a ' for rock mass	0.5159

5 RESULTS AND DISCUSSION

5.1 Overview

This chapter contains the results obtained from the numerical modeling. During the numerical modeling, different cases have been analyzed. They are as

- Excavation of Powerhouse Followed by Transformer Cavern (Case I)
- Excavation of Transformer Cavern followed by Powerhouse (Case II)
- Parallel Excavation of Transformer Caver and Powerhouse (Case III)

During the analysis, the cavern spacing has been varied to analyze the influence of cavern spacing on different cases. Furthermore, in each cavern spacing, mechanical properties have also varied with the variation of GSI to capture the influence of cavern spacing and GSI on the deformation of both caverns.

5.2 Isolated Cavern Behaviour

The powerhouse and transformer caverns were studied separately to determine the deformation of each of the caverns without the interference of the other underground openings. The following resulting displacements are assumed as reference values of the baseline cases of different cavern spacing and GSI. The amplification factor (A.F.) is defined as the ratio of the displacements measured at the interaction cases to the base displacements of single cavern (isolated) displacements.

Table 5.1: Isolated cavern displacement

Cavern	**GSI**	**Left Wall (mm)**	**Right Wall (mm)**	**Crown (mm)**	**Invert (mm)**
Powerhouse	35	93	80	57.4	-
Transformer		57.1	52.6	44.7	59
Powerhouse	50	22.9	23.3	9.65	-
Transformer		15.5	13.8	9.86	14.4
Powerhouse	60	12.7	12.5	3.39	-
Transformer		7.13	6.74	3.32	5.11

The powerhouse has significantly higher displacements than the transformer cavern throughout all locations, which is consistent with its higher cross-sectional

area and stress concentration. In all different case scenarios with different GSI values, it is consistent, which implies that the larger cross-sectional areas are susceptible to higher deformation due to stress concentration around the excavation boundary.

The extent of the yield element and deformation of the cavern depends upon cavern size and rock mass quality. As the rockmass quality increases in this case, represented by GSI, the deformation and extent of the yield element also decrease, which has been presented in Table 5.1 and Figure 5.2 to Figure 5.13 as obtained from Numerical Modeling for different GSI values.

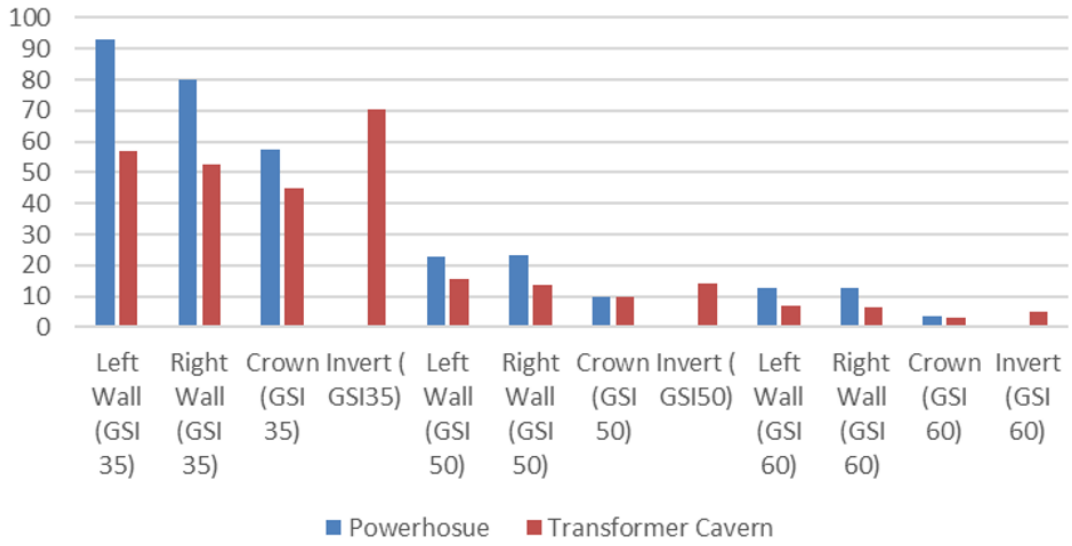

Figure 5.1: Comparison of deformation of PHC and TRC (isolated)

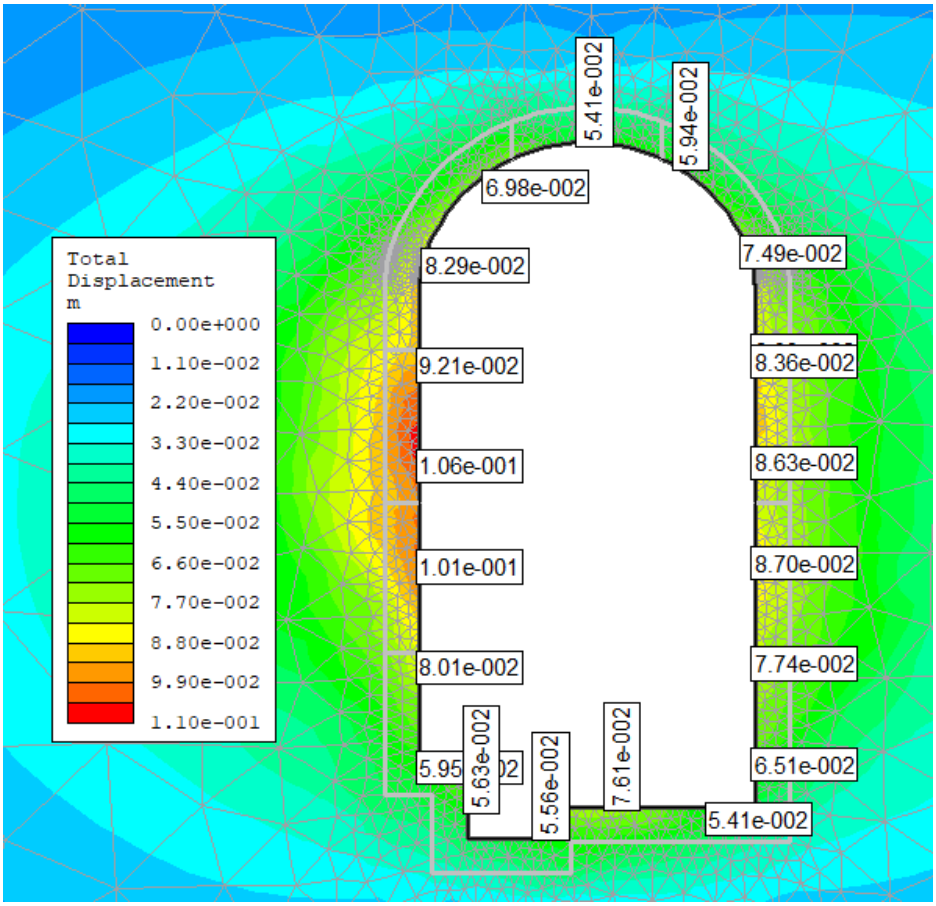

Figure 5.2: Powerhouse deformation (GSI 35)

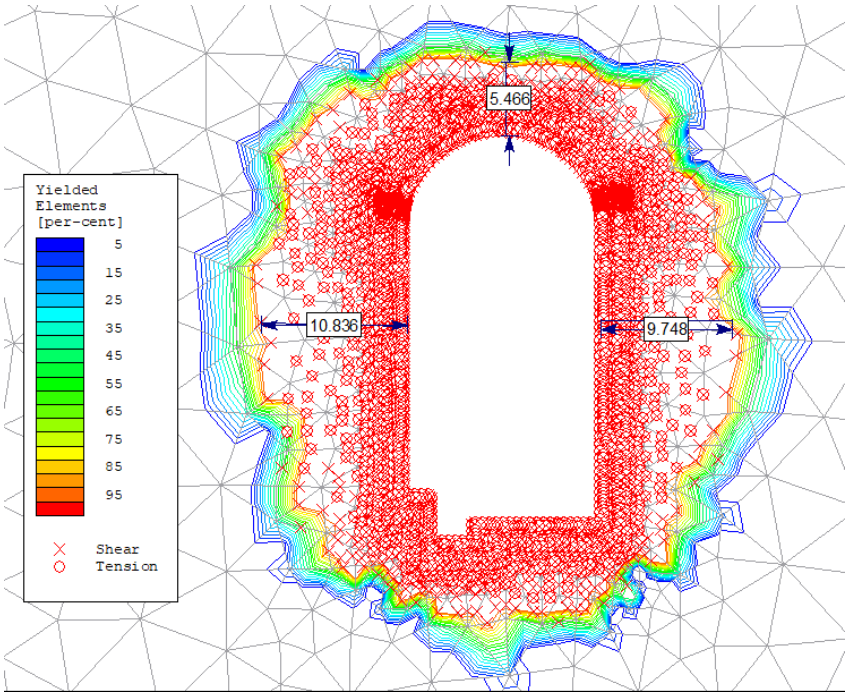

Figure 5.3: Powerhouse cavern, extend of plastic zone (GSI 35)

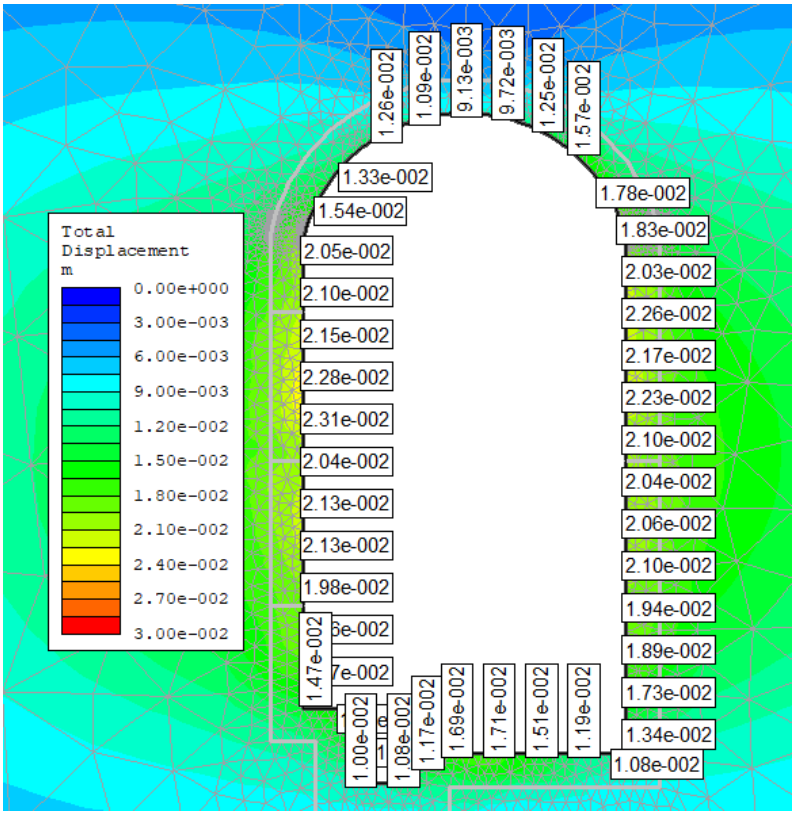

Figure 5.4: Powerhouse deformation (GSI 50)

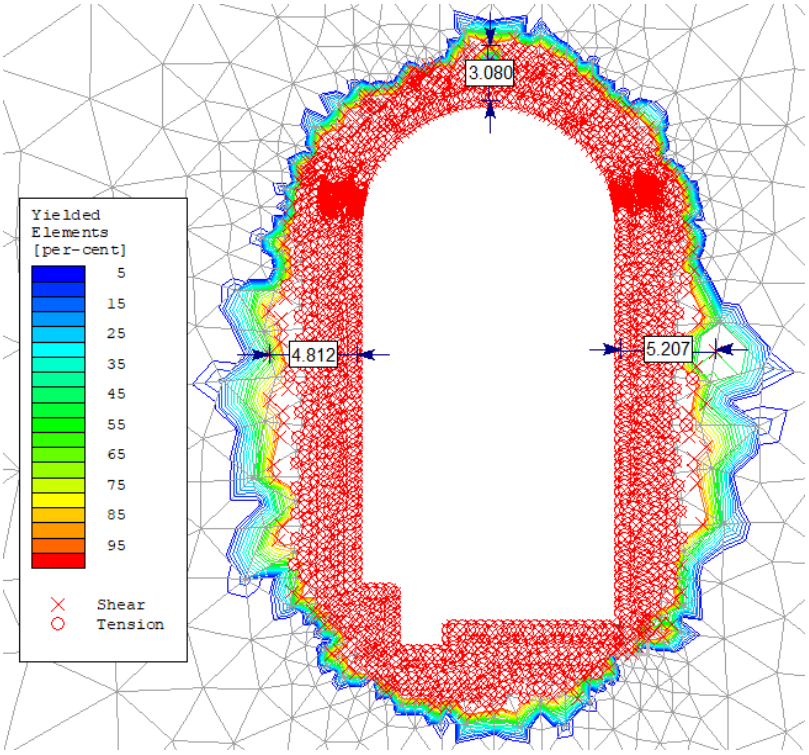

Figure 5.5: Powerhouse cavern, extend of plastic zone (GSI 50

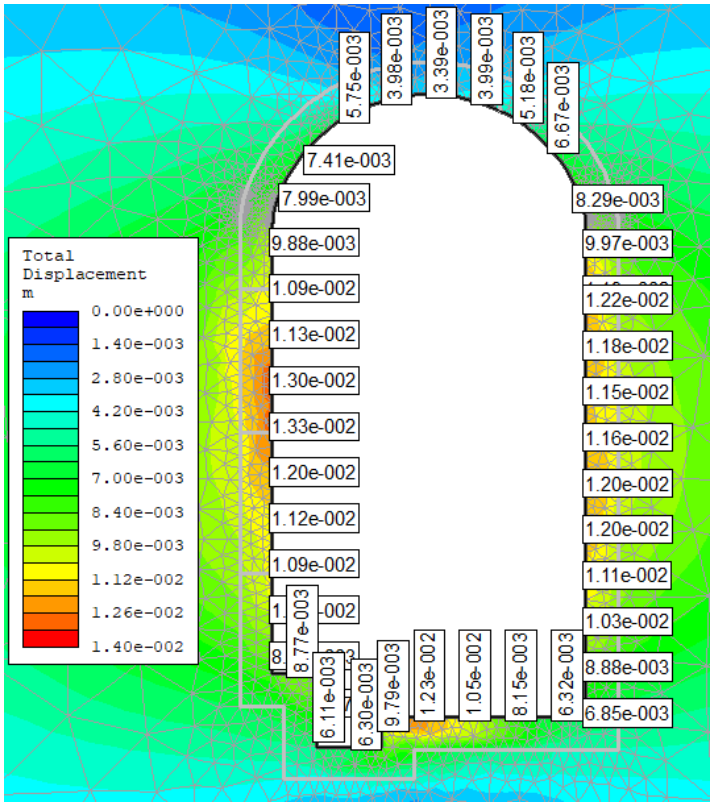

Figure 5.6: Powerhouse deformation (GSI 60)

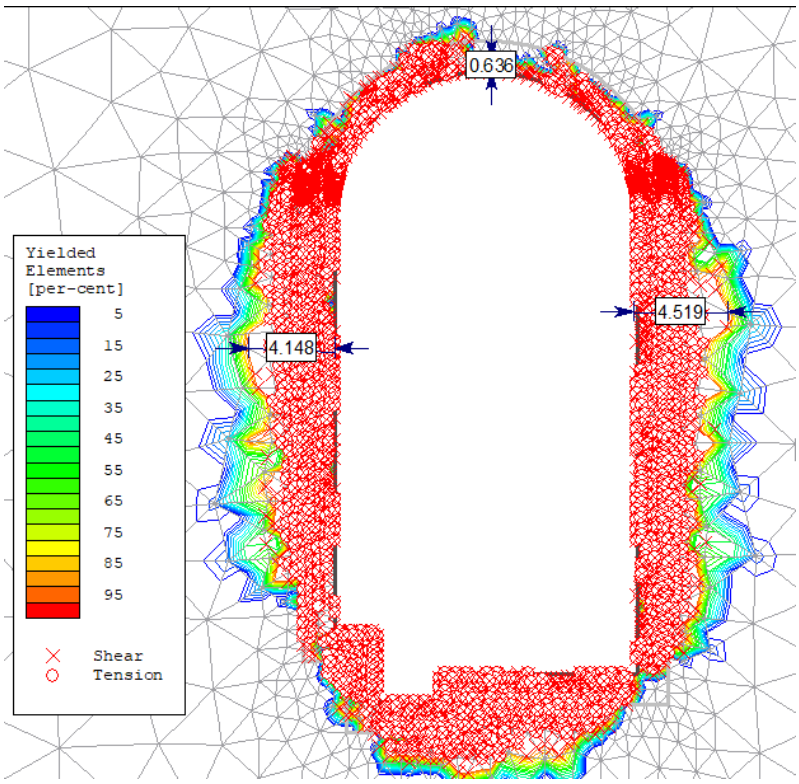

Figure 5.7: Powerhouse cavern extend of plastic zone (GSI 60

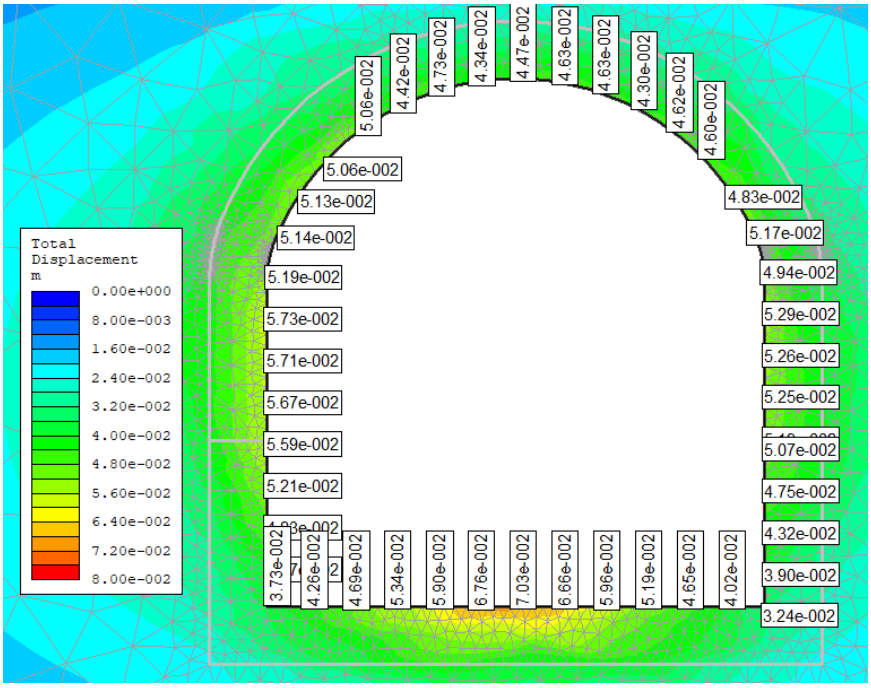

Figure 5.8: Transformer cavern deformation (GSI 35

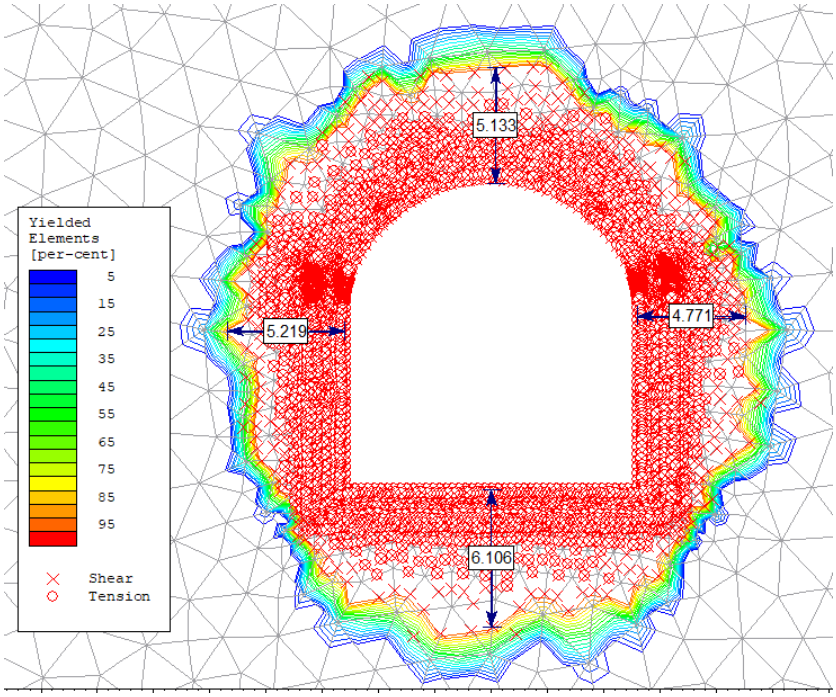

Figure 5.9: Transformer cavern extend of plastic zone (GSI 35)

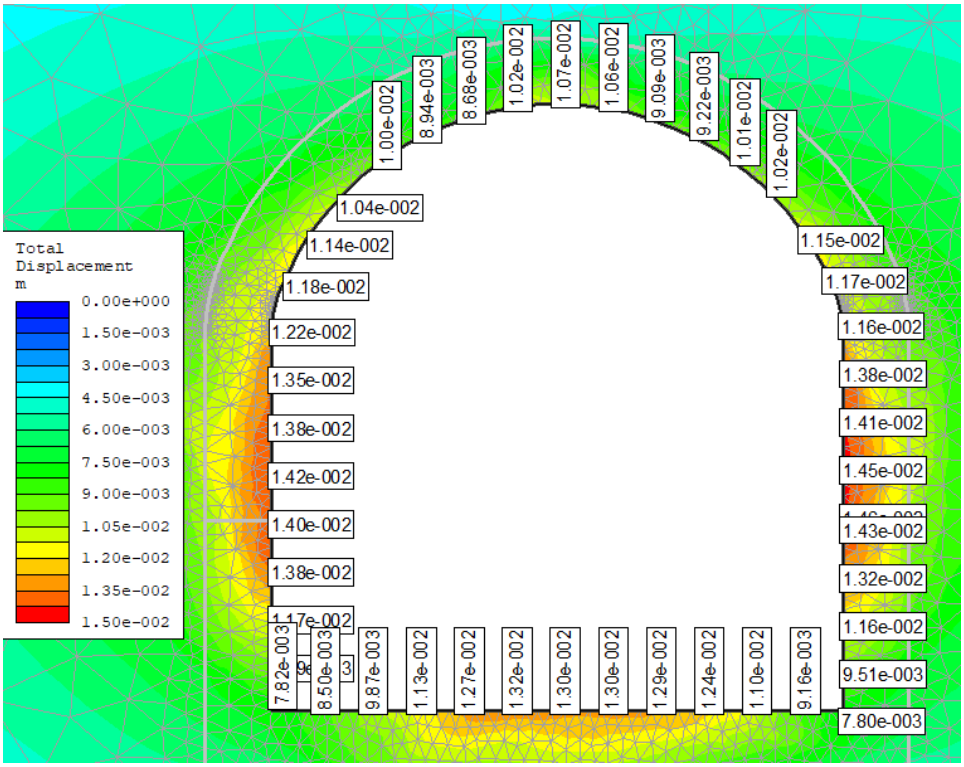

Figure 5.10: Transformer cavern deformation (GSI 50)

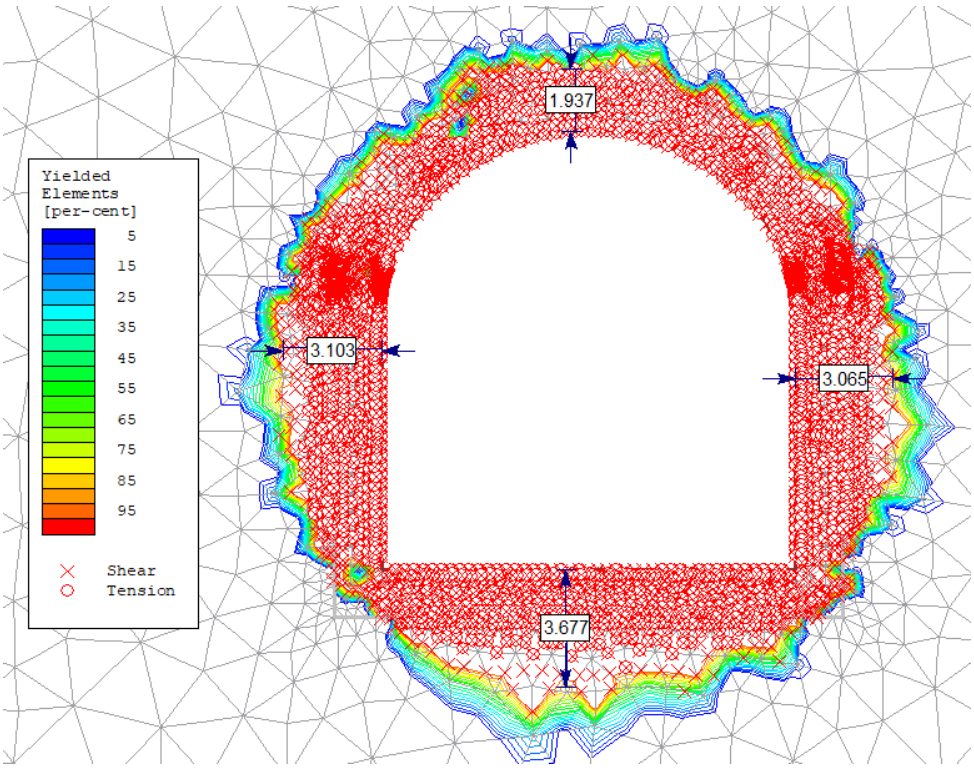

Figure 5.11: Transformer cavern extend of plastic zone (GSI 50)

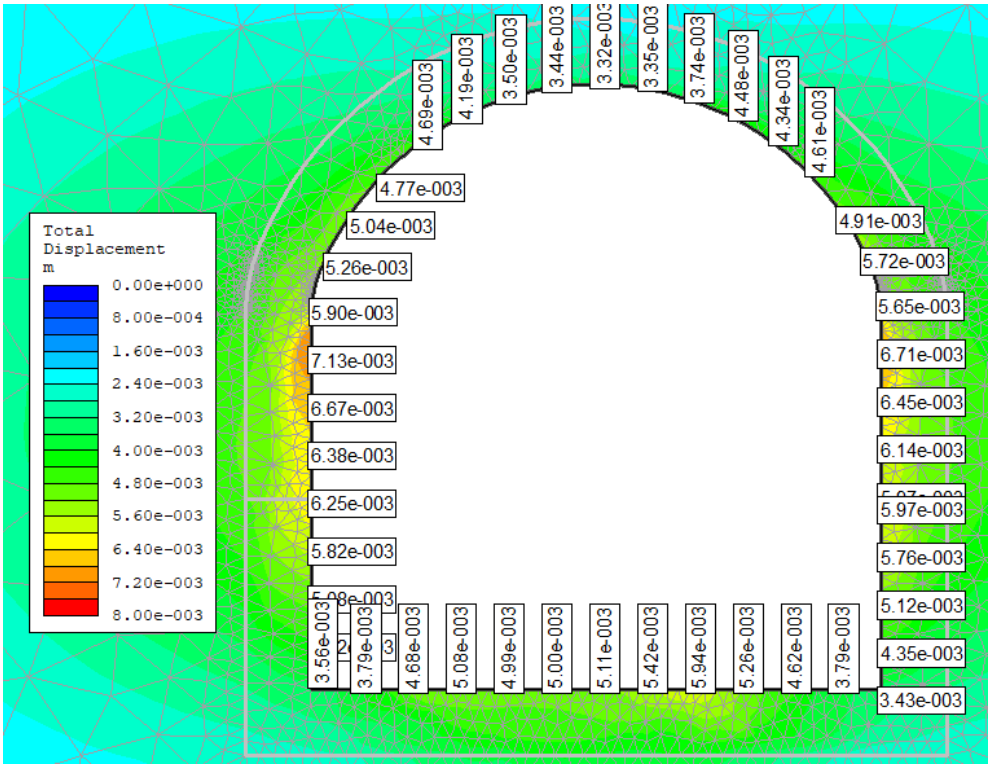

Figure 5.12: Transformer cavern deformation (GSI 60)

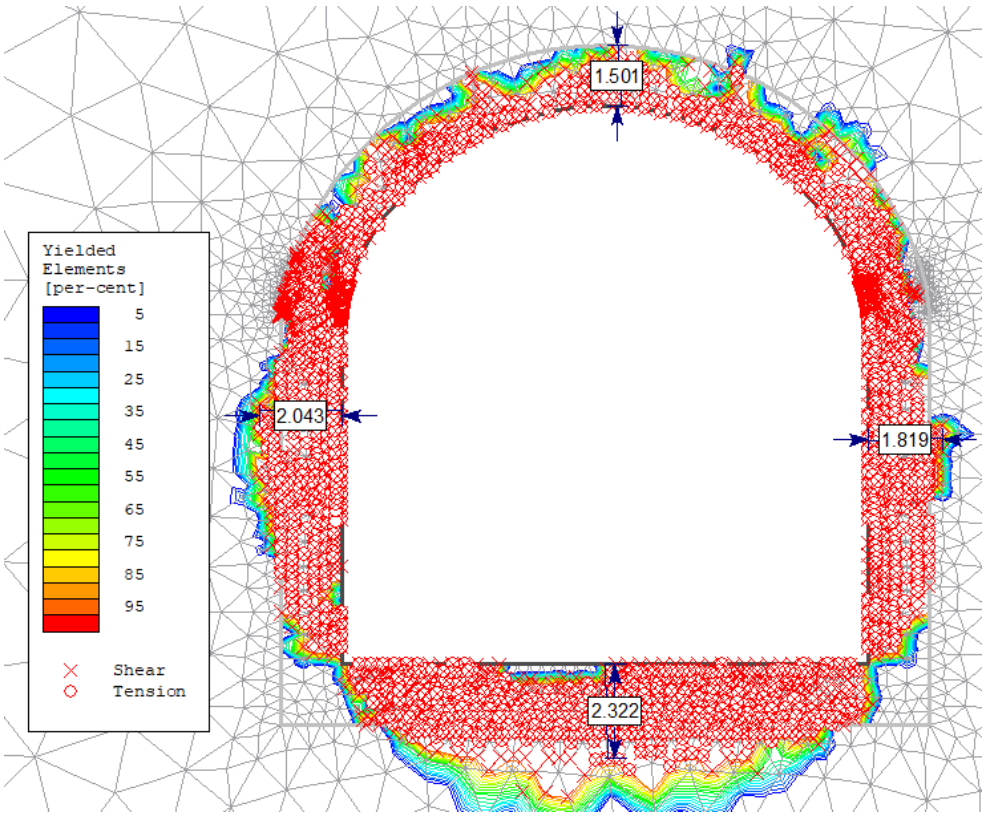

Figure 5.13: Transformer cavern extend of plastic zone (GSI 60)

5.3 Interaction of Caverns At 0.5 Height of Largest Cavern (GSI 35)

The interaction of the PHC and TRC was performed at a cavern spacing equal to 0.5 times the height of the powerhouse cavern. All three excavation sequences show significant amplification of the displacement with reference to the isolated cavern displacement.

Table 5.2: Deformation at 0.5H with GSI 35

Structure Location	**Case I**	**Case II**	**Case III**	**Isolated**	**Max (Cases)**	**Maximum AF** (Max/ Isolated)
	Displacement (mm)					
PH Left Wall	90.3	94.1	98.9	93.0	98.9	1.06
PH Right Wall	189	150.0	153.0	80.0	189.0	2.36
PH Crown	74.6	72.1	71.3	57.4	74.6	1.30
TRC Left Wall	42.9	99.7	112.0	57.1	112.0	1.96
TRC Right Wall	78.2	81.1	84.4	52.6	84.4	1.60
TRC Crown	87.5	85.4	80.9	44.7	87.5	1.96
TRC Invert	74.6	90.8	89.1	59.0	90.8	1.54

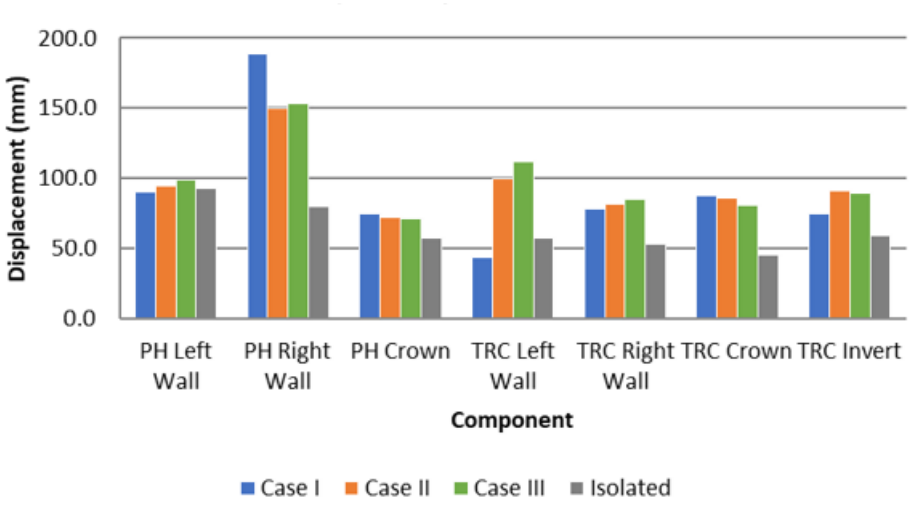

Figure 5.14: Deformation at 0.5H cavern spacing at GSI 35

The most important of the responses is the right wall movement of the powerhouse in Case I (189 mm), which is a 2.36 amplification of the isolated cavern behaviour, 80.0 mm, and this is because the pillar of rock facing the previously yielded transformer cavern is relaxed, and so movement in both directions acts on the rock mass simultaneously and consequently gives a large movement. From Table 5.2,it can be observed that the amplification factor in the transformer cavern is in the range of 2 or greater than 1.5. The excavation sequence of the transformer, followed by the powerhouse, causes the maximum deformation. Deformation at the different locations of the powerhouse is influenced by the different excavation sequences as shown in Table 5.3.

Table 5.3: Influence of excavation sequence at 0.5H and 35 GSI

Structure Location	**Min (Case)**	**Max (Case)**	**Least Critical Case**	**Critical Case**	**Variation %**
	Deformation (mm)				
PH Left Wall	90.3	98.9	Case I	Case III	9.5%
PH Right Wall	150.0	189.0	Case II	Case I	26.0%
PH Crown	71.3	74.6	Case III	Case I	4.6%
TRC Left Wall	42.9	112.0	Case I	Case III	161.1%
TRC Right Wall	78.2	84.4	Case I	Case III	7.9%
TRC Crown	80.9	87.5	Case III	Case I	8.2%
TRC Invert	74.6	90.8	Case I	Case II	21.7%

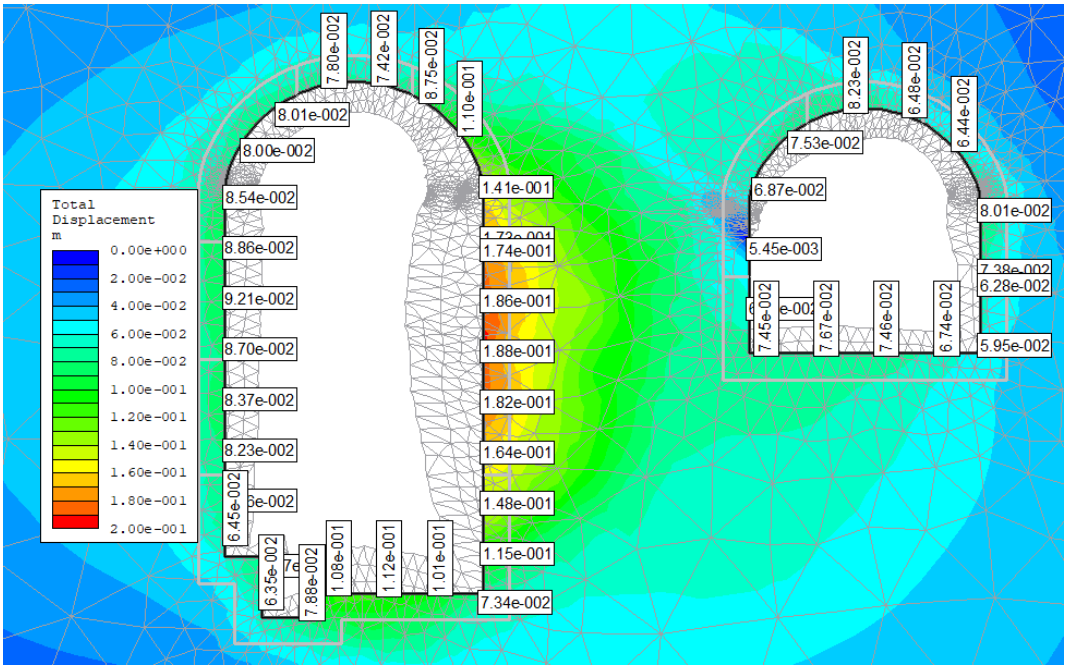

Figure 5.15: Displacement at case I (0.5H, GSI 35)

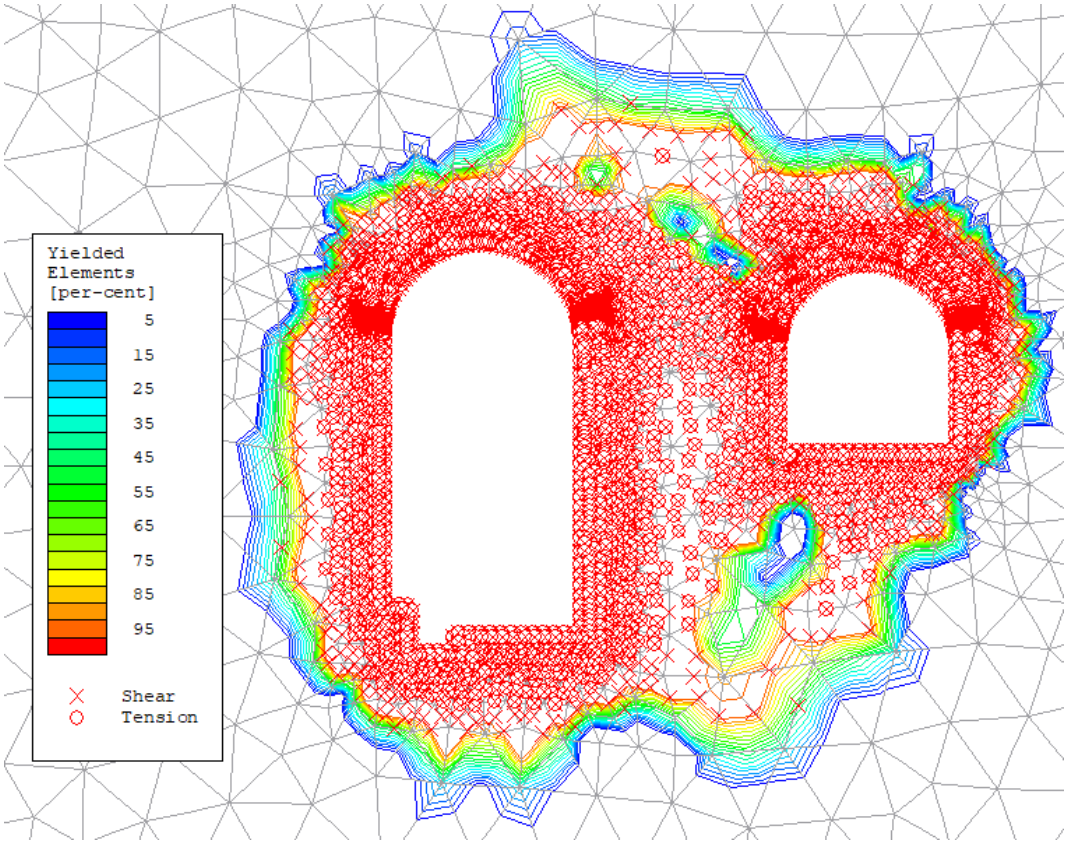

Figure 5.16: Extent of yield element at case I (0.5H, GSI 35)

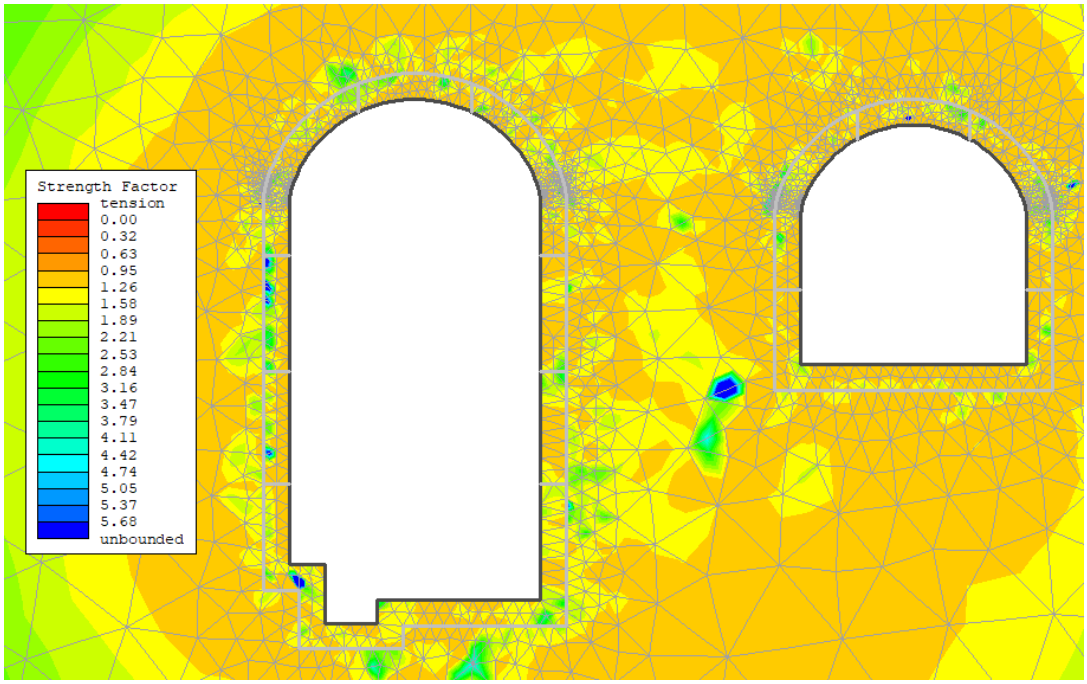

Figure 5.17: Strength factor case I (0.5H, GSI 35)

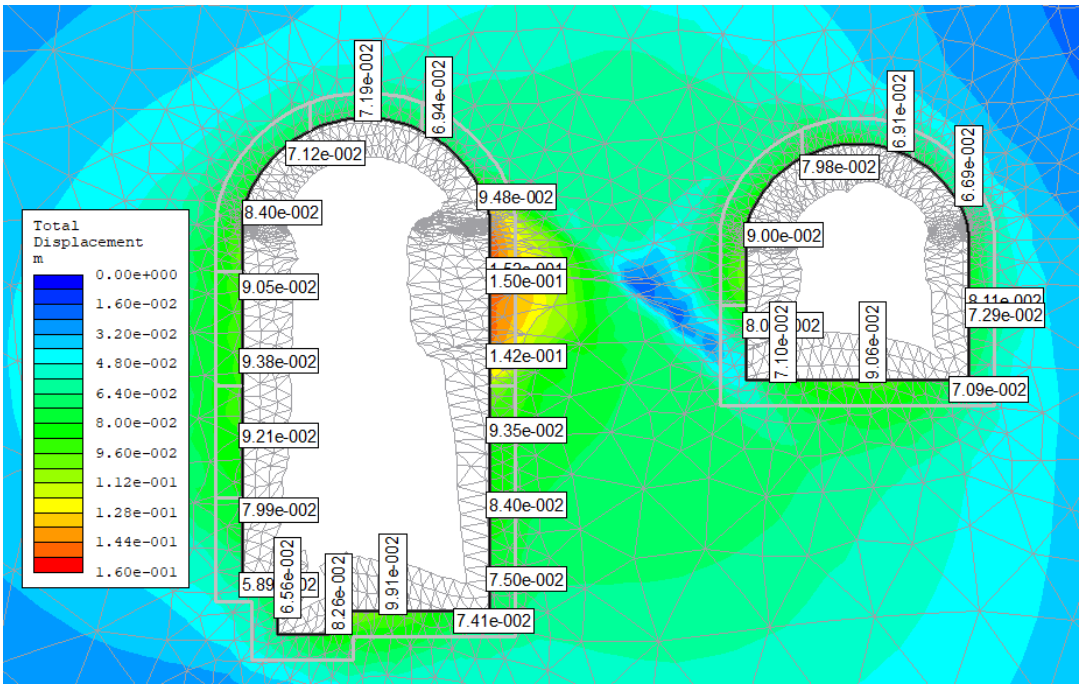

Figure 5.18: Displacement at case II (0.5H, GSI 35)

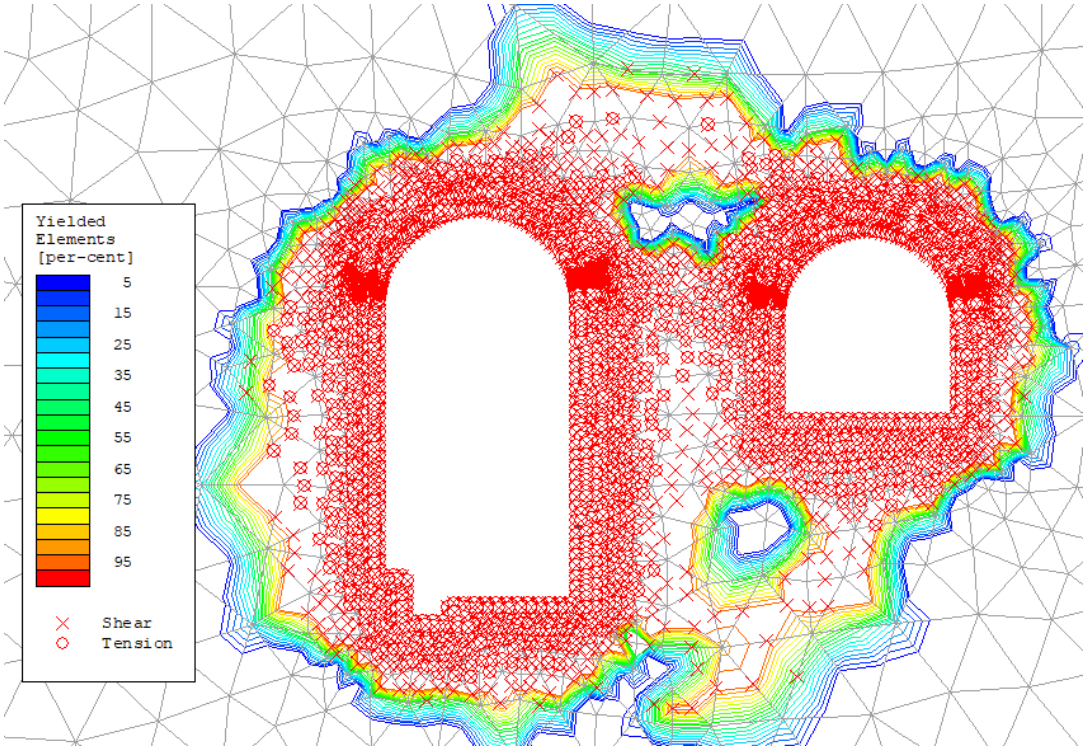

Figure 5.19: Extent of yield element at case II (0.5H, GSI 35)

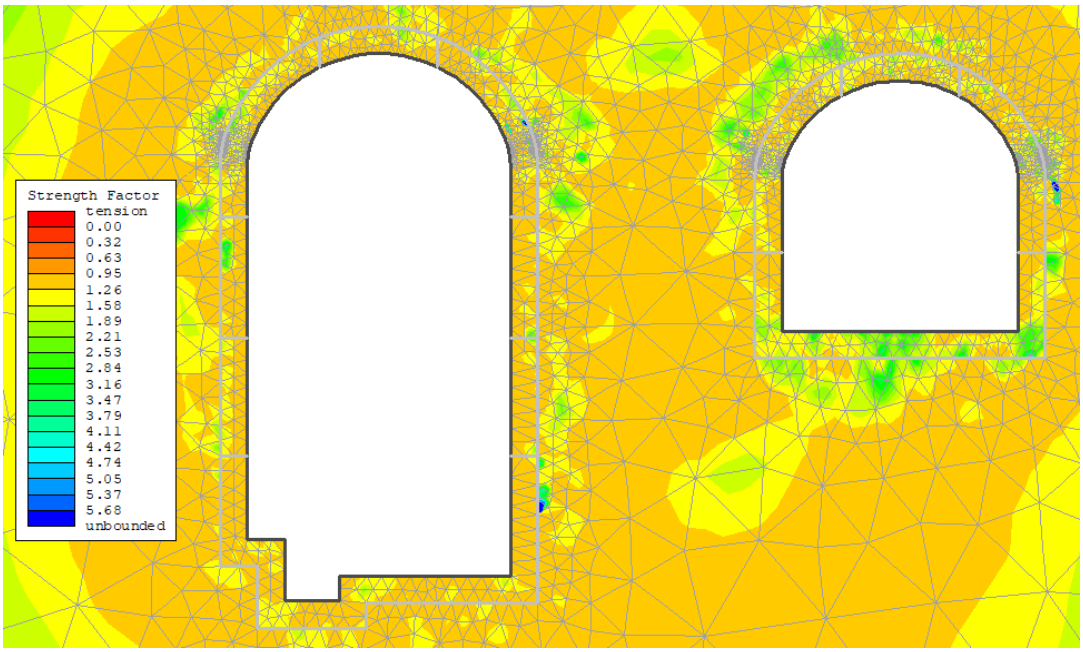

Figure 5.20: Strength factor case II (0.5H, GSI 35)

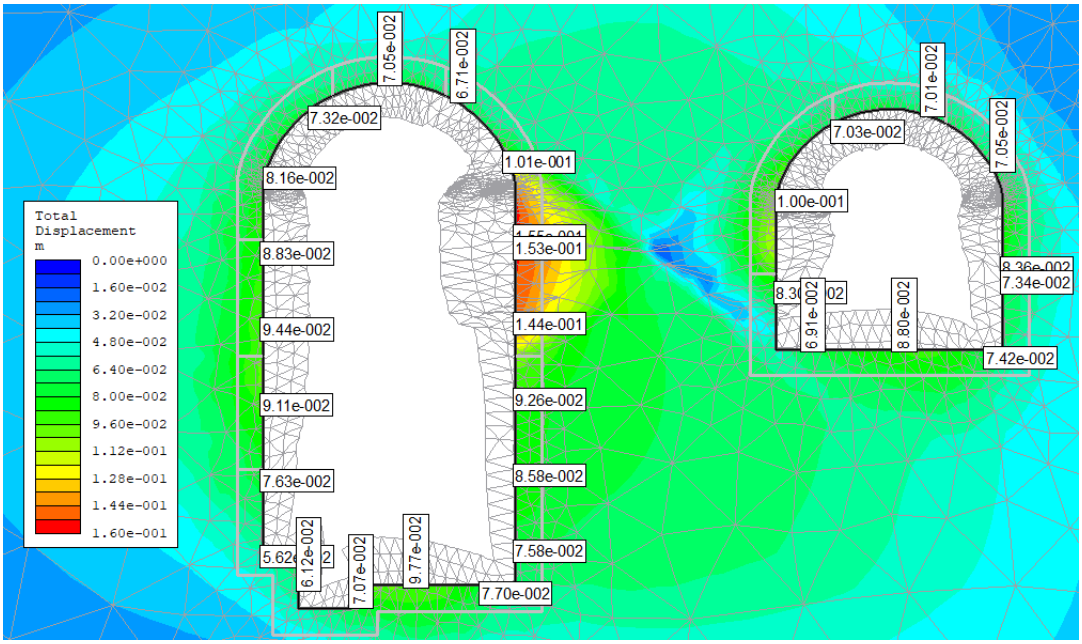

Figure 5.21: Displacement at case III (0.5H, GSI 35)

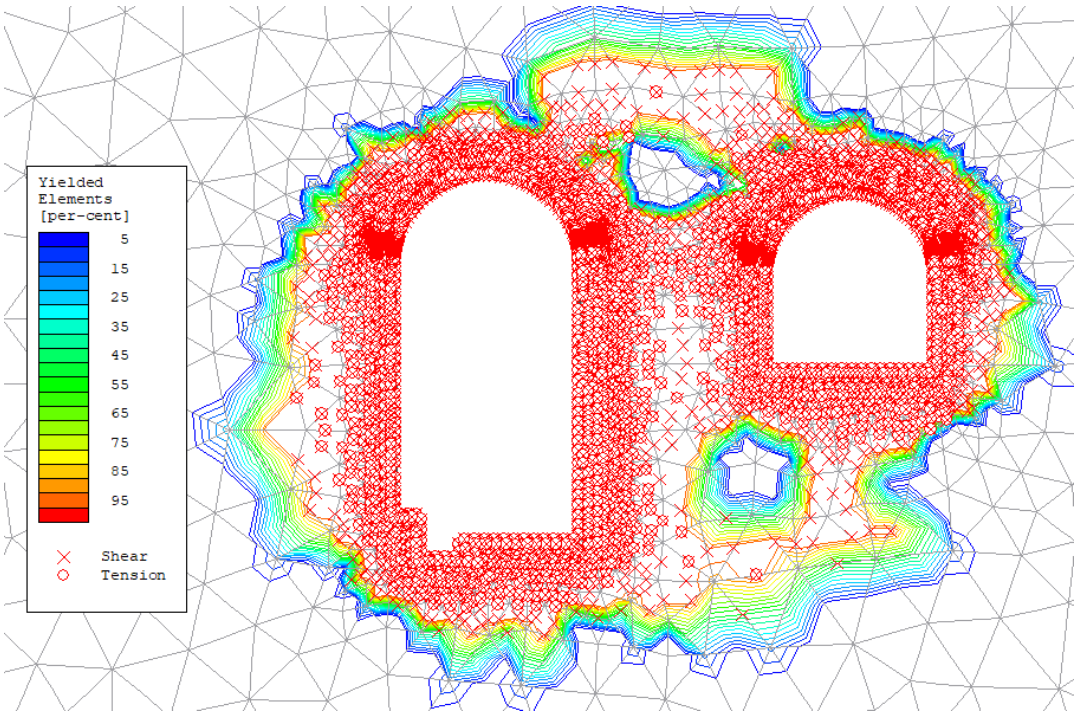

Figure 5.22: Extent of yield element at case III (0.5H, GSI 35)

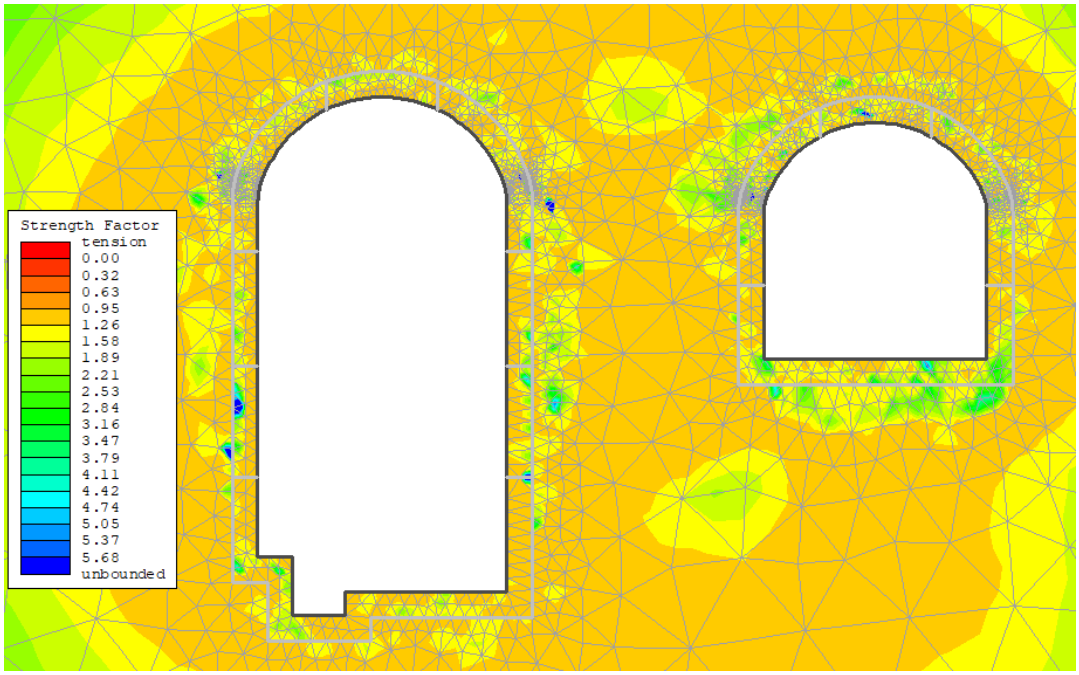

Figure 5.23: Strength factor case III (0.5H, GSI 35)

5.4 Interaction of Caverns At 2/3 Height of Largest Cavern (GSI 35)

The interaction of the PHC and TRC was observed at the cavern spacing equal to (2/3) times the height of the powerhouse cavern. All three excavation sequences show amplification of the displacement with reference to the isolated cavern displacement.

Table 5.4: Deformation at 2/3H with GSI 35

Structure Location	**Case I**	**Case II**	**Case III**	**Isolated**	**Max (Cases)**	**Maximum AF** (Max/ Isolated)
	Deformation (mm)					
PH Left Wall	111.0	118.0	111.0	93.0	118.0	1.27
PH Right Wall	179.0	167.0	145.0	80.0	179.0	2.24
PH Crown	83.0	81.7	72.9	57.4	83.0	1.45
TRC Left Wall	66.6	105.0	79.4	57.1	105.0	1.84
TRC Right Wall	64.1	93.5	65.1	52.6	93.5	1.78
TRC Crown	55.4	71.2	58.8	44.7	71.2	1.59
TRC Invert	63.9	102.0	82.4	59.0	102.0	1.73

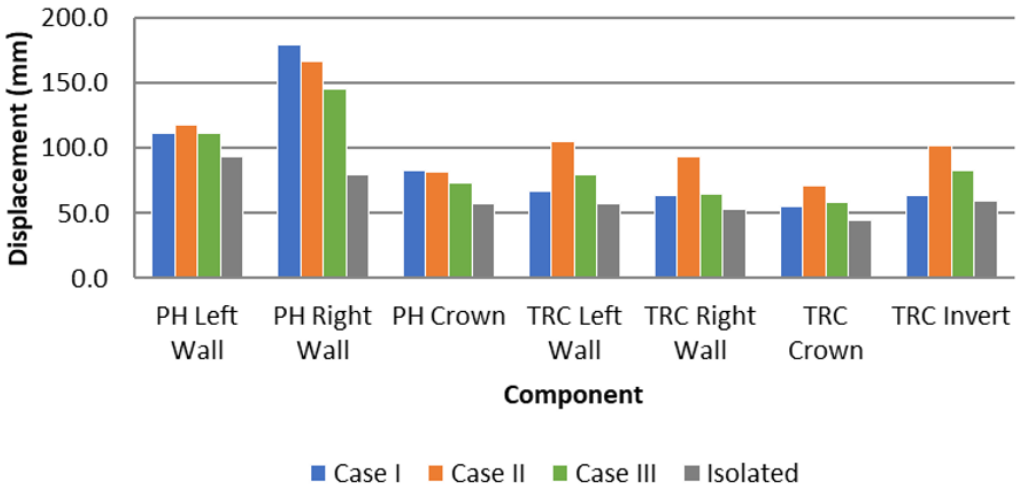

Figure 5.24: Deformation at (2/3)H cavern spacing at GSI 35

The most important of the responses is the right wall movement of the powerhouse in Case III (179 mm), which is a 2.24 amplification of the isolated cavern behaviour, 80.0 mm, and this is because the pillar of rock facing the previously yielded transformer cavern is relaxed, and so movement in both directions acts on the rock mass simultaneously and consequently gives a large movement. From Table 5.4, it can be observed that significant amplification in deformation of the transformer cavern is observed with the amplification factor of greater than 1.5 in the isolated transformer cavern behaviour. However, the amplification factor is slightly decreased in the sidewall and crown of the transformer cavern than in the 0.5H spacing of the cavern. It can also be observed from Table 5.5, that deformation in the transformer cavern is more sensitive to the excavation sequence of the TRC, followed by the PHC.

Table 5.5: Influence of excavation sequence at 2/3H and 35 GSI

Structure Location	**Min (Cases)**	**Max (Cases)**	**Least Critical Case**	**Critical Case**	**% Variation**
	Deformation (mm)				
PH Left Wall	111.0	118.0	Case I	Case II	6%
PH Right Wall	145.0	179.0	Case III	Case I	23%
PH Crown	72.9	83.0	Case III	Case I	14%
TRC Left Wall	66.6	105.0	Case I	Case II	58%
TRC Right Wall	64.1	93.5	Case I	Case II	46%
TRC Crown	55.4	71.2	Case I	Case II	29%
TRC Invert	63.9	102.0	Case I	Case II	60%

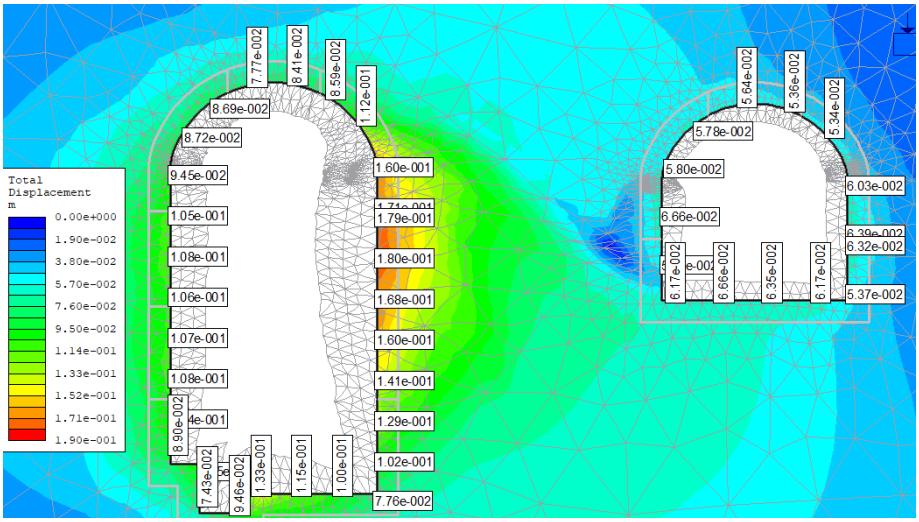

Figure 5.25: Displacement at case I (2/3H, GSI 35)

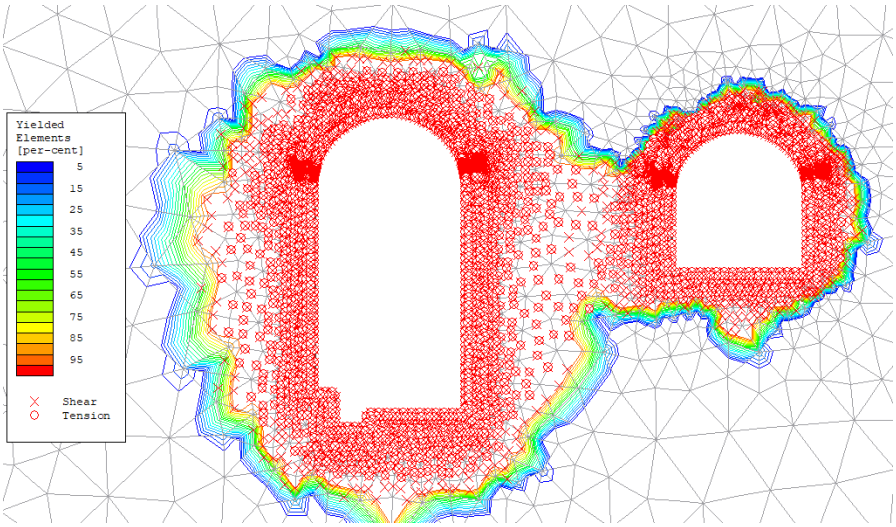

Figure 5.26: Extent of yield element at case I (2/3H, GSI 35)

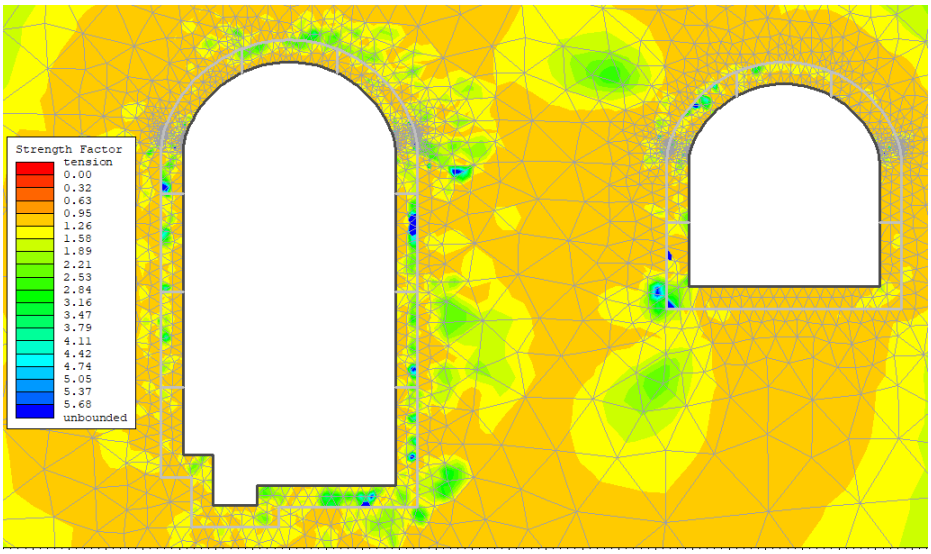

Figure 5.27: Strength factor case I (2/3H, GSI 35)

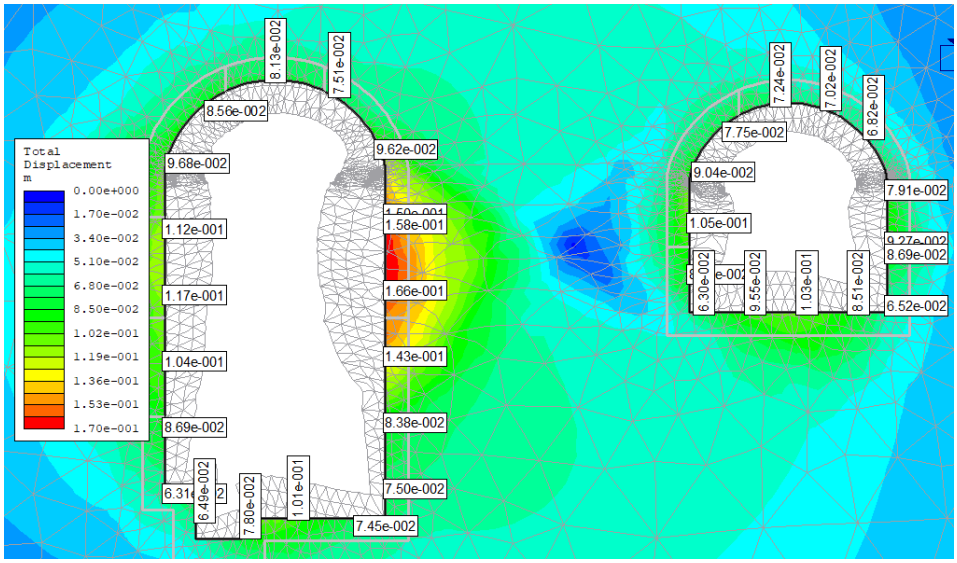

Figure 5.28: Displacement at case II (2/3H, GSI 35)

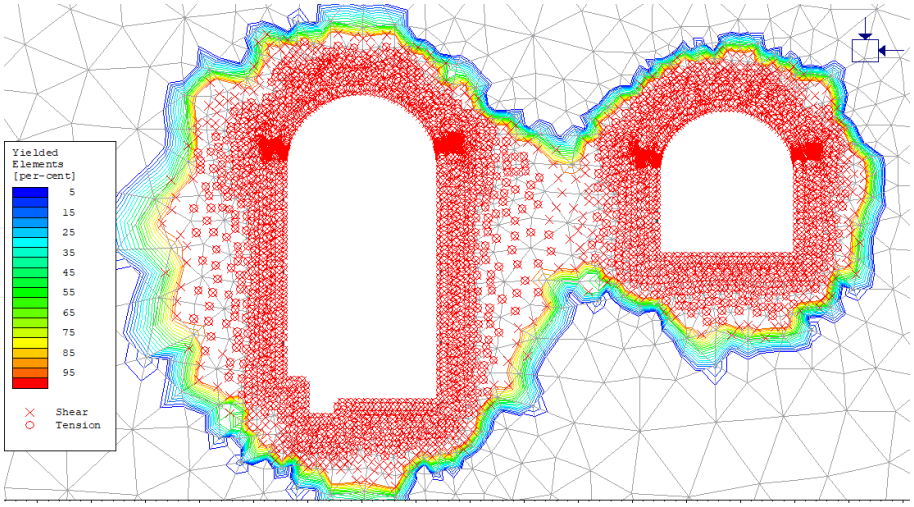

Figure 5.29: Extent of yield element at case II (2/3H, GSI 35)

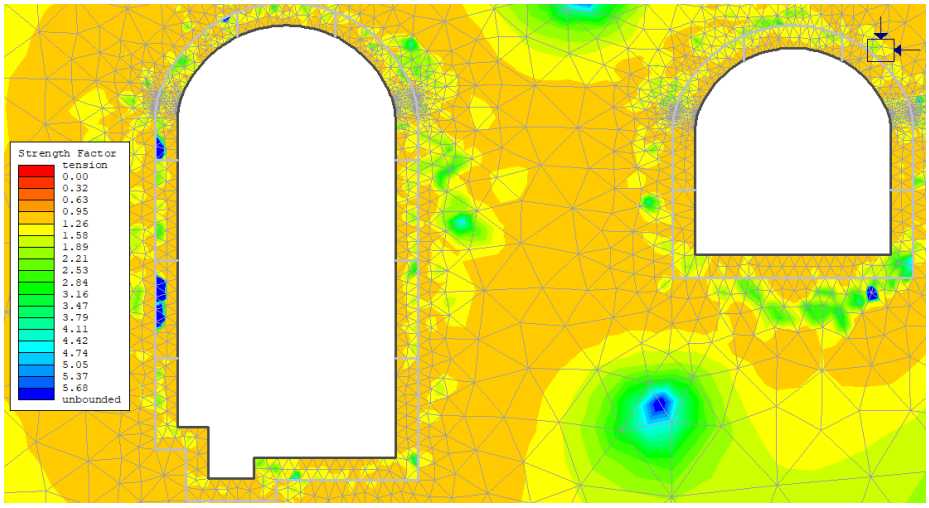

Figure 5.30: Strength factor case II (2/3H, GSI 35)

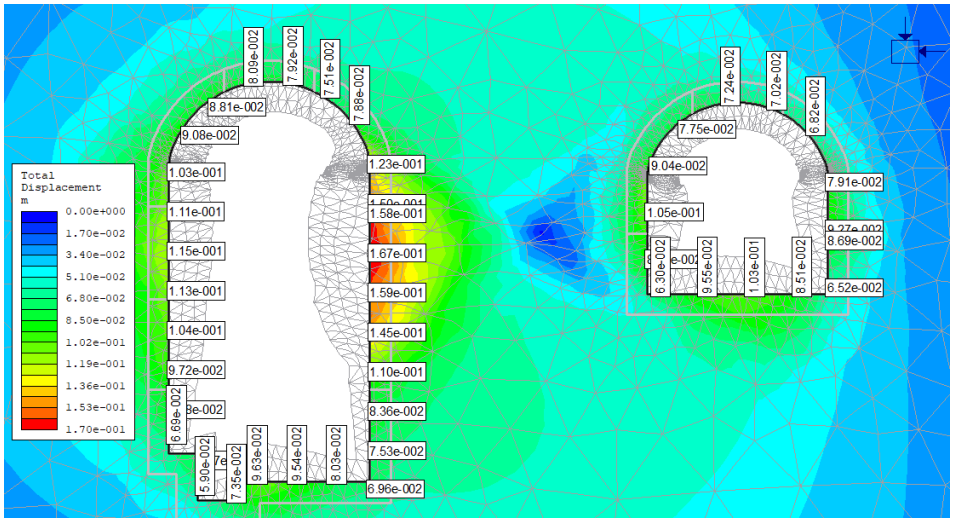

Figure 5.31: Displacement at case III (2/3H, GSI 35)

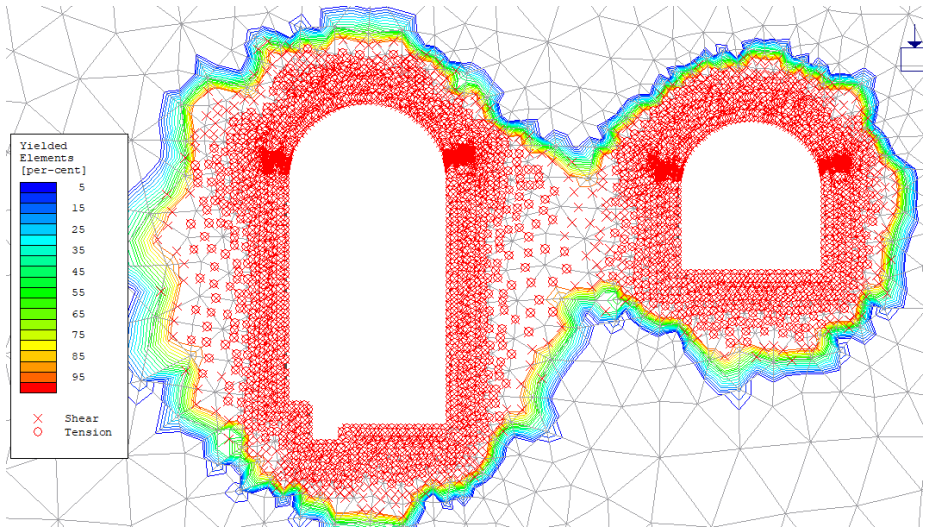

Figure 5.32: Extent of yield element at case III (2/3H, GSI 35)

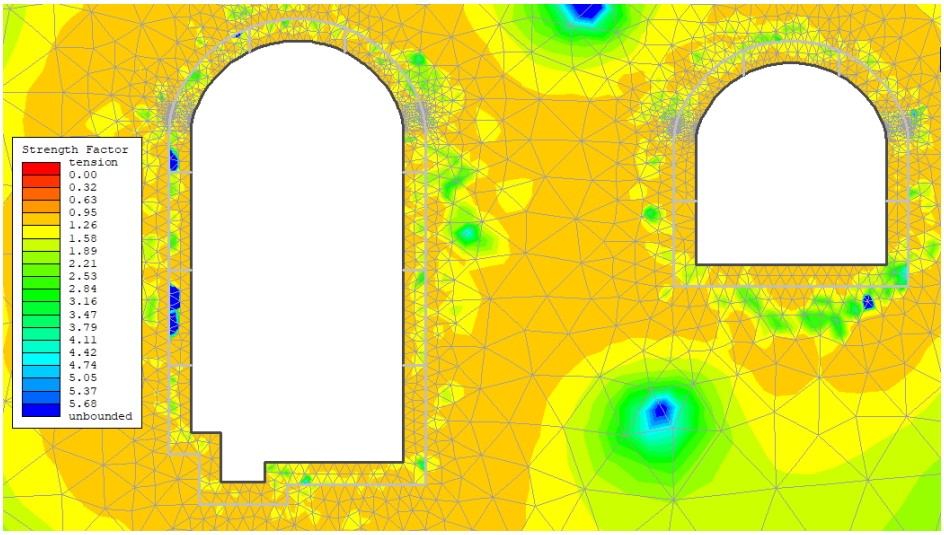

Figure 5.33: Strength factor case III (2/3H, GSI 35)

5.5 Interaction of Caverns at Height Equal to Largest Cavern (GSI 35)

The interaction of the powerhouse and transformer cavern was observed at a cavern spacing equal to the height of the PHC. All three excavation sequences show amplification of the displacement with reference to the isolated cavern displacement.

Table 5.6: Deformation at H with GSI 35

Structure Location	**Case I**	**Case II**	**Case III**	**Isolated**	**Max (Cases)**	**Maximum AF** (Max/ Isolated)
	Deformation (mm)					
PH Left Wall	95.8	100.0	90.7	93.0	100.0	0.94
PH Right Wall	92.5	90.1	85.0	80.0	92.5	1.07
PH Crown	73.9	61.7	56.5	57.4	73.9	1.37
TR Left Wall	9.2	21.3	21.9	57.1	21.9	0.38
TR Right Wall	54.7	61.2	60.6	52.6	61.2	1.16
TR Crown	37.1	58.2	51.4	44.7	58.2	1.30
TR Invert	43.6	59.2	51.8	59.0	59.2	1.00

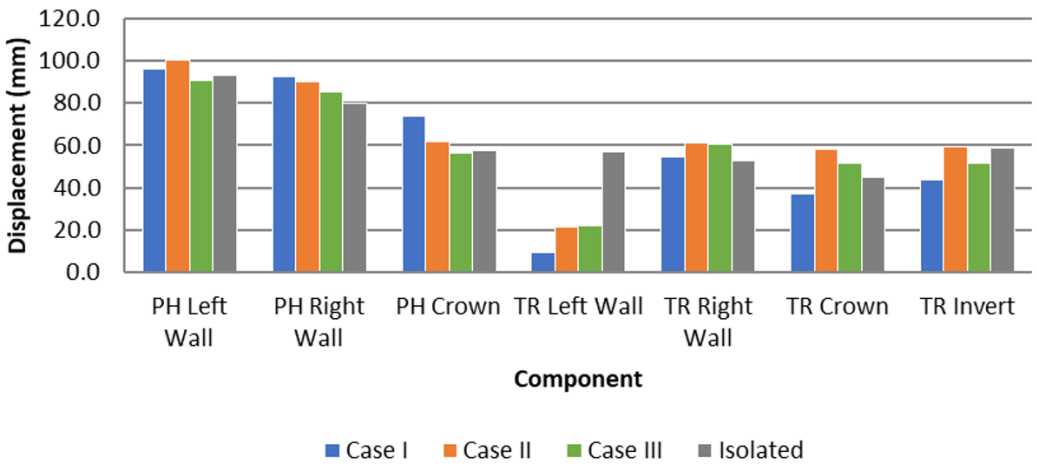

Figure 5.34: Deformation at H cavern spacing at GSI 35

The significant amplification of the sidewall and crown of the powerhouse cavern is not observed. The transformer cavern is showing slight sensitivity due to powerhouse cavern excavation. In the transformer cavern, due to the influence of the powerhouse cavern, the wall closer to the powerhouse is showing less amplification, whereas the right wall, crown, and invert are showing amplification greater than 1.0. The transformer cavern is sensitive to the excavation sequence of the TRC, followed by the PHC. Furthermore, the TRC wall is showing asymmetrical deformation. The influence of the excavation sequence has been shown in Table 5.7.

Table 5.7: Influence of excavation sequence at H and 35 GSI

Structure Location	**Min (Cases)**	**Max (Cases)**	**Least Critical Case**	**Critical Case**	**% Variation**
	Deformation (mm)				
PH Left Wall	90.7	100.0	Case III	Case II	10%
PH Right Wall	85.0	92.5	Case III	Case I	9%
PH Crown	56.5	73.9	Case III	Case I	31%
TR Left Wall	9.2	21.9	Case I	Case III	138%
TR Right Wall	54.7	61.2	Case I	Case II	12%
TR Crown	37.1	58.2	Case I	Case II	57%
TR Invert	43.6	59.2	Case I	Case II	36%

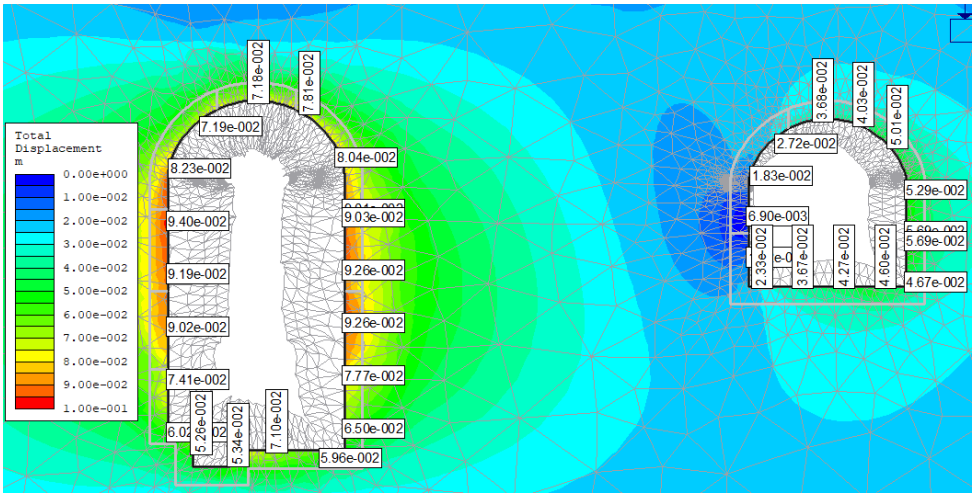

Figure 5.35: Displacement at case I H, GSI 35)

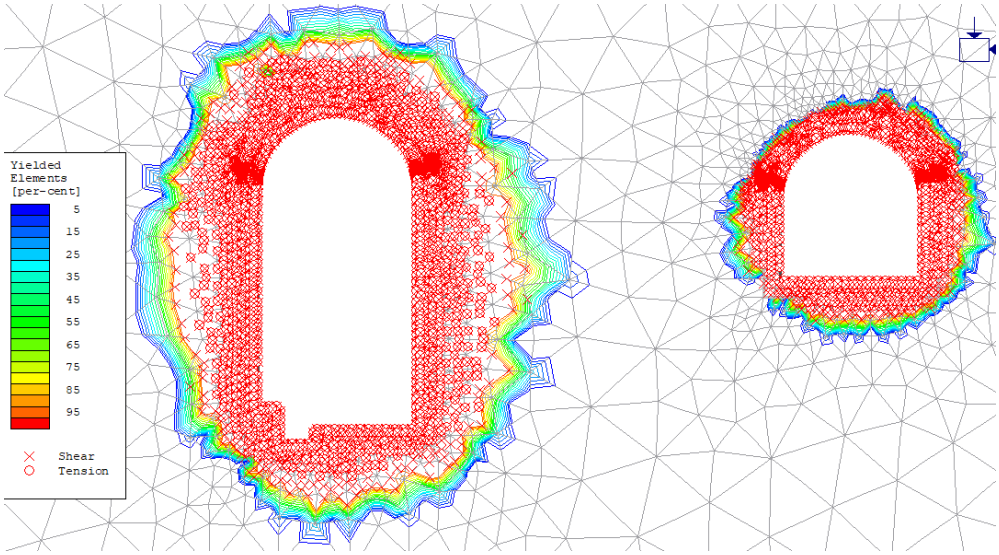

Figure 5.36: Extent of yield element at case I (H, GSI 35)

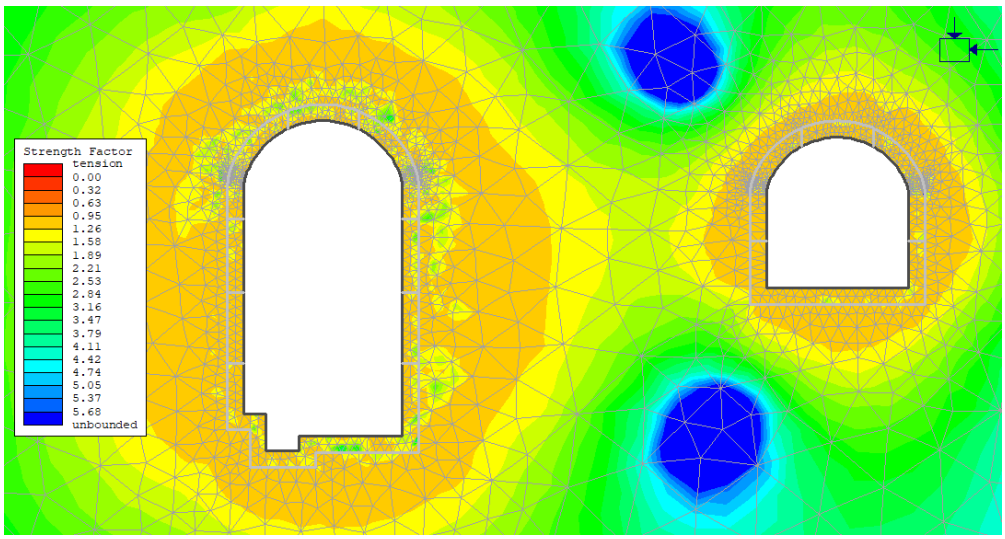

Figure 5.37: Strength factor case I H, GSI 35)

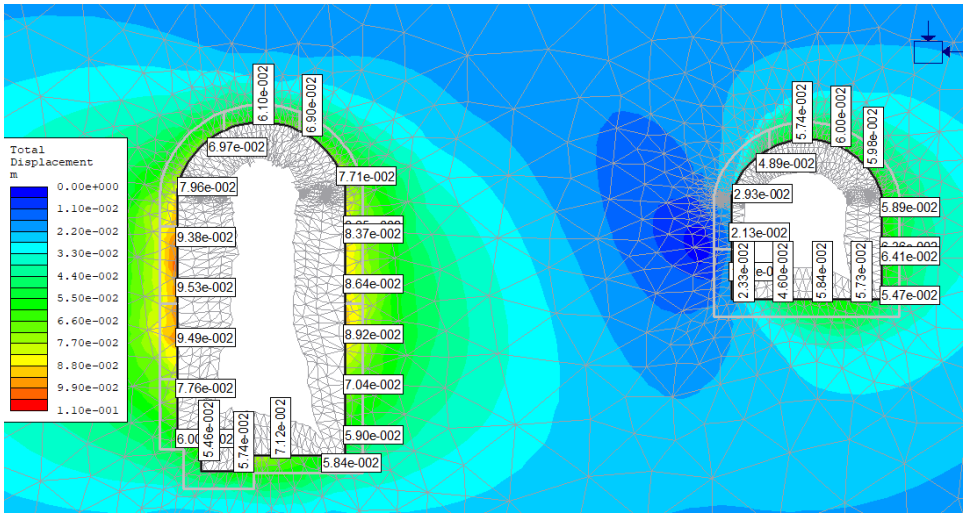

Figure 5.38: Displacement at case II (H, GSI 35)

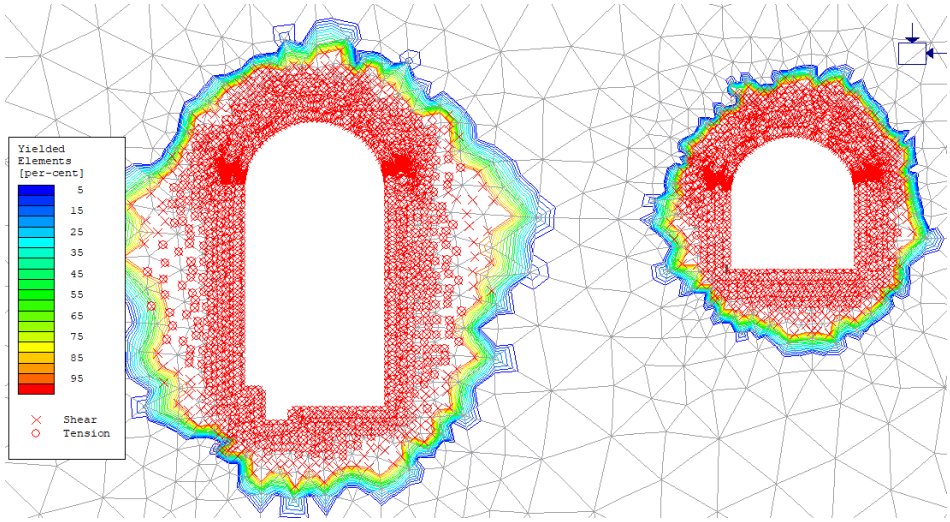

Figure 5.39: Extent of yield element at case II (H, GSI 35)

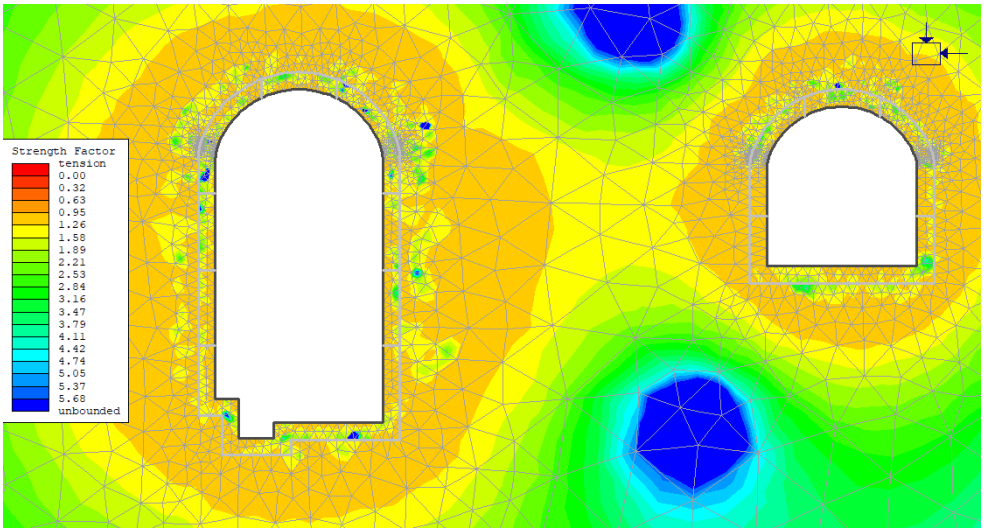

Figure 5.40: Strength factor case II (H, GSI 35)

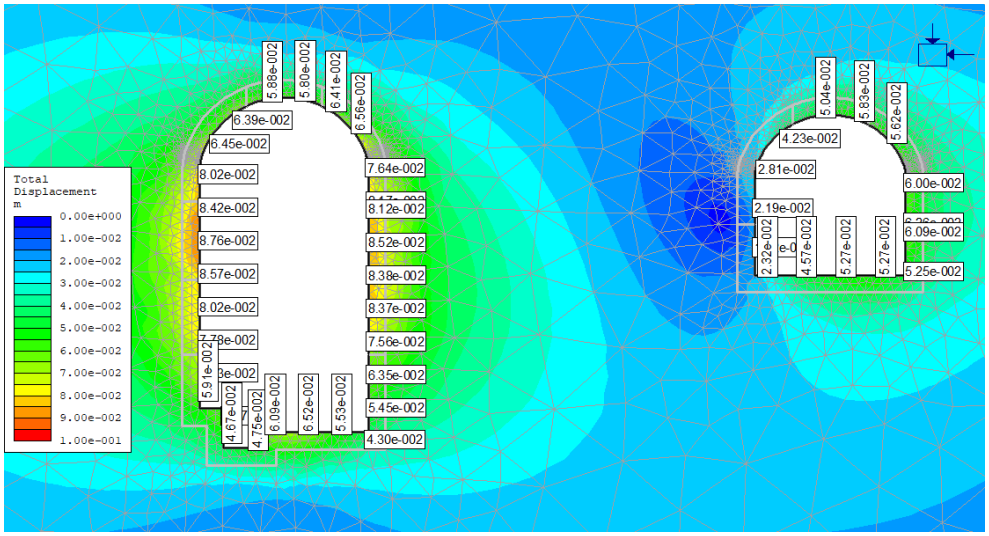

Figure 5.41: Displacement at case III (H, GSI 35)

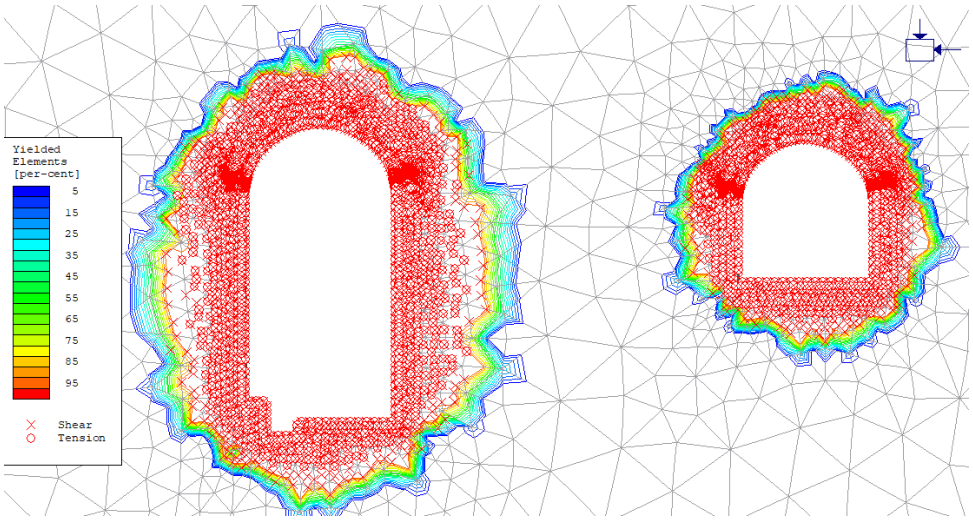

Figure 5.42: Extent of yield element at case III (H, GSI 35)

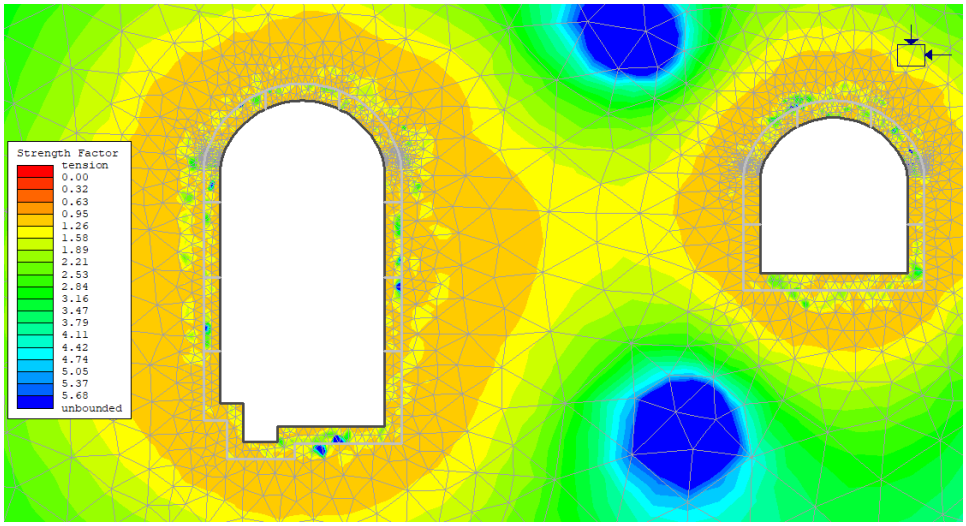

Figure 5.43: Strength factor case III (H, GSI 35)

5.6 Interaction of Caverns At 0.5 Height of Largest Cavern (GSI 60)

The interaction of the powerhouse and transformer cavern was observed at the cavern spacing equivalent to 0.5 times the height of the powerhouse cavern at the GSI 60. The improvement in rockmass shows a significant decrease in deformation of the PHC and TRC.

Table 5.8: Deformation at 0.5H with GSI 60

Structure Location	**Case I**	**Case II**	**Case III**	**Isolated**	**Max (Cases)**	**Maximum AF** (Max/ Isolated)
	Deformation (mm)					
PH Left Wall	11.6	12.3	12.3	11.2	12.7	1.13
PH Right Wall	12.8	12.3	12.3	12.1	12.8	1.06
PH Crown	5.7	6.6	6.6	6.2	6.6	1.07
TRC Left Wall	3.9	2.6	2.6	7.0	3.9	0.56
TRC Right Wall	8.7	9.1	10.1	7.0	10.1	1.44
TRC Crown	5.4	7.2	8.9	5.5	8.9	1.62
TRC Invert	8.3	8.9	8.0	7.0	8.9	1.28

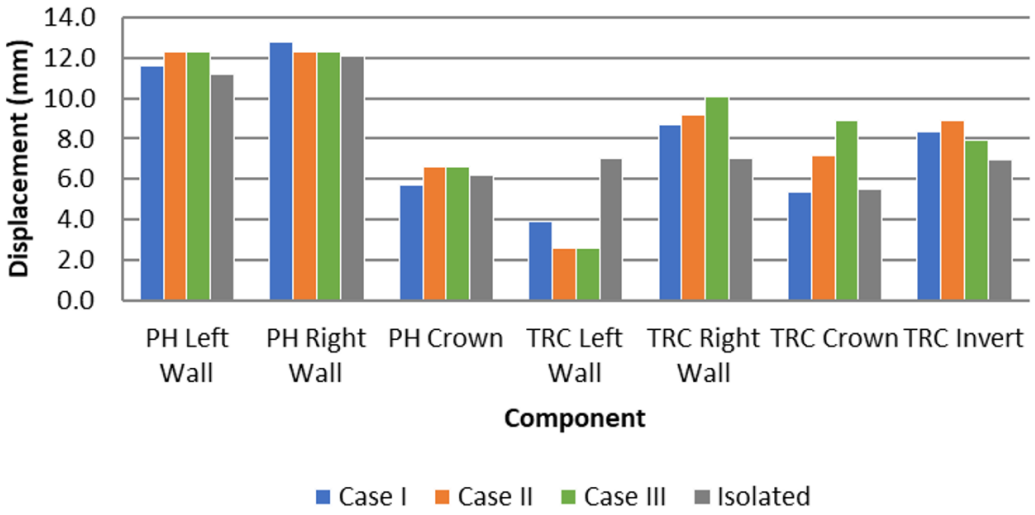

Figure 5.44: Deformation at 0.5H cavern spacing at GSI 60

The slight influence of the cavern interaction can be observed on the powerhouse cavern sidewall and crown at a spacing equivalent to half the height of the PHC. The amplification on the transformer cavern is also significantly decreased, as shown in Table 5.8 and Figure 5.44.

Table 5.9: Influence of excavation sequence at 0.5H and 60 GSI

Structure / Location	**Min (Cases)**	**Max (Cases)**	**Least Critical Case**	**Critical Case**	**% Variation**
	Deformation (mm)				
PH Left Wall	11.6	12.7	Case I	Case II	9%
PH Right Wall	12.3	12.8	Case II	Case I	4%
PH Crown	5.7	6.6	Case I	Case II	16%
TRC Left Wall	2.6	3.9	Case II	Case I	49%
TRC Right Wall	8.7	10.1	Case I	Case III	16%
TRC Crown	5.4	8.9	Case I	Case III	67%
TRC Invert	8.0	8.9	Case III	Case II	12%

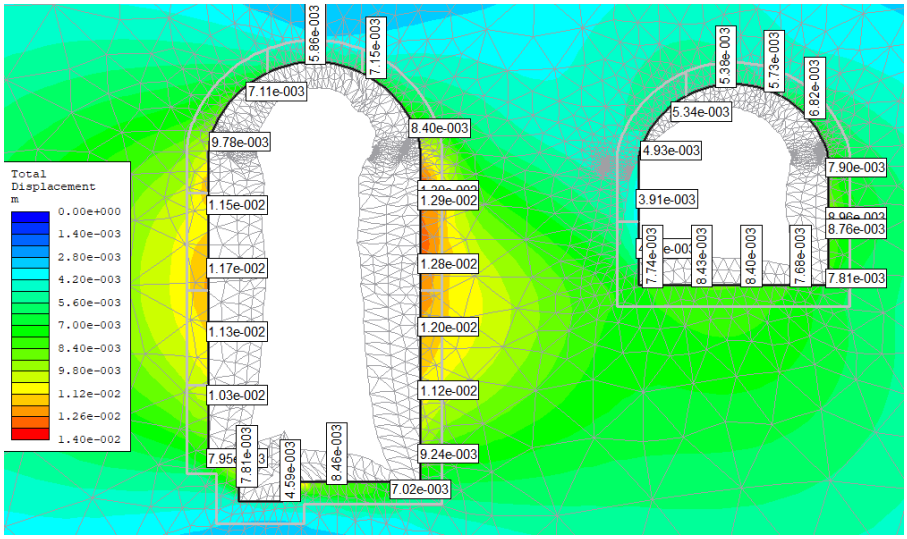

Figure 5.45: Displacement at case I (0.5H, GSI 60)

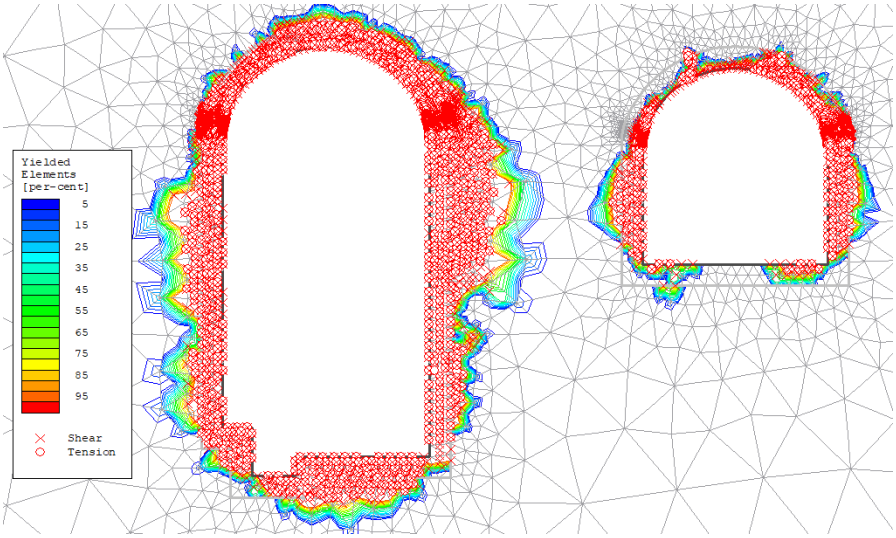

Figure 5.46: Extent of yield element at case I (0.5H, GSI 60)

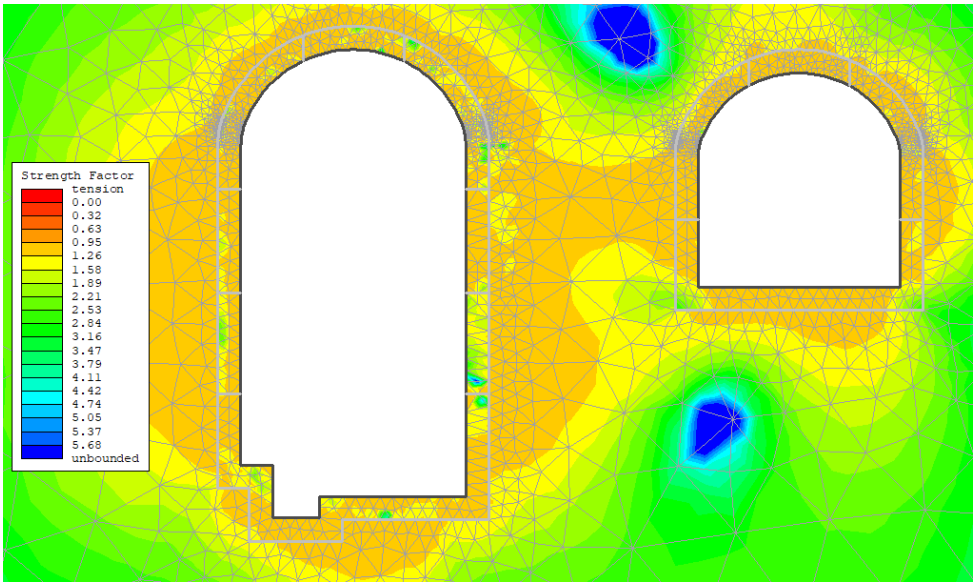

Figure 5.47: Strength factor case I (0.5H, GSI 60)

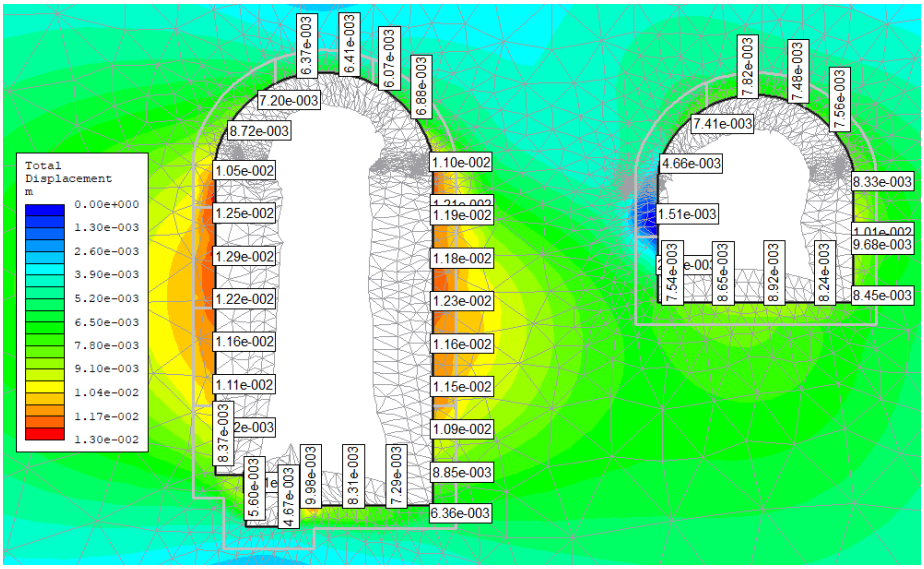

Figure 5.48: Displacement at case II (0.5H, GSI 60)

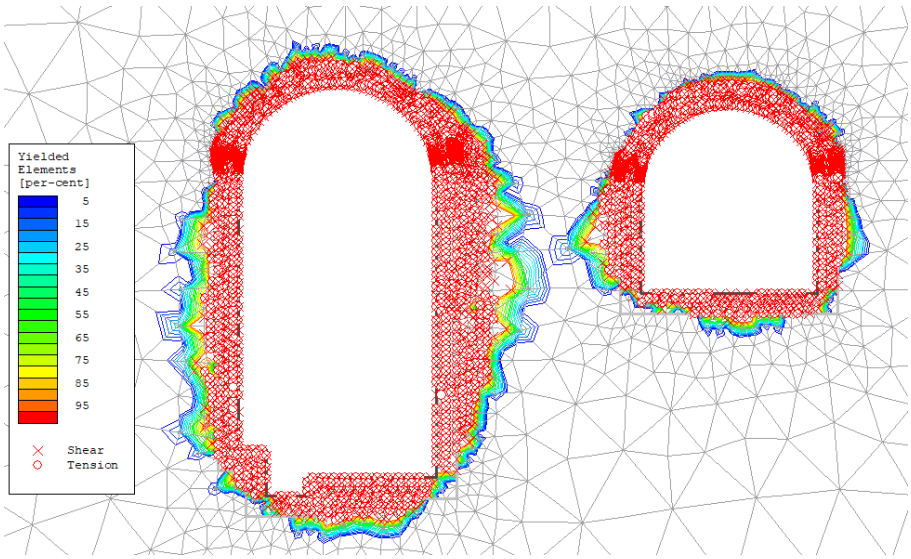

Figure 5.49: Extent of yield element at case II (0.5H, GSI 60)

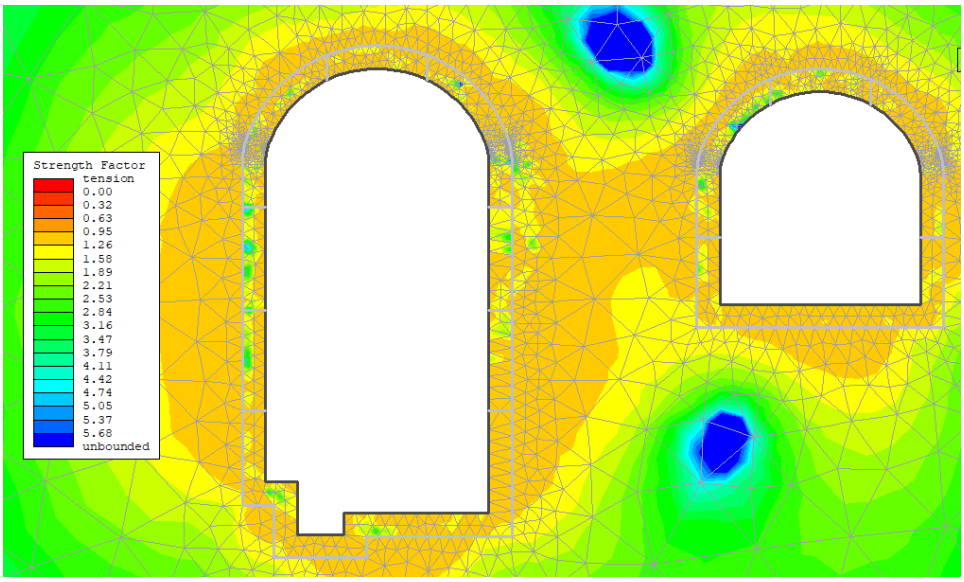

Figure 5.50: Strength factor case II (0.5H, GSI 60)

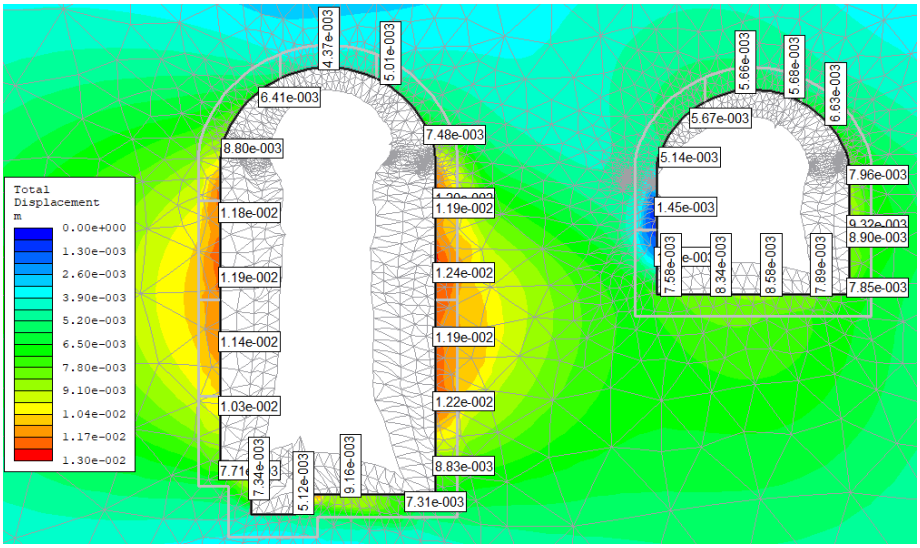

Figure 5.51: Displacement at case III (0.5H, GSI 60)

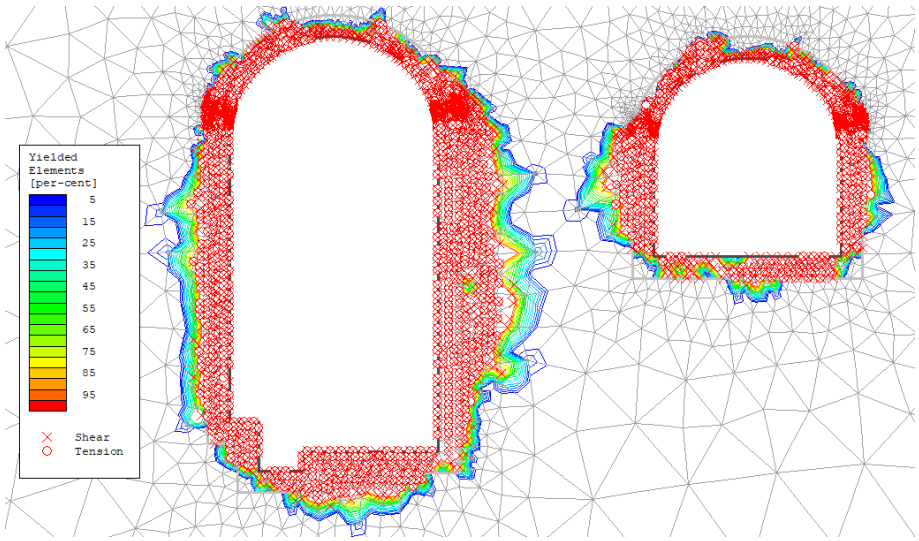

Figure 5.52: Extent of yield element at case III (0.5H, GSI 60)

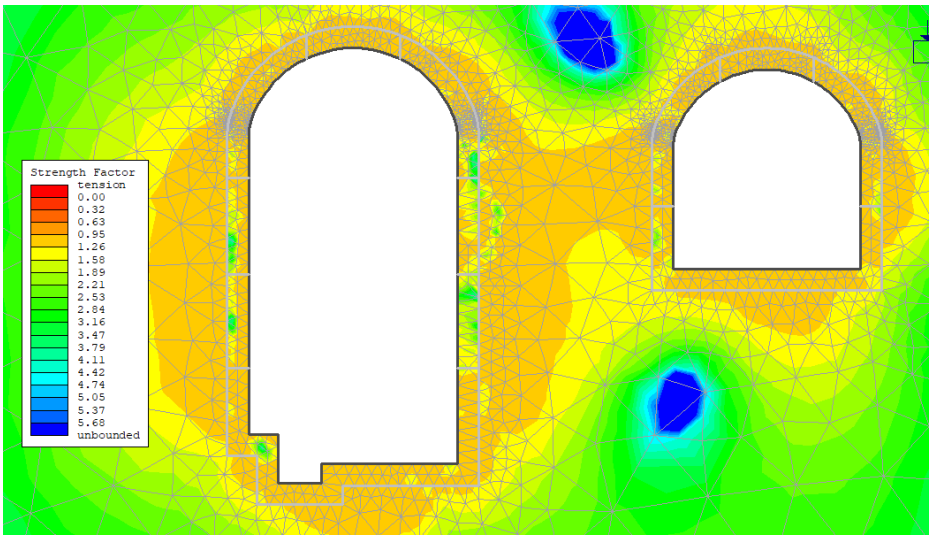

Figure 5.53: Strength factor case III (0.5H, GSI 60)

5.7 Interaction of Caverns at 2/3 Height of Largest Cavern (GSI 50)

The interaction of the powerhouse and transformer cavern was observed at the cavern spacing equal to 2/3 times the height of the powerhouse cavern at the GSI 50. The improvement in rockmass shows a significant reduction in deformation of the powerhouse and transformer cavern.

Table 5.10: Deformation at 2/3H with GSI 50

Structure Location	Case I	Case II	Case III	Isolated	Max (Cases)	Maximum AF (Max/ Isolated)
	Deformation (mm)					
PH Left Wall	25.4	26.1	23.5	21.9	26.1	1.19
PH Right Wall	26.8	24.7	24.2	26.0	26.8	1.03
PH Crown	12.7	12.3	10.3	15.2	12.7	0.84
TRC Left Wall	5.8	7.6	3.8	17.8	7.6	0.43
TRC Right Wall	16.0	18.1	17.0	13.7	18.1	1.32
TRC Crown	10.1	13.3	12.6	13.3	13.3	1.00
TRC Invert	13.9	22.1	14.0	13.4	22.1	1.65

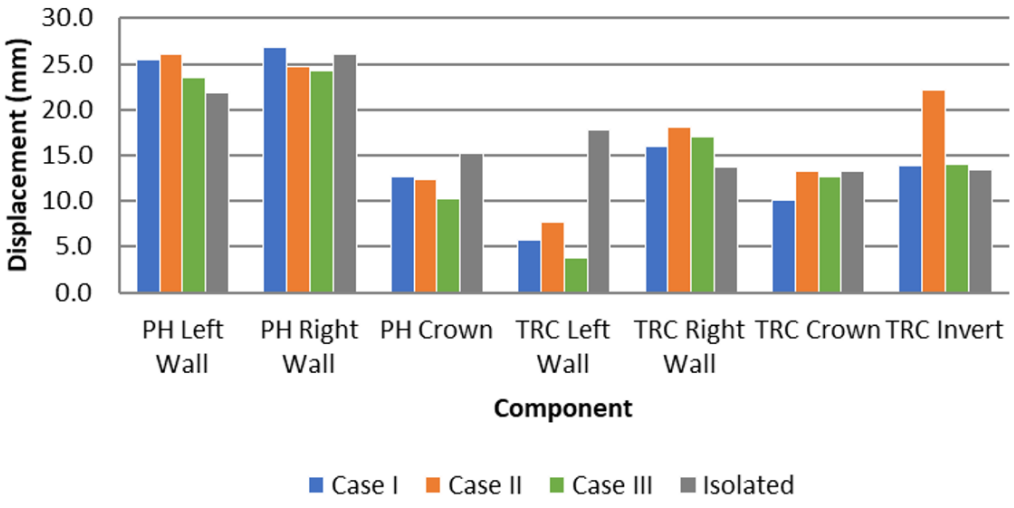

Figure 5.54: Deformation at 2/3H with GSI 50

Table 5.11: Influence of excavation sequence at 2/3H and GSI 50

Structure / Location	Min (Cases)	Max (Cases)	Least Critical Case	Critical Case	% Variation
	Deformation (mm)				
PH Left Wall	27.4	28.8	Case II	Case I	5%
PH Right Wall	22.7	26.4	Case II	Case I	16%
PH Crown	11.4	16.1	Case II	Case I	41%
TRC Left Wall	3.6	6.4	Case I	Case II	78%
TRC Right Wall	14.3	20.8	Case I	Case II	45%
TRC Crown	10.3	13.8	Case I	Case III	34%
TRC Invert	14.0	15.8	Case I	Case II	13%

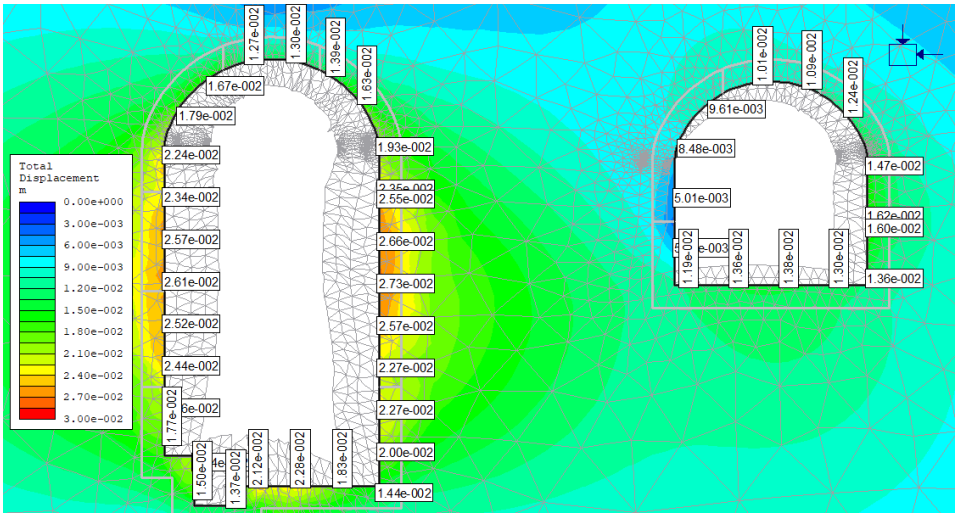

Figure 5.55: Displacement at case I (2/3H, GSI 50)

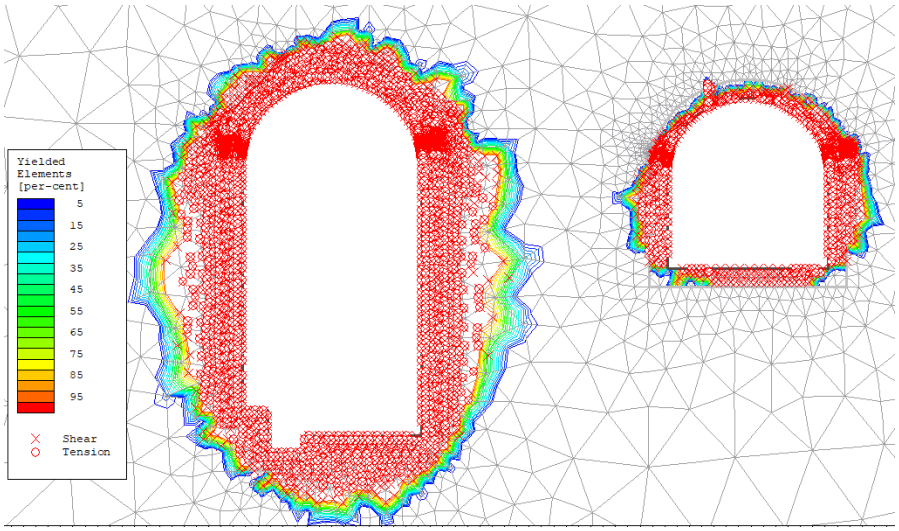

Figure 5.56: Extent of yield element at case I (2/3H, GSI 50)

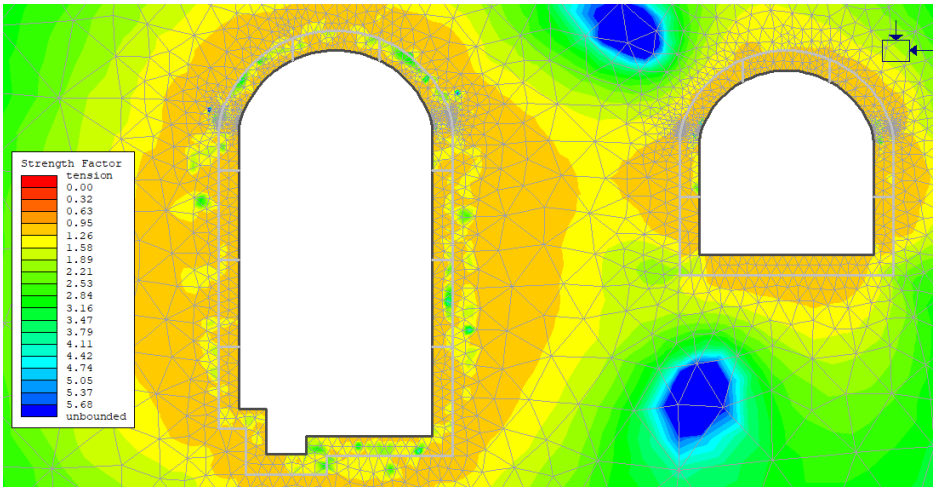

Figure 5.57: Strength factor case I (2/3H, GSI 50)

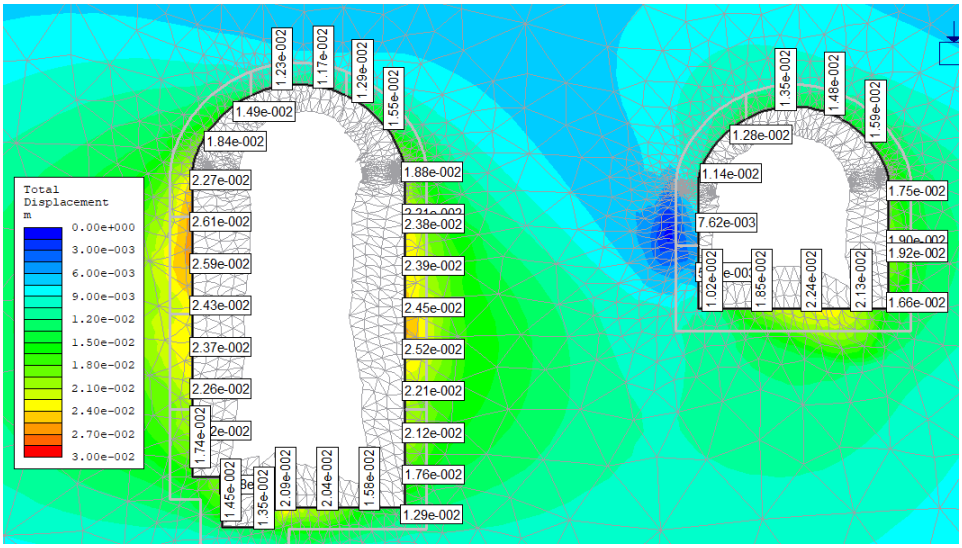

Figure 5.58: Displacement at case II (2/3H, GSI 50)

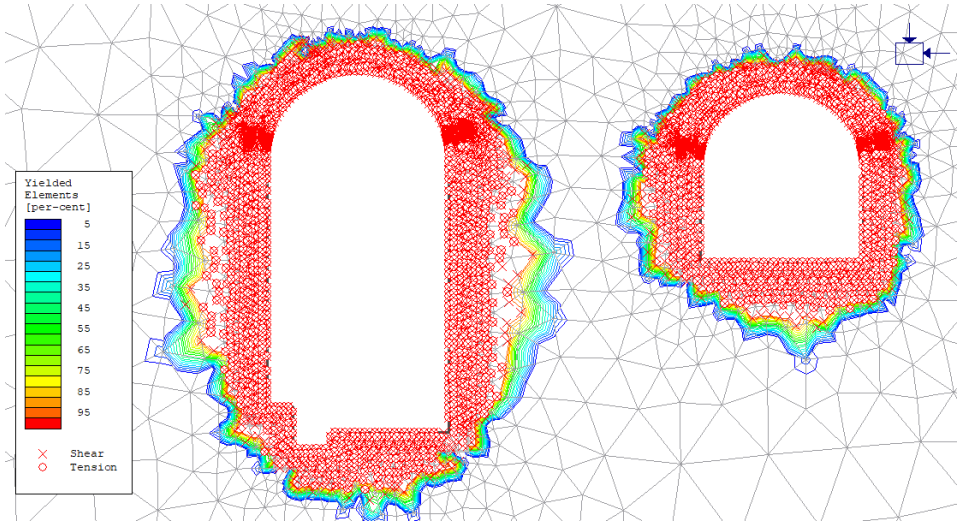

Figure 5.59: Extent of yield element at case II (2/3H, GSI 50)

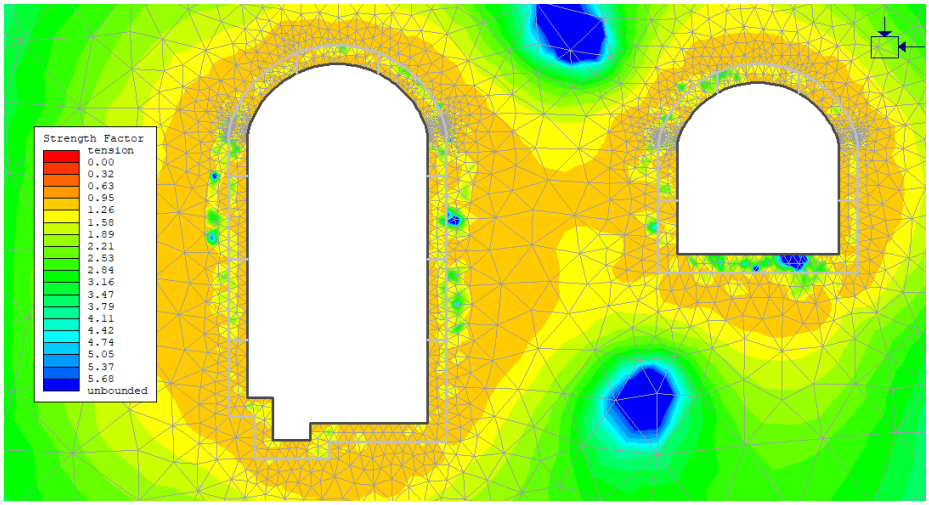

Figure 5.60: Strength factor case II (2/3H, GSI 50)

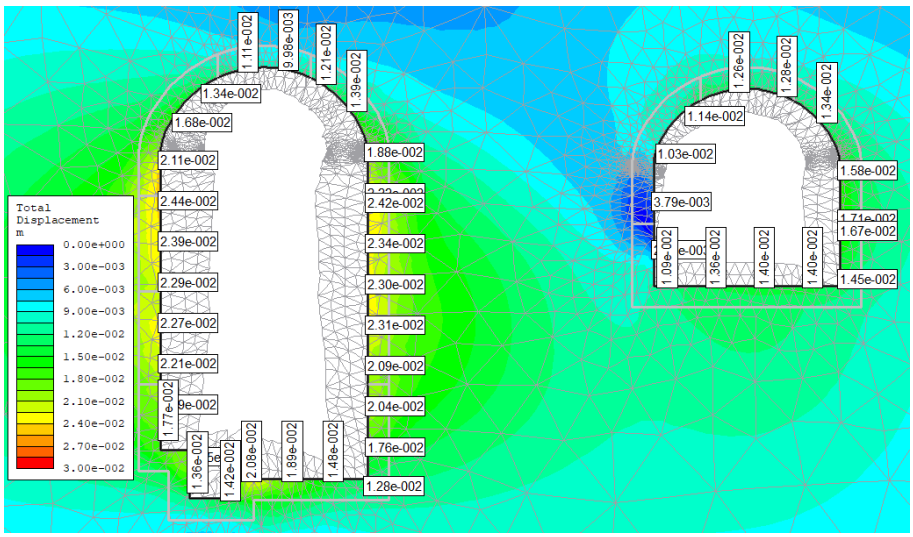

Figure 5.61: Displacement at case III (2/3H, GSI 50)

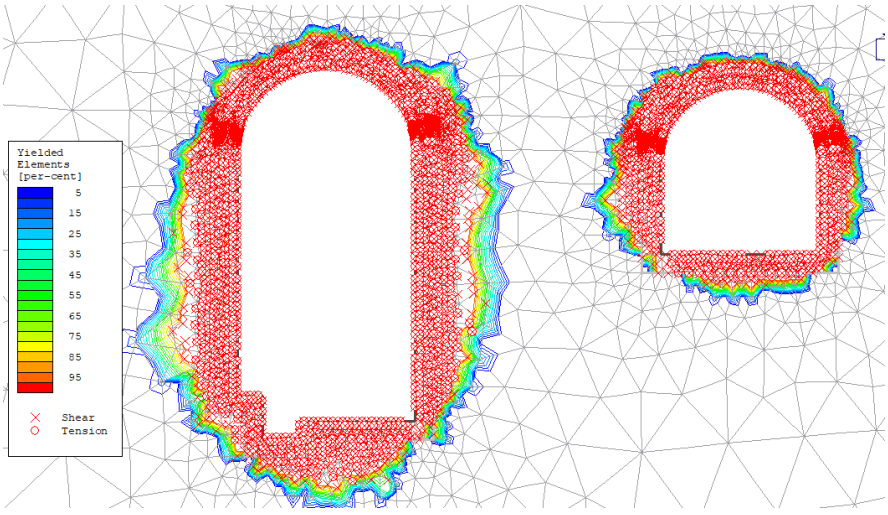

Figure 5.62: Extent of yield element at case III (2/3H, GSI 50)

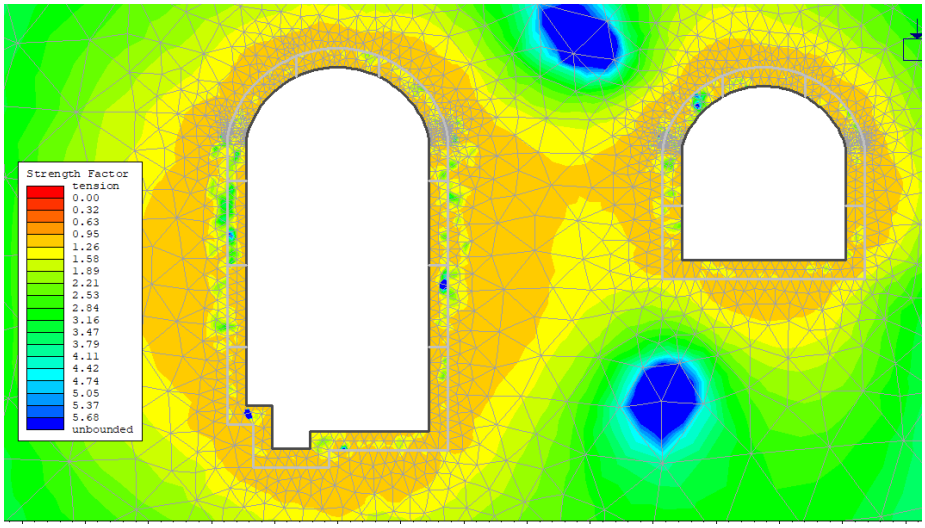

Figure 5.63: Strength factor case III (2/3H, GSI 35)

5.8 Comparison of Cavern Interaction with varying GSI

5.8.1 Cavern interaction at 0.5H with GSI 35 and GSI 60

The direct comparison of displacement magnitude in terms of amplification factor has been made at cavern spacing of 0.5H at GSI 35 and GSI 60. The comparison with cavern spacing equivalent to the height of the PHC with GSI also presented in Table 5.12.

Table 5.12: Comparison of AF (0.5H (GSI 35 and GSI60), H (GSI 35))

Structure / Location	**GSI 35**		**GSI 60**		**GSI 35 (H Spacing)**	
	Maximum AF	Critical Case	Maximum AF	Critical Case	Maximum AF	Critical Case
PH Left Wall	1.06	Case III	1.13	Case II	1.08	Case II
PH Right Wall	2.36	Case I	1.06	Case I	1.16	Case I
PH Crown	1.30	Case I	1.07	Case II	1.29	Case I
TRC Left Wall	1.96	Case III	0.56	Case I	0.38	Case III
TRC Right Wall	1.60	Case III	1.44	Case III	1.16	Case II
TRC Crown	1.96	Case I	1.62	Case III	1.30	Case II

Structure / Location	GSI 35		GSI 60		GSI 35 (H Spacing)	
	Maximum AF	Critical Case	Maximum AF	Critical Case	Maximum AF	Critical Case
TRC Invert	1.54	Case II	1.28	Case II	1.00	Case II

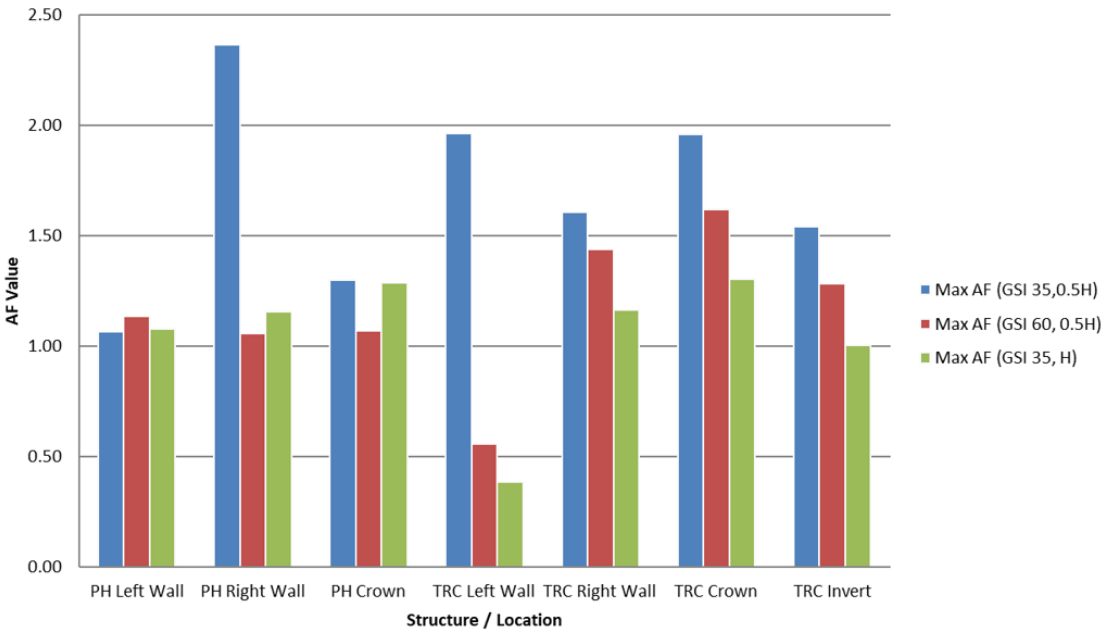

Figure 5.64: Comparison of amplification factor at 0.5H

5.8.2 Cavern Interaction at 2/3H with GSI 35 and GSI 50

The direct comparison of displacement magnitude in terms of amplification factor has been made at cavern spacing of 2/3H at GSI 35 and GSI 50, and the comparison with cavern spacing equal to the height of the powerhouse has been made and presented in Table 5.13.

Table 5.13: Comparison of AF (2/3H (GSI 35 and GSI 50), H (GSI 35))

Structure / Location	GSI 35		GSI 60		GSI 35 (H Spacing)	
	Maximum AF	**Critical Case**	**Maximum AF**	**Critical Case**	**Maximum AF**	**Critical Case**
PH Left Wall	1.27	Case II	1.19	Case II	1.08	Case II
PH Right Wall	2.24	Case I	1.03	Case I	1.16	Case I
PH Crown	1.45	Case I	0.84	Case I	1.29	Case I

Structure / Location	GSI 35		GSI 60		GSI 35 (H Spacing)	
	Maximum AF	Critical Case	Maximum AF	Critical Case	Maximum AF	Critical Case
TRC Left Wall	1.84	Case II	0.43	Case II	0.38	Case III
TRC Right Wall	1.78	Case II	1.32	Case II	1.16	Case II
TRC Crown	1.59	Case II	1.00	Case II	1.30	Case II
TRC Invert	1.73	Case II	1.65	Case II	1.00	Case II

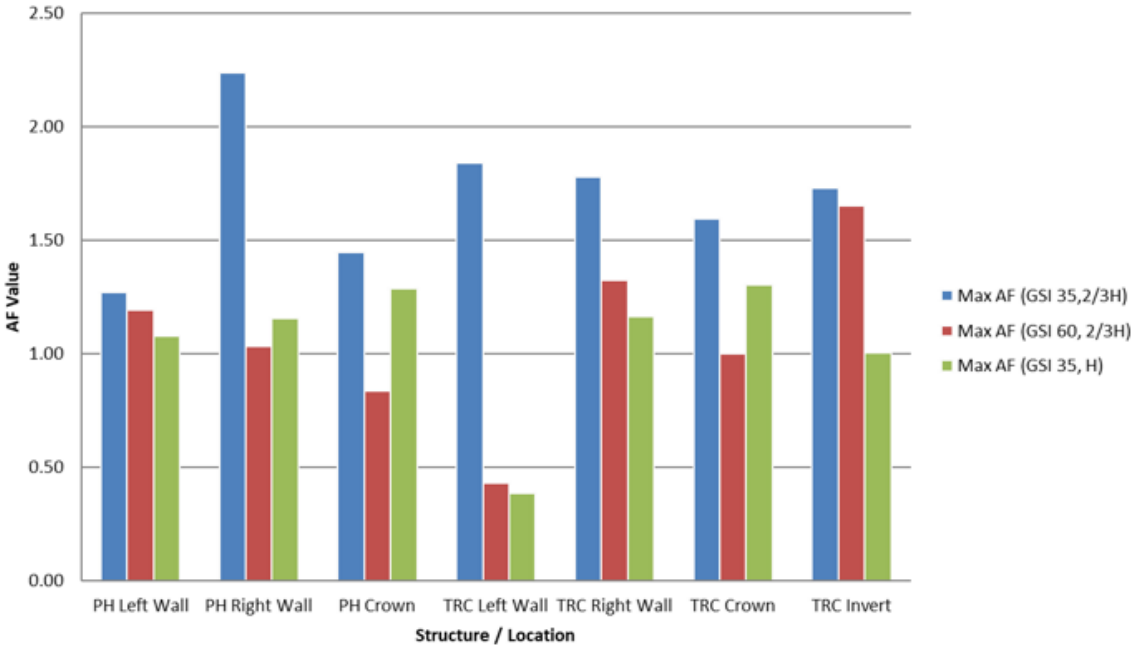

Figure 5.65: Comparison of amplification factor at 2/3H

Table 5.14: Summary of amplification factor with spacing and GSI

Structure / Location	0.5H, GSI35		2/3H, GSI35		H, GSI35		0.5H, GSI60		2/3H, GSI50	
	Min AF	Max AF	Min AF	Max AF	Min AF	Max AF	Min AF	Max AF	Min AF	Max AF
PH Left Wall	0.97	1.06	1.19	1.27	0.98	1.08	1.04	1.13	1.07	1.19

PH Right Wall	1.88	2.36	1.81	2.24	1.06	1.16	0.96	1.05	0.90	1.00
PH Crown	1.24	1.30	1.27	1.45	0.98	1.29	1.87	2.05	1.55	1.72
TRC Left Wall	0.75	1.96	1.17	1.84	0.16	0.38	1.65	1.81	1.32	1.47
TRC Right Wall	1.49	1.60	1.22	1.78	1.04	1.16	1.65	1.81	1.72	1.91
TRC Crown	1.81	1.96	1.24	1.59	0.83	1.30	2.11	2.30	1.77	1.96
TRC Invert	1.26	1.54	1.08	1.73	0.74	1.00	1.67	1.83	1.75	1.95

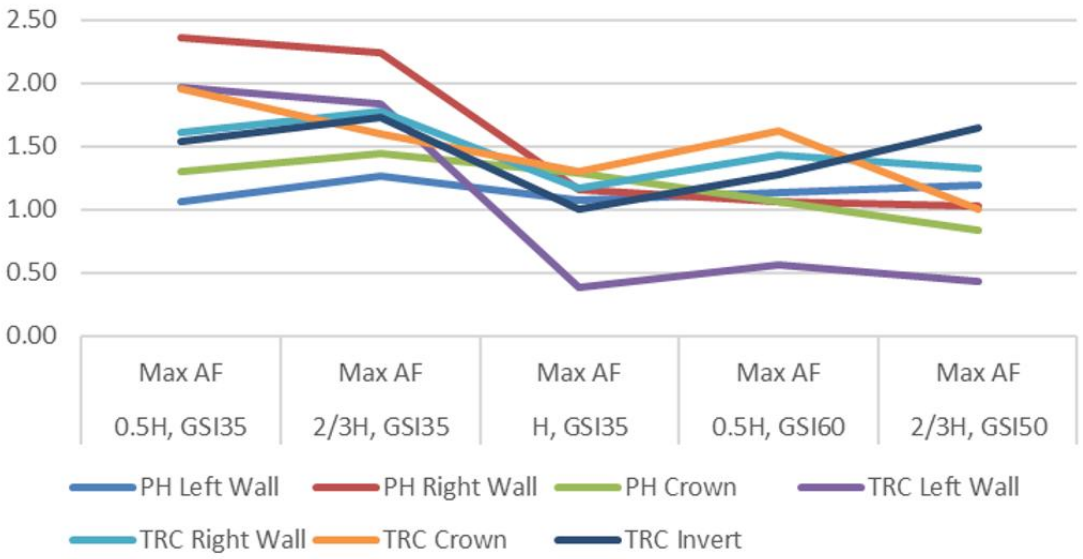

Figure 5.66: Plot of maximum AF with varying GSI and spacing

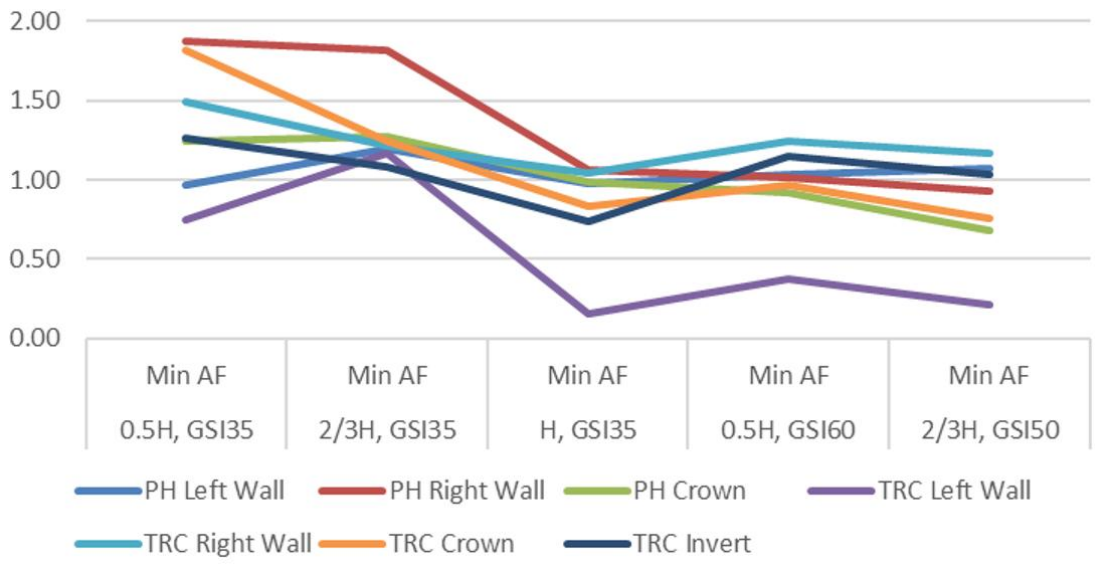

Figure 5.67: Plot of minimum AF with varying GSI and spacing

5.9 Influence of Excavation Sequence

Table 5.15: Occurrence of critical excavation sequence

Structure / Location	0.5H, GSI 35	2/3H, GSI 35	H, GSI 35	0.5H, GSI 60	0.5H, GSI 50	Occurrence of Event			Dominant Case
	Critical Case					Case I	Case II	Case III	
PH Left Wall	Case III	Case II	Case II	Case II	Case II	0	4	1	Case II
PH Right Wall	Case I	Case I	Case I	Case I	Case I	5	0	0	Case I
PH Crown	Case I	Case I	Case I	Case II	Case I	4	1	0	Case I
TRC Left Wall	Case III	Case II	Case III	Case I	Case II	1	2	2	Case II
TRC Right Wall	Case III	Case II	Case II	Case III	Case II	0	3	2	Case II

Structure / Location	0.5H, GSI 35	2/3H, GSI 35	H, GSI 35	0.5H, GSI 60	0.5H, GSI 50	Occurrence of Event			Dominant Case
	Critical Case					Case I	Case II	Case III	
TRC Crown	Case I	Case II	Case II	Case III	Case II	1	3	1	Case II
TRC Invert	Case II	Case II	Case II	Case II	Case II	0	5	0	Case II
Total of Event and Dominant Case						11	18	6	Case II

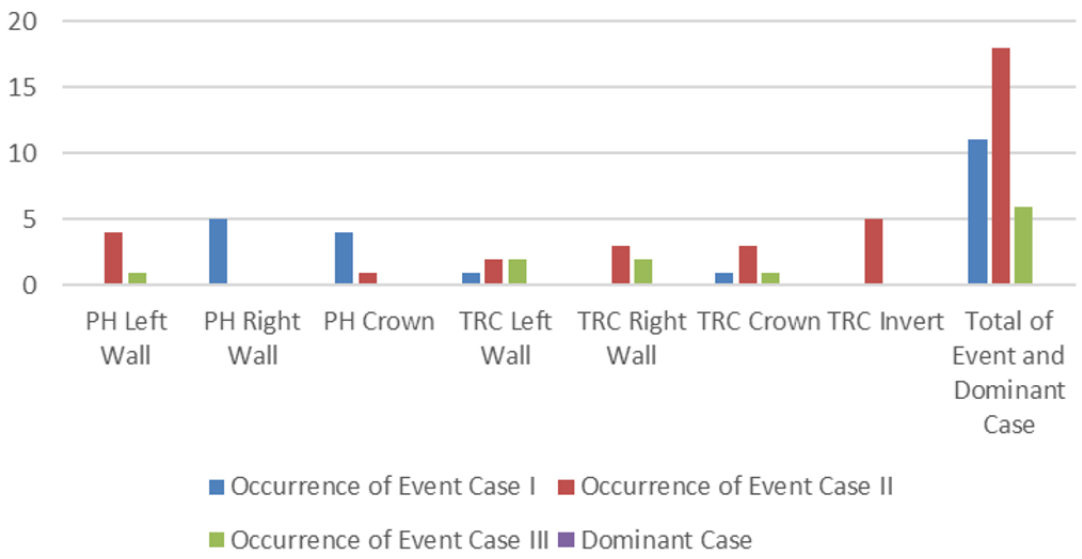

Figure 5.68: Graphical Representation of Critical Excavation Sequence

Table 5.16: Occurrence of the Least Critical Excavation Sequence

Structure / Location	0.5H, GSI 35	2/3H, GSI 35	H, GSI 35	0.5H, GSI 60	0.5H, GSI 50	Occurrence of Event			Dominant Case
	Least Critical Case					Case I	Case II	Case III	
PH Left Wall	Case I	Case I	Case III	Case I	Case III	3	0	2	Case I
PH Right Wall	Case II	Case III	Case III	Case II	Case III	0	2	3	Case II
PH Crown	Case III	Case III	Case III	Case I	Case III	1	0	4	Case II
TRC Left Wall	Case I	Case I	Case I	Case II	Case III	3	1	1	Case I
TRC Right Wall	Case I	Case I	Case I	Case I	Case I	5	0	0	Case I
TRC Crown	Case III	Case I	Case I	Case I	Case I	4	0	1	Case I
TRC Invert	Case I	Case I	Case I	Case III	Case I	4	0	1	Case I
Total of Event and Dominant Case						20	3	12	**Case I**

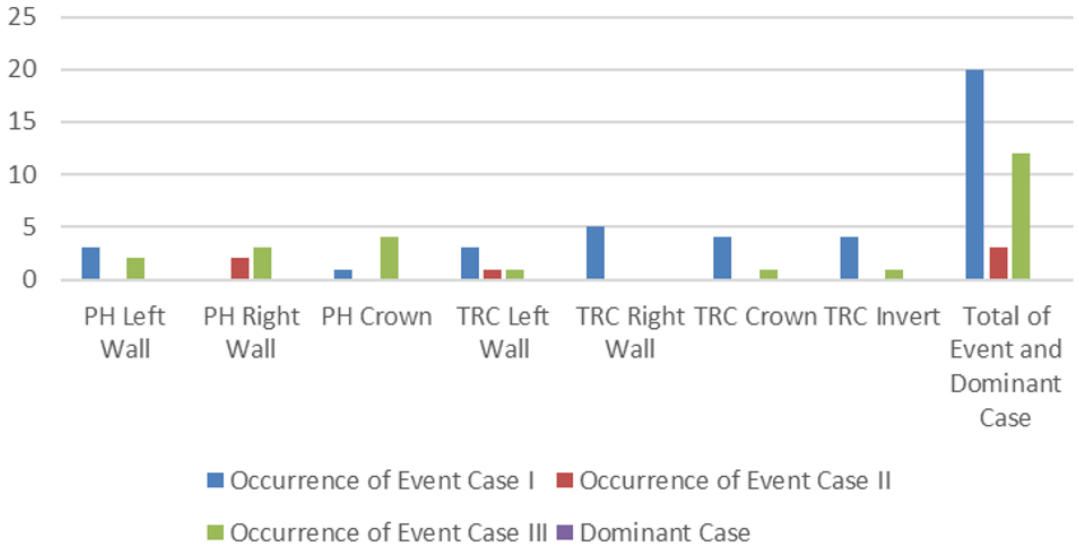

Figure 5.69: Graphical representation of the favorable excavation sequence

From Table 5.15 and Table 5.16, the critical excavation sequence is Case II, which is the excavation of the transformer cavern followed by the powerhouse, and the most favourable excavation sequence is the excavation of the PHC followed by the TRC.

5.9.1 Conclusion

In the analysis, the Geological Strength Index (GSI) was modulated to check the effect of the rock mass quality on the deformation behaviour of various cavern spacing arrangements. Figure 5.66 and Figure 5.67, shows the amplification factors of different locations in the PH and TRC. As the quality of rock mass changes to good conditions (increasing GSI value), the size of the plastic zone also diminishes, as well as the amplification factor. The relationship shows that rock mass competency is important in regulating stress redistribution and deformation in the surroundings of underground excavations. Based on Table 5.12 and Table 5.13, the AF is mainly observed in the TRC and the left side of the PH near the TRC.

As illustrated in Table 5.1, PHC side wall near to TRC undergo significant deformation. From study, TRC is found to be more vulnerable to deformation than the PH. The amplification factors are greater in TRC, and this implies that TRC is shadowed under the PH zone of influence, causing deformation.

6 CONCLUSIONS AND RECOMMENDATIONS

The study focuses on the influence of the cavern interaction due to excavation sequence, deformation modulus of rock mass, and spacing between the caverns. The study also highlights the major influence zone due to cavern interaction. Some of the conclusions of the study have been highlighted below

6.1 Conclusions

- The effect of GSI is the most controlling factor for the deformation modulus and cavern interaction behaviour in cavern design. It is more influential than the excavation sequence and cavern spacing. The deformation, extent of plastic zone and inter cavern influence decreased considerably for GSI ranging from 35 to 60. Therefore, accurate characterization of GSI is critical as underestimation leads to excessive support design while overestimation compromises structural safety.

  The excavation sequence is the second controlling factor and represents a controllable design variable, unlike rock mass properties and cavern spacing which are often site constraints. It directly alters stress redistribution patterns. When caverns fall within each other's zone of influence, the second excavation experiences amplified stress concentrations and increased displacements due to prior stress redistribution.

  Cavern spacing is the tertiary controlling parameter, largely governed by rock mass quality. Although spacing influences the level of cavern interaction, its effect varies with GSI. The critical spacing and interaction level are therefore primarily governed by GSI, which represents the overall rock mass quality. This relationship aids in optimizing cavern arrangement by balancing stability, cost, and construction risk.

- From the analysis and study of different case scenarios, as highlighted below, a higher deformation modulus allows a reduction in spacing. The general observation observed from the study has been provided as follows: The influence of discontinuity and different stress conditions has not been considered. The table shown below can be taken as the reference, whereas

a detailed numerical analysis is required for the determination of appropriate cavern spacing.

Rock Quality	GSI	Recommended Spacing
Weak	≤35	≥H
Intermediate	≥50	2/3H
Good	≥60	0.5H

- A consistent observation throughout the study is that the sidewall of the transformer cavern adjacent to the powerhouse cavern undergoes lesser deformation than the opposite sidewall. This indicates that the smaller cavern is attracted toward the larger cavern, resulting in non-uniform deformation and consequently requiring non-uniform support design.

  The powerhouse right wall adjacent to the transformer cavern experiences significant deformation. The transformer cavern undergoes an overall increase in deformation.
- The deformation and extent of the plastic zone decrease with an increase in quality of rock mass. The overlapping of plastic zone and yielding of deformation decreases with an increase in rockmass quality and cavern spacing.

  Excavation sequence plays a significant role in controlling deformation. The most desirable sequence is to excavate the larger cavern first, followed by the smaller cavern. In the least desirable sequence, where the smaller cavern is excavated first, the induced stresses may overwhelm the existing support system which may require additional support measures on smaller cavern.

6.2 Recommendations

The present analysis has been performed considering a plain strain 2D model, which does not fully capture the three-dimensional stress redistribution and deformation mechanisms characteristics of complex underground excavation. Furthermore, several connecting tunnels to the powerhouse and transformer cavern have not been considered, which can be better analyzed through a 3D model. The dynamic loading induced by excavation-related vibrations has not been incorporated, potentially underestimating the actual deformation response. The numerical results indicate that the transformer cavern sidewall adjacent to

the powerhouse cavern exhibits susceptibility to instability, which could be analyzed in a further stage of study. Since the present analysis has been performed without support systems, it is recommended that further investigations incorporate systematic support elements through parametric studies correlating support requirements with varying rock mass quality to develop optimized support spacing and excavation sequence.

7 REFERENCES

Amadei, B., & Stephansson, O. (1997). *Rock Stress and Its Measurement*. Springer Netherlands. https://doi.org/10.1007/978-94-011-5346-1

Barton, N. (2002). Some new Q-value correlations to assist in site characterisation and tunnel design. *International Journal of Rock Mechanics and Mining Sciences*, *39*(2), 185–216. https://doi.org/10.1016/S1365-1609(02)00011-4

Barton, N., Lien, R., & Lunde, J. (1974). Engineering classification of rock masses for the design of tunnel support. *Rock Mechanics Felsmechanik Mecanique Des Roches*, *6*(4), 189–236. https://doi.org/10.1007/BF01239496

Bellapu, H. V. S., Sinha, R. K., & Naik, S. R. (2023). Estimation of Modulus of Deformation Using Rock Mass Rating—A Review and Validation Using 3D Numerical Modelling. *Sustainability*, *15*(7), 5721. https://doi.org/10.3390/su15075721

Bieniawski, Z. T., & Bieniawski, Z. T. (1989). *Engineering rock mass classifications: A complete manual for engineers and geologists in mining, civil, and petroleum engineering*. Wiley.

Bilham, R., Larson, K., & Freymueller, J. (1997). GPS measurements of present-day convergence across the Nepal Himalaya. *Nature*, *386*(6620), 61–64. https://doi.org/10.1038/386061a0

Brady, B. H. G., & Brown, E. t. (2004). *Rock Mechanics for Underground Mining* (3rd ed.). https://doi.org/https://doi.org/10.1007/978-1-4020-2116-9

Brown, E. T., & Hoek, E. (1978). Analytical and Computational Methods in Engineering Rock Mechanics. In *Analytical and Computational Methods in Engineering Rock Mechanics*.

Cai, M. (2010). Practical Estimates of Tensile Strength and Hoek–Brown Strength Parameter m i of Brittle Rocks. *Rock Mechanics and Rock Engineering*, *43*(2), 167–184. https://doi.org/10.1007/s00603-009-0053-1

Carranza-Torres, C., & Fairhurst, C. (2000). Application of the Convergence-Confinement method of tunnel design to rock masses that satisfy the Hoek-Brown failure criterion. *Tunnelling and Underground Space Technology*, *15*(2), 187–213. https://doi.org/10.1016/S0886-7798(00)00046-8

Chern, J. C., Yu, C. W., & Shiao, F. Y. (1998). *Tunnelling in squeezing ground and support design*. (2), 119–136.

Clarke, B. G. (2023). *Pressuremeters in geotechnical design* (Second edition). CRC Press.

Copley, A., Avouac, J., & Royer, J. (2010). India-Asia collision and the Cenozoic slowdown of the Indian plate: Implications for the forces driving plate motions. *Journal of Geophysical Research: Solid Earth*, *115*(B3), 2009JB006634. https://doi.org/10.1029/2009JB006634

Eberhardt, E. (2012). *The Hoek–Brown Failure Criterion*. University of British Columbia.

Hammett, R. D., & Hoek, E. (1981). *Design of Large Underground Caverns for Hydroelectric Projects with Particular Reference to Structurally Controlled Failure Mechanisms*. ASCE Spring Convention.

Hoek, E. (1994). *Strength of rock and rock masses*.

Hoek, E. (2007). *Practical Rock Engineering*. Rocscience. https://www.rocscience.com/learning/practical-rock-engineering

Hoek, E., & Brown, E. T. (1980a). Empirical Strength Criterion for Rock Masses. *American Society of Civil Engineers (ASCE)*, *106*(GT9), 1013–1035.

Hoek, E., & Brown, E. T. (1980b). *Underground excavations in rock* (Rev). Institution of Mining and Metallurgy.

Hoek, E., & Brown, E. T. (1997). Practical estimates of rock mass strength. *International Journal of Rock Mechanics and Mining Sciences*, *34*(8), 1165–1186. https://doi.org/10.1016/S1365-1609(97)80069-X

Hoek, E., Carranza-Torres, C., & Corkum, B. (2002). Hoek–Brown Failure Criterion – 2002 Edition. *Proceedings of the 5th North American Rock Mechanics Symposium (NARMS-TAC 2002)*, 267–273.

Hoek, E., Carranza-Torres, C., Diederichs, M. S., & Corkum, B. (2008). *The 2008 Kersten Lecture: Integration of geotechnical and structural design in tunneling*.

Hoek, E., Kaiser, P. K., & Bawden, W. F. (2006). *Support of underground excavations in hard rock* (Nachdr.). Tayler & Francis.

Hubbert, M. K., & Willis, D. G. (1957). Mechanics Of Hydraulic Fracturing. *Transactions of the AIME*, *210*(01), 153–168. https://doi.org/10.2118/686-G

Hudson, J. A., & Harrison, J. P. (2009). *Engineering rock mechanics. 1: An introduction to the principles*. Pergamon.

Jaeger, J. C., Cook, N. G. W., Zimmerman, R. W., & Jaeger, J. C. (2011). *Fundamentals of rock mechanics* (4. ed., [Nachdr.]). Blackwell Publ.

Karl, T., & Richart, F. E. (1952). Stresses in Rock About Cavities. *Géotechnique*, *3*(2), 57–90. https://doi.org/10.1680/geot.1952.3.2.57

Krishna K. Panthi (2006), Analysis of Engineering Geological Uncertainties Related to Tunnelling in Himalayan Rock Masses. (n.d.).

Labuz, J. F., & Zang, A. (2012). Mohr–Coulomb Failure Criterion. *Rock Mechanics and Rock Engineering*, *45*(6), 975–979. https://doi.org/10.1007/s00603-012-0281-7

Li, C. C. (2017). Principles of rockbolting design. *Journal of Rock Mechanics and Geotechnical Engineering*, *9*(3), 396–414. https://doi.org/10.1016/j.jrmge.2017.04.002

Lunardi, P. (2008). *Design and Construction of Tunnels*. Springer Berlin Heidelberg. https://doi.org/10.1007/978-3-540-73875-6

Mair, R. J., & Muir Wood, D. (1987). *Pressuremeter testing: Methods and interpretation*. CIRIA ; Butterworths.

Marions, P., & Hoek, E. (2000). GSI: A geologically friendly tool for rock mass strength estimation. *Proceedings of the GeoEng2000 International Conference on Geotechnical and Geological Engineering*. GeoEng2000.

Molnar, P., & Tapponnier, P. (1975). Cenozoic Tectonics of Asia: Effects of a Continental Collision: Features of recent continental tectonics in Asia can be interpreted as results of the India-Eurasia collision. *Science*, *189*(4201), 419–426. https://doi.org/10.1126/science.189.4201.419

NGI. (2025). *Using the Q-System: Rock Mass Classification and Support Design (Q-Handbook 2025)* (p. Oslo). NGI. https://www.ngi.no/globalassets/bilder/forskning-og-radgivning/bygg-og-anlegg/q-handbook_2025_english_final.pdf

Nilsen, B., & Palmström, A. (2000). *Engineering geology and rock engineering: Handbook. No. 2 / [authors: Björn Nilsen; Arild Palmström]*. Norwegian Group for Rock Mechanics.

Nilsen, B., & Thidemann, A. (1993). *Rock engineering*. Norwegian Inst. of Technology.

Palmstrom, A., & Broch, E. (2006). Use and misuse of rock mass classification systems with particular reference to the Q-system. *Tunnelling and Underground Space Technology*, *21*(6), 575–593. https://doi.org/10.1016/j.tust.2005.10.005

Pantelidis, L. (2009). Rock slope stability assessment through rock mass classification systems. *International Journal of Rock Mechanics and Mining Sciences*, *46*(2), 315–325. https://doi.org/10.1016/j.ijrmms.2008.06.003

Phangkawira, F., Ong, D. E. L., & Choo, C. S. (2025). Interpretation of Pressuremeter Test in Fractured and Weathered Phyllite for Back-Analysis of Pipe Jacking Forces. *Rock Mechanics and Rock Engineering*, *58*(2), 2013–2029. https://doi.org/10.1007/s00603-024-04220-x

Ray, A. K. (2009). *Influence of cutting sequence and time effects on cutters and roof falls in underground coal mine—Numerical approach* [PhD, West Virginia University Libraries]. https://doi.org/10.33915/etd.3491

Sakurai, S. (1983). Displacement Measurements Associated with the Design of Underground Openings. *International Symposium on Field Measurements in Geomechanics*, *2*, 1163–1178.

Sengupta, S. (1998). *Influence of Geological Structures on In Situ Stresses* [Ph.D. Thesis]. Indian Institute of Technology.

Sheorey, P. R. (1994). A theory for In Situ stresses in isotropic and transverseley isotropic rock. *International Journal of Rock Mechanics and Mining Sciences & Geomechanics Abstracts*, *31*(1), 23–34. https://doi.org/10.1016/0148-9062(94)92312-4

Shrestha, G. (2021). *Rock Engineering Handbook on Design of Tunnel and other Underground Structures*.

Shukla, A. K., Mishra, A. K., Mazumder, T., & Raju G, D. (2024). Study on significance of pillar dimensions on stability of caverns in rocks with high overburden. *Heliyon*, *10*(12), e31838. https://doi.org/10.1016/j.heliyon.2024.e31838

Singh, B., & Goel, R. K. (1999). *Rock Mass Classification*. Elsevier. https://doi.org/10.1016/B978-0-08-043013-3.X5000-7

Sivakugan, N., Shukla, S. K., & Das, B. M. (2013). *Rock mechanics: An introduction*. Taylor & Francis.

Stephansson, O. (1993). Rock Stress in the Fennoscandian Shield. In *Rock Testing and Site Characterization* (pp. 445–459). Elsevier. https://doi.org/10.1016/B978-0-08-042066-0.50024-0

Sun, N., Li, X., Li, S., Hu, D., Hu, M., Zhang, F., Zhong, Y., Dong, M., & Li, Z. (2023). The Deformation Law of a Soft-Rock Cavern by Step Excavation in a Pumped

Storage Power Station. *Applied Sciences*, *13*(15), 8970. https://doi.org/10.3390/app13158970

Ulusay, R. (Ed.). (2015). *The ISRM Suggested Methods for Rock Characterization, Testing and Monitoring: 2007-2014*. Springer International Publishing. https://doi.org/10.1007/978-3-319-07713-0

Vlachopoulos, N., & Diederichs, M. S. (2009). Improved Longitudinal Displacement Profiles for Convergence Confinement Analysis of Deep Tunnels. *Rock Mechanics and Rock Engineering*, *42*(2), 131–146. https://doi.org/10.1007/s00603-009-0176-4

Wang, M., Shi, A.-C., Li, H.-B., Yan, H.-C., Fan, G., & Zhou, J.-W. (2023). Mechanism Analysis of Surrounding Rock Mass Failure Induced by the Multi-Cavern Effect in a Large-Scale Underground Powerhouse. *Applied Sciences*, *13*(7), 4376. https://doi.org/10.3390/app13074376

Yin, A. (2006). Cenozoic tectonic evolution of the Himalayan orogen as constrained by along-strike variation of structural geometry, exhumation history, and foreland sedimentation. *Earth-Science Reviews*, *76*(1–2), 1–131. https://doi.org/10.1016/j.earscirev.2005.05.004

Zang, A., & Stephansson, O. (2010). *Stress Field of the Earth's Crust*. Springer Netherlands. https://doi.org/10.1007/978-1-4020-8444-7

Zhang, W., & Goh, A. T. C. (2015). Numerical study of pillar stresses and interaction effects for twin rock caverns. *International Journal for Numerical and Analytical Methods in Geomechanics*, *39*(2), 193–206. https://doi.org/10.1002/nag.2306

Zhao, B., & Ma, Z. (2009). Influence of cavern spacing on the stability of large cavern groups in a hydraulic power station. *International Journal of Rock Mechanics and Mining Sciences*, *46*(3), 506–513. https://doi.org/10.1016/j.ijrmms.2008.10.002

Zhu, W., Li, S., Li, S., Chen, W., & Lee, C. F. (2003). Systematic numerical simulation of rock tunnel stability considering different rock conditions and construction effects. *Tunnelling and Underground Space Technology*, *18*(5), 531–536. https://doi.org/10.1016/S0886-7798(03)00070-1

ANNEX I: INSITU AND LAB RESULT

Table 7-0.1:Summary of lab test result of core samples

S.N	Sample ID	Depth (m)	Rock Type	UCS (MPa)	Young's Modulus (Secant) (GPa)	Young's Modulus (Avg.) (GPa)	Young's Modulus (Tangent) (GPa)	Poisson's Ratio (Secant)	Poisson's Ratio (Avg.)	Poisson's Ratio (Tangent)
1	PH03	6.53–6.67	Gneiss	74.4	36.95	43.65	45.34	0.26	0.35	0.37
2		13.20–13.35	Gneiss	65.51	38.26	44.49	47	0.25	0.34	0.36
3		14.00–14.24	Gneiss	93.52	37.87	39.52	40.82	0.21	0.25	0.26
4		14.27–14.46	Gneiss	86.14	28.17	39.36	41.12	0.2	0.34	0.37
5		21.00–21.25	Gneiss	52.3	29.05	36.46	39.13	0.15	0.24	0.27
6	PH04	10.00–10.28	Gneiss	48.48	23.68	34.91	35.54	0.16	0.29	0.29
7		12.00–12.15	Gneiss	77.33	33.15	47.48	45.58	0.14	0.26	0.25
8		12.63–12.81	Gneiss	46.13	23.59	35.27	37.05	0.1	0.2	0.21
9		12.81–13.00	Gneiss	39	22.83	31.19	31.47	0.1	0.17	0.17

Table 7-0.2: Dilatometer test results at powerhouse location

Borehole No.	Test section (mbgl)	Em (MN/m2) (initial load)	Em (MN/m2) (1st unload/reload cycle)	Em (MN/m2) (2st unload/reload cycle)	Em (MN/m2) (3st unload/reload cycle)	G (MN/m2) (initial load)	G (MN/m2) (1st unload/reload cycle)	G (MN/m2) (2st unload/reload cycle)	G (MN/m2) (3st unload/reload cycle)	Inferred UCS (MPa)	Co officiant of Earth Pressure at rest (K_0)	in-situ total lateral earth stresses (kPa)
PH-03	13.55-14.20	832.20	18583.00	4144.80	-	243.90	7433.20	1657.90	-	27.00	2.01	800
PH-03	18.65-19.30	277.40	975.30	2477.00	1872.9	119.6	395.30	988.60	786.90	15.30	1.64	752
PH-03	20.85-21.50	1084.00	6944.10	13118.30	17555.50	467.20	2993.10	5511.90	7376.31	10.6	1.43	772
PH-04	4.10-4.75	141.10	2610.80	4716.90	4676.00	60.80	1087.80	1965.40	1948.30	11.9	2.32	657
PH-04	9.00-9.65	334.40	1693.50	3793.30	6658.90	144.20	705.60	1580.60	2774.60	15.7	2.16	700
PH-04	13.00-13.65	1295.70	13944.00	19098.70	21952.70	589.00	5959.00	8161.80	9381.50	14.3	2.12	758

ANNEX II: PHOTOGRAPHS

Figure 7-0.1: Excavated powerhouse cavern (crown and first bench)

Figure 7-0.2: Extracted core sample from PH cavern

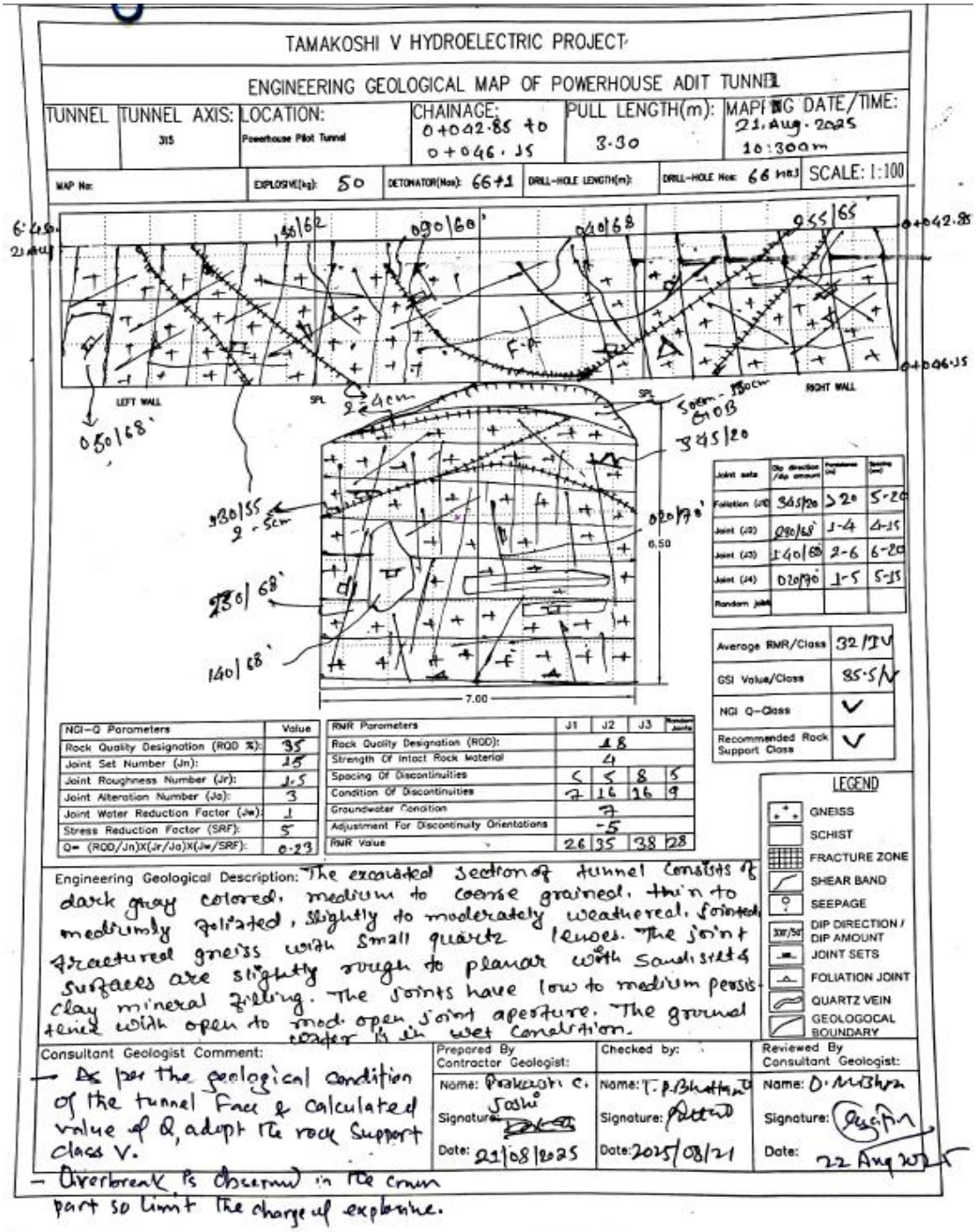

Figure 7-0.3: Geological face map

Figure 7-0.4: Preparation of pressuremeter test at powerhouse cavern

Figure 7-0.5: Tunnel connecting powerhouse and transformer cavern

ANNEX III: LIST OF PUBLICATIONS

Conference Paper:

G. Pathak and S.K. Yadav, "Numerical Investigation on Influence of Excavation Sequence and Parametric Analysis on Cavern Interaction (A Case Study of Tamakoshi V Hydroelectric Project)" in *18th IOE Graduate Conference (2026),* Lalitpur, Nepal